STUDIES ON OPTICAL PROPERTIES OF METHACRYLATE-BASED PHOTOPOLYMERS FOR 3D PRINTED OPTICAL WAVEGUIDES

by

Kunal Sharma

A Dissertation Submitted in Partial Fulfillment of the Requirements for the Degree of Doctor of Engineering in Nanotechnology

Examination Committee:	Dr. Tanujjal Bora (Chairperson)
	Dr. Waleed Mohammed (Co-Chairperson)
	Dr. Loc Thai Nguyen
	Dr. Gabor Louis Hornyak
External Examiner:	Prof. Teyuan Chung
	Department of Optics and Photonics
	National Central University
	Taiwan
Nationality:	Indian
Previous Degree:	Master of Engineering in Mechatronics
	Asian Institute of Technology
	Thailand
Scholarship Donor:	Ideal Fastener Asia Ltd., Hong Kong - AIT Fellowship

Asian Institute of Technology

School of Engineering and Technology

Thailand

December 2021

AUTHOR'S DECLARATION

I, Kunal Sharma, declare that the research work carried out for this dissertation was in accordance with the regulations of the Asian Institute of Technology. The work presented in it are my own and has been generated by me as the result of my own original research, and if external sources were used, such sources have been cited. It is original and has not been submitted to any other institution to obtain another degree or qualification. This is a true copy of the dissertation, including final revisions.

Date: 05-12-2021

Name: Kunal Sharma

Signature: *Kunel Sherme*

ACKNOWLEDGMENTS

ABSTRACT

In this study the optical properties of methacrylate-based photopolymers were explored, using the stereolithography-based 3D printed optical waveguides. A first-order model was developed to estimate surface scattering losses in the waveguide and how the transmission of the light through the waveguide would change when the waveguide interacts with solvents. This study revealed that in the presence of solvents, a dynamic gain in the optical power through the 3D printed waveguide was observed due to the formation of a swelling layer at the surface producing a cladding effect. The degree of swelling depends on the solvent's absorption affinity for the methacrylate-based polymer and the refractive index of the individual solvents here had a trivial role to play in the optical power gain. When physically interacted with solvents, the methacrylate-based waveguide exhibited significant optical gain in the transmitted light, confirming the theoretical observations. When the waveguide was tested with solvents having different absorption affinities for the methacrylate-based polymer but having a similar refractive index, the highest optical gain was produced by the solvent with the highest absorption affinity for the photopolymer, as it develops more homogenous and thicker swelling layer and hence effective cladding. This showed that the effectiveness of the swelling layer to act as cladding depends on how well the given solvent can be absorbed in the polymer rather than the refractive index of the solvent. The methacrylate-based waveguide was further studied for its temperature-dependent properties. It was found that the optical transmittance through the waveguide changes with a change in the ambient temperature. However, the methacrylate-based waveguide did not show a consistent optical output and failed to produce a change in the optical output when tested for multiple cycles. To address this issue, we embedded gold nanoparticles in the polymer matrix. When tested, the gold nanoparticle incorporated waveguides showed more stable results. For a change of surrounding temperature from room temperature to 45 °C, we observed consistent optical transmittance change between 90 to 98%, respectively and up to 20 repeated heating and cooling cycles the waveguide exhibited similar behavior.

Keywords: Methacrylate-based photopolymer, Nanoparticles embedded waveguides, 3D printed waveguides, Solvent absorption, Polymeric swelling

CONTENTS

LIST OF TABLES

LIST OF FIGURES

LIST OF ABBREVIATIONS AND SYMBOLS

NPs = Nanoparticles

Vis = Visible

UV = Ultraviolet

T_c = Transmittance through gold nanoparticle embedded waveguide

CAD = Computer Added Design

SLA = Stereolithography

n_{poly} = Refractive index of photopolymer

n_{sw} = Refractive index of swelling layer

n_{sol} = Refractive index of the given solvent

n_{air} = Refractive index of air

ε = Dielectric constant of a material

PMMA = Polymethyl-methacrylate

PDMS = Polydimethylsiloxane

D_m = Coefficient of mutual diffusion

CA = Contact Angle

EM = Electromagnetic

DI = De-ionized

VOC = Volatile Organic Compound

v/v = Volume by volume

T = Temperature

d_t = Thickness of swelling layer

k = Extinction coefficient

κ = Attenuation coefficient

P_{guid} = Guided optical power through photopolymer waveguide

V_f = Volume fraction

SEM = Scanning Electron Microscopy

WV = Waveguide

CHAPTER 1
INTRODUCTION

1.1 Background of the Study

Innovations in the field of materials and methods for optical components and photonic devices have gained significant pace recently to overcome the fabrication complexity associated with commonly used traditional methods like chemical vapor deposition, sputtering, lithography, etc. that requires sophisticated equipment and facilities making these methods expensive (Imoto et al., 1983). Photopolymers, in this regard, have drawn significant attention lately because of their ability to get cured easily with direct exposure to light (N. Sakai, 2009), high refractive indices (Venkatraman & Alsberg, 2018), large working dimensions (typically from 100nm to 100s of microns), and low cost. Transparent photopolymers have shown an efficient light transmission in the visible and near infra-red region of the electromagnetic spectrum with low production cost. The ease of handling these photopolymers, generally at ambient conditions, makes the fabrication process more convenient.

At present, photopolymers are being used in a variety of photonics applications like waveguides (Madani & Azarinia, 2017), deformable lenses (Falahati et al., 2019), electro-optic modulators (Yongqiang Shi et al., 2000), light-emitting diodes (Schmitz et al., 2001) and flexible displays (Fujikake et al., 2016). Fabrication of waveguides using photopolymers is one of the most valuable applications in integrated optics and has broad applications in areas like optical communication, microwave signal processing, and sensing. Waveguides with high aspect ratios, rapid duplication, and customized sizes make photopolymers a potential material to be used for integrated optical devices. Photopolymers are generally available in liquid suspension form, which makes them suitable ink material for 3D printing methods such as stereolithography (SLA) where photopolymers are cured when exposed to an inbuilt UV light source (Dall'Argine et al., 2020).

A CAD file of the specified design is uploaded to a 3D printer, which prints the entire 3D structure in a layer-by-layer format in a single-step fabrication process. This flexibility, with practical correctness, makes photopolymers a viable option for integrated optical devices fabrication. Photopolymers can also be doped with different

chemical functional groups which help to impart some unique properties to photopolymers such as mechanical strength, hardness, transparency, and color (Sinha et al., 2020). Photopolymers are special kinds of polymers that are cured by the light of a specific wavelength to convert liquid resin into a hard polymer. Poly-methyl methacrylate (PMMA) is the most commonly used photopolymer in the stereolithography process.

The main repeating unit in PMMA is methyl methacrylate (MMA), but often other monomers and co-polymers are added to implant different physical properties in the final product. PMMA shows good physical properties like tensile strength, flexural strength, transparency, grinding ability, refractive index, and economic viability over other photonics polymers like polycarbonate (PC) when extremely high strength is not necessary (Hamdi, 2020). Unlike PC, PMMA does not have bisphenol-A which is toxic (Le et al., 2008). For this reason, PMMA is used for biomaterial applications like dentures and prosthetics in joint replacement. PMMA exhibits hydrolytic stability against acid and base hydrolysis (Rodriguez et al., 2018) and solid PMMA is inert to ordinary aminolysis (Henry et al., 2000) which makes PMMA chemically stable under common working conditions.

1.2 Statement of the Problem

Studies have been conducted to evaluate the optical properties of photopolymers for their potential use in integrated optical devices (Peters, 2011). Methacrylate photopolymers are widely studied and numerous sensing applications have been reported (Fuchs et al., 2012). Methacrylate-based photopolymers are easy to handle and provide decent mechanical stability to the optical components. They, however, are not stable in high acidic or basic conditions, as well as at high temperatures, and react with most of the organic chemicals. Typically, in optical sensing applications, optical components are expected to get exposed to any kind of chemical atmosphere depending on the application area. For example, a photopolymer-based chemical sensor will be exposed to a chemical environment to sense the target chemical, where the atmosphere can be corrosive or can contain other chemicals mixed with the target chemical, which can interfere with the optical properties of the photopolymer.

Robustness of methacrylate-based photopolymers in such applications is a desired property and the understanding of the material's chemical nature is a key factor to

fabricate robust optical components. Till date very few studies have been conducted to understand the interaction of methacrylate-based photopolymers with commonly used solvents and their effects on the optical properties of the polymer. Methacrylate-based polymers are generally hydrophilic in nature and exhibit swelling whenever they meet solvents like water and alcohol (Miller-Chou & Koenig, 2003). Swelling of the polymers also can occur due to the presence of humidity and VOCs (H. Guo et al., 2020) in the ambient environment. The extent of such swelling mostly depends on the temperature of the environment and the concentration of the chemicals. Recent research conducted on polyacrylic acid hydrogel (Okudan & Altay, 2019) shows that the degree of swelling is being affected by the change in the solvent temperature.

Polymers are long-chain networks that are cross-linked with each other. During the crosslinking process some void spaces within the polymer chains are created. Solvent molecules have the ability to diffuse inside these polymer chains (Vrentas & Vrentas, 1994) and acquire the void spaces. When solvent molecules come in contact with the polymer, they eventually fill these void spaces (Vrentas & Duda, 1977), and the net effective volume of the polymer, therefore, increases. This process is termed as *swelling* which mainly depends on the mutual diffusion between the polymer and the solvent. For example, polymethyl-methacrylate (PMMA) has a strong affinity to absorb less polar solvents, like acetone and toluene, while it has a poor affinity to absorb water which is a highly polar solvent (Ballenger et al., 2002).

It has been shown that exposure to varying concentrations of ethanol in water, the swelling of methacrylate-based polymers also varies (Malacarne-Zanon et al., 2009). The degree of swelling is maximum in the case where the concentration of ethanol is the highest. A similar analysis was reported on poly-vinylpyrrolidone (PVPON) and poly-acrylic (PAA) thin films (Q. Han et al., 2014) and it was found that the extent of swelling depends on the concentration of ethanol in the solvent. This process of absorption of solvent in the polymer will continue till a saturation state is reached (Gervasio et al., 2015).

During the swelling process, solvent molecules penetrate the polymer network affecting the natural properties of the polymer. Effect of swelling on the structural properties of polymers, like tensile strength (Mat-Shayuti et al., 2017), compressive strength (Krasucka et al., 2018), cyclic loading (Abdul Hamid et al., 2020), etc., have

been studied. However, the effect of swelling on the optical properties of polymers has not been studied in detail. To use photopolymers in integrated optics, particularly for the fabrication of sensing devices, it is important to understand the effect of swelling on their optical properties.

1.3 Research Questions

Based on the above discussion following are the research questions that lead to take-up this doctoral research work.

1. How would the optical transmission in a methacrylate-based photopolymer waveguide change due to swelling of the polymer resulting from the absorption of a solvent in the polymer network? Would this change be similar or different for different solvents?

2. What are the factors that contribute to this change of optical transmission in a methacrylate-based photopolymer due to swelling? Would this depend on, the refractive index of the solvent or the swelling capacity of the polymer, or the concentration of the solvent? Also, is the effect of swelling on the optical properties of the photopolymer a reversible effect?

3. How would the optical transmission of a photopolymer waveguide will be affected by the change in the temperature of its ambient? Since temperature affects the swelling process, any change around the surrounding temperature of the photopolymer waveguide should affect optical transmission through it. Can this effect of temperature on the optical transmission in the polymer be affected by embedding nanoparticles in the polymer?

1.4 Objectives of the Study

Following are the specific objectives of this doctoral study.

1. Explore the effects of solvent-photopolymer interaction on the optical properties of a methacrylate-based 3D printed waveguide and find the relationship of the swelling of the polymer with different types of commonly used solvents.

2. Develop a solvent-photopolymer diffusion model explaining the reduction of surface scattering and dynamic optical gain in the 3D printed waveguide.

3. Study the effect of temperature on the optical properties of the methacrylate-based photopolymer waveguide.

4. Study the role of gold nanoparticles embedded in the waveguide on its temperature dependent optical behavior.

1.5 Hypothesis of the Study

It is hypothesized that the optical transmission through the methacrylate-based photopolymer waveguide can be affected by polymeric swelling which depends on the ability of the solvent to interact with the polymer and temperature of the ambient. The developed swelled layer in the photopolymer waveguide due to solvent absorption would act as a natural cladding layer which would reduce the interaction of light with the rough waveguide surface and eventually yield a reduction in surface scattering loss. This would induce an optical gain in the photopolymer waveguide as the transmission through the photopolymer waveguide will be enhanced. The change in the temperature of the ambient can also alter the refractive index of the methacrylate-based photopolymer waveguide by affecting the optical transmission through it.

1.6 Organization of the Report

This report is organized in the following steps:

Chapter 1: Introduction, in this chapter the background of the research and the need to do the research on the swelling-induced optical properties of photopolymers are established. Research questions and specific objectives of the research work are explained.

Chapter 2: Literature Review, in this chapter literature review relevant to this research, is described. This includes usage of polymers in integrated optics, properties of photopolymers, 3D printing, solvent absorption by the polymers, formation of the swelling layer, and effect of temperature on the optical properties of the polymers are discussed in detail.

Chapter 3: Methodology, in this chapter the methods for both theoretical and experimental studies that have been applied to conduct this research are described. This includes characterization of the photopolymer, 3D printing of the waveguide, development of the theoretical model for the swelling process and how it affects

surface scattering losses in the waveguide, conducting physical experiments to verify actual swelling and effect of temperature, and any other experiments conducted in this research are explained.

Chapter 4: Results and Discussion, in this chapter the results obtained from both theoretical models and experiments are mentioned and discussed. This includes UV-Vis absorption spectroscopy and hydrophilicity of photopolymer, microscopic images of the 3D printed waveguide, theoretical results for swelling layer thickness, increase in optical power through the waveguide due to solvent-polymer interaction, and transmittance variation with respect to temperature of the ambient.

Chapter 5: Conclusion and Future Recommendation, in this chapter conclusions from the findings of this research work are explained and recommendations to conduct further research are given.

CHAPTER 2
LITERATURE REVIEW

This chapter provides the substantial impression of the study done previously by other researchers which are referred to find research gaps to conduct this doctoral study. It introduces the framework to find answers to the research questions while keeping the research focus on the objective of doctoral study. The chapter opens with the usage of polymers in integrated optics applications and subsequently, photopolymers have been introduced with their synthesis principle. Next, stereolithography-based 3D printers and their working technique has been explained which is the main fabrication method in this research. This is followed by scattering losses in waveguides, swelling of polymers due to absorption of solvent, and the possibility of the swelled layer to act as cladding is described. This chapter ends with explaining the effect of temperature on polymers which possibly affect the optical properties of the polymer.

2.1 Polymers and Their Application in Integrated Optics

Polymers have been used as an economical and easily available alternative for traditional photonic materials such as silicon or quartz (Paquet & Kumacheva, 2008). Polymers such as polymethacrylates (PMA), Polyurethanes (PU), and Polycarbonate (PC) have shown a refractive index in the range of 1.4-1.6 (Liu & Ueda, 2009). These polymers are clear polymers and transparent like glass which makes them suitable for the fabrication of optical components like lenses and waveguides. In recent times, researchers have developed polymers-based optical fibers (Bhowmik & Peng, 2019) as an alternative to silica-based optical fibers and conducive polymers-based antennas (Chen et al., 2016) for wireless sensor applications.

With the addition of doping agents like silicones, the siloxanes polymers can show a refractive index of around 1.54 (Yang et al., 2013). Another advantage of these polymers is their availability in both solid and liquid forms which give the user convenience during the fabrication process and by changing the concentration of monomers and doping agents (Obreja et al., 2006), properties like physical strength, hardness, and flexibility of the polymers can be improved. Some methacrylate-based polymers can be recycled by dissolving them in a suitable solvent (Esmizadeh et al., 2018) which makes them sustainable for some of the applications. Refractive indices

of some common polymers that have been used in the photonics application are mentioned in Table 2.1.

Table 2.1

Common Polymers that have been Used in Photonics Applications with Their Refractive Indices at 632nm (Sudarsan, 2012)

Sr. No	Polymer Type	Refractive Index
1.	Polymethyl-methacrylate (PMMA)	1.4887
2.	Polycarbonate (PC)	1.5863
3.	Polyvinyl chloride (PVC)	1.5400
4.	Polydimethylsiloxane (PDMS)	1.4283
5.	Polyvinyl alcohol (PVA)	1.4766

Polymers can be cured with different techniques, for example, PMMA based polymers are cured in Ultra-Violet (UV) light (Mendes-Felipe et al., 2019) that is why they are also called photopolymers or light-sensitive polymers. Other polymers like Polydimethylsiloxane (PDMS) are cured by applying heat (Yingli Shi et al., 2020), while some polymers can also be electro-cured by applying suitable voltage and current (M. Hossain, 2020). There is a new class of polymers known as self-cured polymers (Reddy et al., 2020) which get cross-linked when polymers chains come in contact with each other, that's is why they are also called self-healing polymers as they can repair any damage that happened in the structure.

Polymers can be used in a wide variety of dimensional ranges, pairing with the right technique the working dimensions with polymers can be as low as 100 nm (Kuila et al., 2013) to as high as in 100s of microns (Horák, 2003). This makes them suitable for the fabrication of optical and photonics components which required complex geometry and precise dimensions. The lower density of the common polymers (Bernardo et al., 2019) helps them in the fabrication of lightweight optical components in comparison to glass. Selecting the right polymer with a desirable

refractive index and pairing it with an appropriate fabrication technique, can make polymers a promising material in the future of integrated optics.

2.2 Formation Mechanism of Photopolymers

Photopolymers draw their names from the word '*photo*' which means light, and this is because light plays an important role in the synthesis of these types of polymers. Polymers are long-chain supra-molecules that contain an initiator, a monomer, and oligomers (Naka, 2021). The purpose of the initiator is to start the polymerization mechanism and the most common method is the formation of free radicals (Bisht & Chatterjee, 2001). Photo-initiators molecules when exposed to the light of specific wavelengths get decomposed to an active fractured segment called free radicals. These free radicals combined with monomers and oligomers to create a long chain of polymer networks.

Monomers are the smallest part of polymers joined in a repeated fashion to create a new molecule called a polymer. Oligomers are binder molecules that are repeated units of monomers present in smaller quantities. Together these three make long chains of polymers and the process propagates further till the polymer chain is terminated. After the formation of long-chain molecules, individual polymer chains further absorb light and stronger bonds are formed among different chains which is called crosslinking (Tawade et al., 2021). The final product formed is a crosslinked structure which is a supra-molecule as shown in the below mechanism and this process is commonly known as curing of the polymer.

$$\text{Light + Photo-initiator} \longrightarrow \text{Active Compound}$$

$$\text{Active Compound + Monomers \& Oligomers} \longrightarrow \text{Polymer Chains}$$

$$\text{Polymer Chains + Light} \longrightarrow \text{Cross-linked Structure}$$
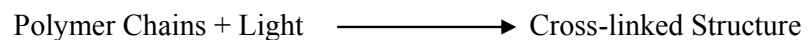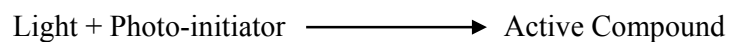
A specific type of photopolymers that absorbs ultra-violet light for the polymerization process is commonly called a UV-Resin. UV-resin generally absorbs light wavelength from around 250 nm to 410 nm (Shukla et al., 2004). Light in this electromagnetic region has a higher frequency which contributes to higher energy (hυ) resulting in better excitation of the initiators to begin the polymerization process. Also, the light

of higher energy can penetrate polymer structure better (Araujo et al., 2019) which results in a faster process, stronger structure, and higher working dimensions. The common examples of photopolymers are acrylated polyesters, acrylated urethanes, acrylated silicones (J. Guo et al., 2012). The most common monomer that is present in UV-Resin is methacrylate and in general, these resins or photopolymers are called methacrylate-based resins. An example of the synthesis of PMMA through free radical polymerization is presented in Figure 2.1.

Figure 2.1

Synthesis of Poly (Methyl Methacrylate) Through Free Radical Polymerization (Darvell, 2018)
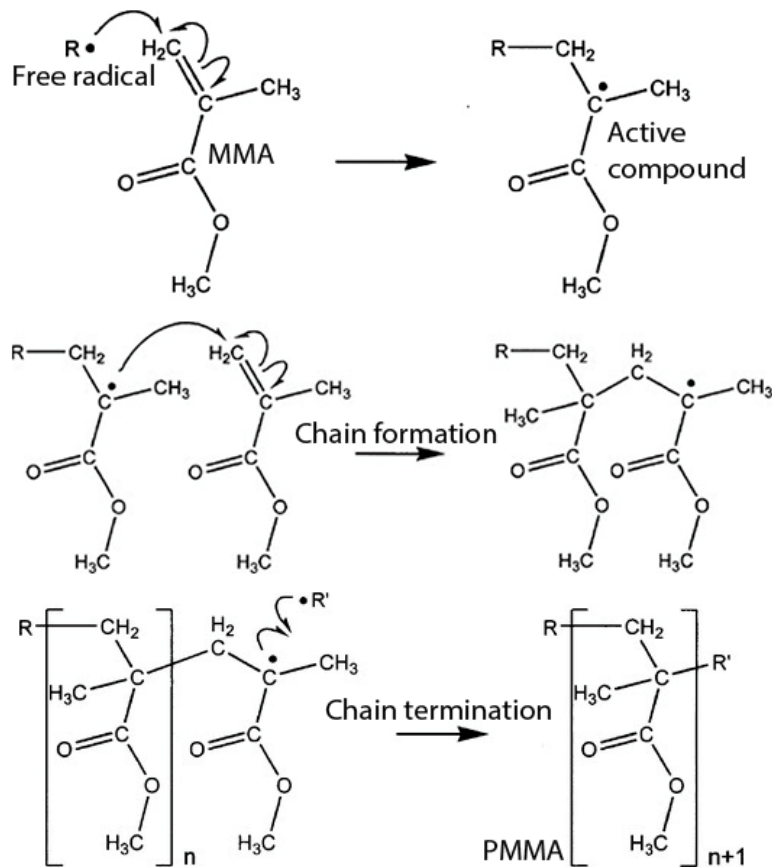
The refractive index of PMMA, a common methacrylate-based polymer is around 1.48-1.50 (Ali et al., 2015) which can serve as an efficient optical material that can be

used in optical fibers, waveguides, and lenses. Due to the presence of a highly active double bond in its chemical structure (Leggat et al., 2009) the free radical activity of methacrylate to undergo polymerization is high. Also, its ability to combine with different functional groups like epoxies, urethanes, amides, imides, ethers, hydrocarbons, esters, and siloxanes (Yoshida et al., 2019) makes methacrylate-based resin the most sought after polymers for the UV-cured class of polymers. With the ability to produce desirable results and being environmentally friendly methacrylate-based polymers first have been used in dental implants in 1975 (Leigh, 1975) and then in 2006, they were used as prosthetics in orthopedic surgeries (Frick et al., 2006) for knee, hips, and shoulders.

2.3 Stereolithography Based 3D Printing

3D (or 3-Dimensional) printing is the technology that has provided much ease and flexibility in the fabrication process. The term "3D printing" was originally generated through a process that deposits a binder material onto a bed with an inkjet printer head in a layer-by-layer mechanism (Horvath, 2014). Since the deposition is done in a layer-by-layer format, the height or the Z-axis can be controlled as well, and hence this technology gives us printouts where all three-dimensional axis (X, Y, and Z) can be designed and fabricated as per the specific requirements. In the 3D printer, a CAD file (generally in STL format) is uploaded, and the respective software of the 3D printer converts this CAD file into G-codes which are further read by the printer's controller to move all 3-axis to produce the required print. Selecting a commercial 3D printer with high resolution can help achieve dimensions as low as 10s of the microns (Maines et al., 2021) and good surface finishing.

Using the raw material available in different colors, also provide attractive looks to the finished products for their commercial usage. Commercially available 3D printers are also categorized according to the raw material and printing technology they use for 3D printing, like fused deposition modeling (FDM) which uses thermoplastic filament (Ngo et al., 2018) and stereolithography (SLA) which uses light-sensitive resin or photopolymers, selective laser sintering (SLS) that uses a laser as power supply to form 3D printed objects (Huang et al., 2020). Amongst these, SLA-based 3D printers have created a huge interest as they use light-sensitive resin to create sophisticated 3D objects. In an SLA-based 3D printer, an inbuilt UV-light source is

placed inside the body of the printer and under a transparent screen that can be able to project this UV-light. Above the screen, the transparent tank is placed which is used to fill liquid resin and a movable holder is placed above the tank as shown in Figure 2.2 which is controlled by a micro-controller that is attached with the printer. This holder moves up-down in the Z-axis to control the height of the structure that is intended to print.

Figure 2.2

Up-Side-Down 3D Printer Schematic
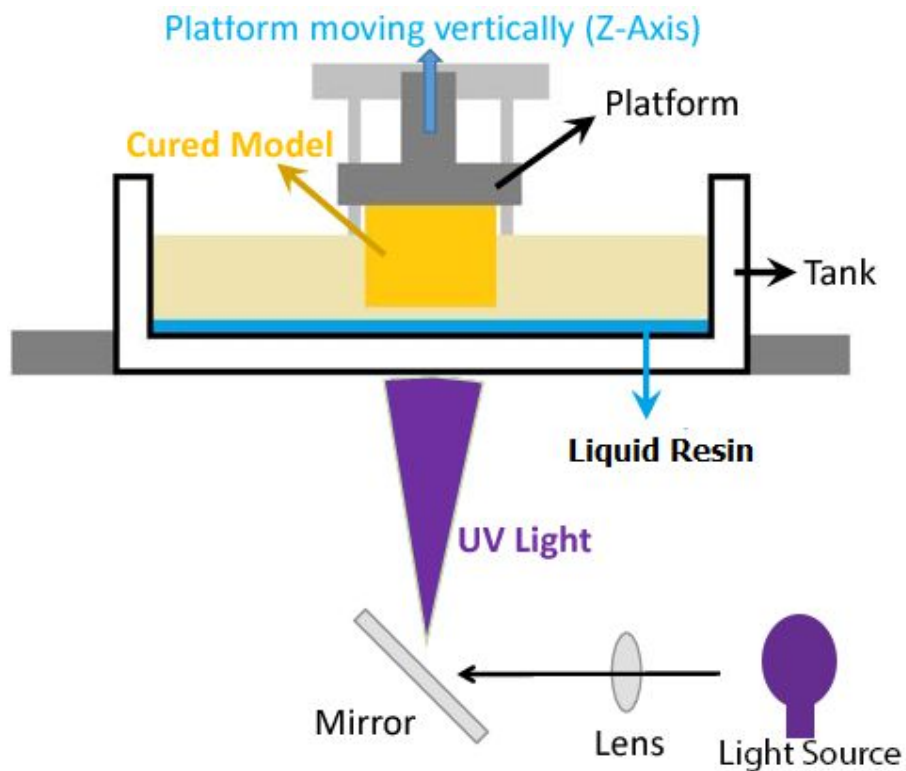
The G-code generated by the software are projected on the screen which gets cured when the inbuilt light source flashes, the XY-coordinates are directly projected from the G-codes of the design while the Z-axis can further be controlled in a layer-by-layer format, which means the printer software divides the total height of the design in small layers and the thickness of each layer can be decided by the user which can vary from 10 µm to 100 µm as per the user's requirement (Ravi & Shiakolas, 2021). This

process is called slicing. This gives more flexibility and finesse in the fabrication and helps to generate surfaces with the desired finishing. Since the print is generated on the printer holder as shown in Figure 2.2, this kind of printing style is called upside down because the downside of the design is printed first on the holder and then the holder keeps moving up in the increments of the layer (which is decided by the user). SLA-based 3D printers are compact, relatively cheaper, convenient to use and with much flexibility in fabrication (Quan et al., 2020) gives them an edge over traditional fabrication methods.

2.4 3D-Printed Waveguides and Their Scattering Losses

3D printing is an effective and convenient fabrication method that can be used for the fabrication of polymeric waveguides for integrated optics applications. Waveguides of different aspect ratios and geometries can be 3D printed within practical limits of tolerances in dimensions. The simplicity of the 3D printing process gives it a major advantage over traditional methods like lamination, doctor-blading, and extrusion which are complex and time-consuming (Han et al., 2018). But, like any other fabrication method, 3D printing also creates irregularity within the 3D printed waveguide which results in scattering losses. Due to scattering, light deviates from its original path within the waveguide, and the net transmittance through the waveguide is decreased. The main reasons for the occurrence of scattering losses in the 3D printed waveguide are molecular level defects, volumetric defects, and surface defects which are described below.

1. Molecular-level defects in the 3D printed waveguide occur due to inhomogeneities in photopolymer material which results in structural irregularities and disordered molecular bonding (Elson, 2003). At times, due to inaccurate blending of monomers and oligomers in the photopolymer resin, the crosslinking among different photopolymer chains are not homogenous which results in the variation of the photopolymer chain length, density, and size of voids within photopolymer structure (Xavier, 2003). These imperfections in the photopolymer structure optically result in the variation of the refractive index within the same photopolymer waveguide. In general, these material imperfections are

smaller in comparison to the wavelengths in the visible region (Trost et al., 2013) and result in lesser power losses in the waveguide.

2. Volumetric defects in the 3D printed waveguide occur due to irregular 3D printing mechanism. During the 3D printing, the air bubbles present in the resin tank of the printer get entrapped inside the 3D printed structure which results in the formation of an internal cavity (Maruyama et al., 2020). At times, due to uneven projection of UV-light by the printer, some part of the waveguide gets cured lesser than the other which results in the formation of different optical zones within the same 3D printed waveguide (Berglund & Tkaczyk, 2019). With the development of sophisticated 3D printers, the occurrence of volumetric losses in the waveguides has been lowered by controlling the slicing thickness, speed of the holder, and movement of the printer in all three directions.

3. Surface defects in 3D printed waveguides include surface roughness, sidewall roughness, and surface irregularities in the waveguide geometry which mostly occurs at core/air interfaces of the waveguide (Verrina et al., 2020). The propagating light in the waveguide gets distorted when the interface has large surface irregularities (Barwicz & Haus, 2005) which results in a portion of the light spreading away from its regular path. The extent of such loss also depends on factors like the length of the waveguide, the wavelength of light, the refractive index of waveguides, and the surrounding environment (Grillot et al., 2008). A detailed discussion on surface scattering losses in 3D printed waveguides is presented in the next sections.

2.4.1 Scattering Losses Due to Surface Roughness

Optical losses mostly depend on two things: raw material and the fabrication process (Ramponi et al., 2002). Since the quality of raw materials used for waveguide fabrication, lesser or more is the same hence what matters the most is the choice of the fabrication method. Because losses like absorption and sub-surface defects depend on the raw material it is safe to say that it is the surface scattering losses that contribute to most of the optical defects as they mostly depend on surface quality which in turn depends on the fabrication method used (Ying Shi et al., 2020). When the light interacts at the junction of two medium which has rough surfaces, a large

part of the light is scattered and get wasted as shown in Figure 2.3. It has been observed that surface roughness can be minimized but it is not possible to totally eliminate it from the waveguides. Effect of surface roughness becomes more critical for small-sized waveguides (Fang et al., 2008) because there is lesser scope to control physical parameters during the fabrication process. Hence it would be better to use this surface roughness as a useful tool in integrated optics like sensing.

Figure 2.3

Scattering Losses in Waveguide Due to Rough Surfaces
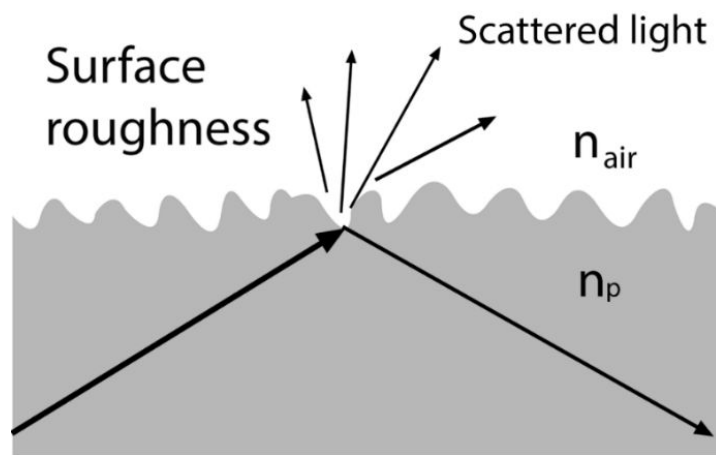
Note. n_p is the refractive index of the polymer material which is used for 3D printing of waveguide and n_{air} is the refractive index of the environment in which the waveguide is placed, most commonly air.

2.4.2 Surface Roughness in 3D Printed Waveguides

Like other fabrication techniques, SLA-based 3D printing also induces surface roughness on the printed components. The extent of surface roughness induced in an object printed by an SLA-based printer can be influenced by factors like the resolution of the printer, the thickness of each layer in the Z direction, minimum structural dimensions, the complexity of the design, and the type of polymer used (Vidakis et al., 2020). Among them the most important part is played by the thickness of each layer which comes because of slicing in the Z direction, hence at the juncture of every layer, there will be some gap that accounts for most of the surface roughness as shown in Figure 2.4. This is called the staircase effect (Xue & Fu, 2014) which is

mostly observed in surfaces with contours. How much roughness this juncture will create depends on the resolution of the printer as well as the type of photopolymer used (Hartcher-O'Brien et al., 2019). Printers having higher resolution combined with good curing ability of polymers can be crosslinked well and the extent of surface roughness can be lowered while having a poor resolution with poor curing ability cause products with high surface roughness and uneven surface finish.

Figure 2.4

Staircasing Effect in an SLA-based 3D Printer Which Leads to Surface Roughness in the Print and its Dependence on the Thickness of the Slicing Layer (Brooks et al., 2011)
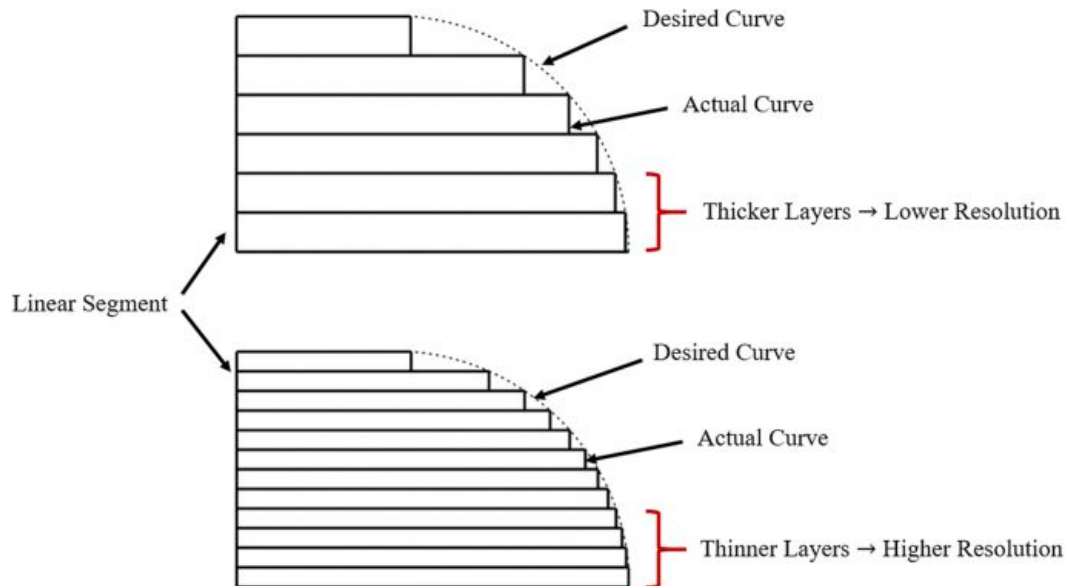
The main reason which leads to the formation of staircase, poor surface quality, and inaccuracies is due to the slicing process (Ravi, 2020). Mostly SLA-based 3D printers use a CAD model as a reference to print a structure that is being sliced by the printer's software. During slicing an algorithm is generated by the printer software that cuts the structure into a certain number of slices having equal thickness. Hence in this approach, the print that we get would be a precise approximation of the original CAD model but not the exact copy (Hällgren et al., 2016). So, there is a possible loss of

geometries if the design is complex with many contours and arches. This loss of geometry that happens in the Z direction due to slicing is called as staircase effect. Researchers have solved this problem by adjusting the slicing process by either reducing the thickness of the sliced layer or slicing a structure with a mathematically calculated model (Ahamed et al., 2016). Reducing the staircase leads to lesser surface roughness and high finishing in the printed product.

2.4.3 Role of Cladding in Reducing Surface Scattering Loss

Cladding layer has been applied to optical fibers and waveguides for better light confinement and to improve guided light transmission. It has been already explained previously that whatever method and material that we choose to fabricate waveguides there will always be some surface roughness that would lead to surface scattering losses. Because of this optical signal is both attenuated and distorted (Maradudin & Mendez, 2007). The output that we get is weak and at times it degrades beyond an acceptable level. To solve this problem, a thin layer of cladding material whose refractive index is smaller than the waveguide material (Addanki et al., 2018) but higher than the air or the environment of the waveguide is applied as shown in Figure 2.5. The cladding layer causes light to remain confined in the core of the waveguide by reducing the forward scattering and increasing the backward scattering at the boundary between the two (Suzuki et al., 2018).

Figure 2.5

Role of Cladding Layer in Reducing Optical Losses in Waveguides
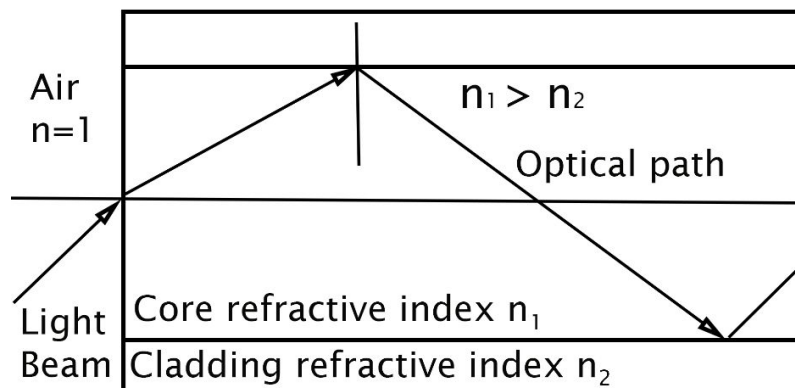
The light that was earlier getting wasted due to the interaction between waveguide-air boundary is now confined in the waveguide which adds in optical signal gain. Another important reason for the use of cladding in optical transmission is to utilize the advantage of total internal reflection (Mahoney et al., 2020). During propagation, light tends to bend outwards from normal when it travels from high refractive index medium to low refractive index medium. When the refracted angle exceeds the critical angle, the light ray reflects into the core of the waveguide and this principle is called total internal reflection. Therefore, the refractive index of the cladding materials for waveguides is kept lower in comparison to the core (Sinchenko et al., 2013). At present, there are a variety of materials like silica, glass, and quartz being used for cladding but with increasing usage of polymer in optics, the next section explores the potential usage of polymers as a cladding material.

2.4.4 Application of Polymers as Cladding Material

In recent times application of polymers has been widely increased in the field of light transmission. Polymers have replaced the traditional glass and silica-based optical fibers and polymer optical fibers (POF) are being frequently used for optical signal transmission. POF can demonstrate high flexibility and other physical properties that include high bending strength, fracture toughness, elastic strain, potential negative thermo-optic coefficients (Beckers et al., 2017). Also, by doping or adding different functional groups optical properties of the polymer can be modified to exhibit a range of lower refractive indices compared to the optical core of the waveguide or optical fiber contributed to the extensive use of polymers for cladding applications (Stajanca et al., 2018). The ease in handling, simpler fabrication process, and low cost make polymers a favorable choice as a cladding material over traditional material like silica or quartz (Cennamo et al., 2021).

Certain polymers can be doped with nanomaterials such as silica nanoparticles and quantum dots (C. Y. Yu et al., 2007) which further improves optical transmission by reducing scattering and reflection losses in the waveguide. However, with many benefits polymers have certain limitations as well. At times, the waveguides are used for a certain specific application like high temperature or in corrosive environments, which limits the usage of polymers as cladding materials. The glass transition temperature (T_g) of common polymers like PVC, PMMA, etc. is around 100 °C which

does not allow these polymers to function properly at high temperatures (Abiad et al., 2009).

Typically, polymers used for cladding are acrylic polymers, silicones, polyimides, polyether, and polyurethanes which can go structural changes when high temperature is applied which can affect optical transmission through the waveguide (Uyor et al., 2020). Also, a corrosive environment that may include alkanes, toluene or chloroform can dissolve the polymers like PMMA as these polymers have very high solubility for these solvents (Evchuk et al., 2005). In this situation, the polymer structure will be disturbed and will affect the optical transmission through the waveguide. Even though polymers suffer from these problems, research is going on to improve their performance by cross-linking, using different copolymers, fluorination, and doping but we are aware that this is a long way to go.

2.5 Solvent Absorption by Polymers

The absorption of a solvent by a polymer matrix can be described by Flory-Huggin's theory. When a solvent encounters the polymer, whether the solvent molecule would be diffused inside the polymer matrix or not will depend on the change in free energy of mixing of this process which is denoted as ΔG_{mix}. For a solvent-polymer combination if the $\Delta G_m < 0$, the solvent will always be absorbed by the polymer matrix (Brinke, 2012). The derived equation (Bussamra et al., 2021) for ΔG_{mix} is presented in Eq. (2.1) and it shows that ΔG_{mix} depends on the number of moles of solvent (n_1) and polymer (n_2), the volume fractions of solvent (f_1), and polymer (f_2), and the polymer-solvent interaction parameter (χ). For crosslinked polymer networks, the term $n_2 ln f_2$ approximated as 0 considering that fully crosslinked networks are essentially made up of one molecule (Sudhakar et al., 2018), hence Eq. (2.1) can be further modified to Eq. (2.2)

$$\Delta G_{mix} = RT(n_1 ln f_1 + n_2 ln f_2 + \chi n_1 f_2) \tag{2.1}$$

$$\Delta G_{mix} = RT(n_1 ln f_1 + \chi n_1 f_2) \tag{2.2}$$

From Eq. (2.2), if the moles and volume fraction of solvent and polymers are kept constant and the temperature remains the same, it is the interaction parameter on which ΔG_{mix} will be depending. The value of the interaction parameter depends on the difference between the solubility parameters of the polymer and the solvent ($\delta_p - \delta_s$)

(Tian et al., 2019). The solubility parameter is a numerical value associated with the relative solvency behavior of a substance mostly used for solvent and polymers. In 1936 Joel H. Hildebrand proposed the square root of the cohesive energy density as a numerical value indicating the solvency behavior of a solvent (Roughton et al., 2011). In 1950, the term solubility parameter was specified for this value and symbolized by δ (values for some common solvents are presented in Table 2.2). Eq. (2.2) shows that the lower value of χ is preferred to keep ΔG_{mix} as low as possible, hence it can be said that the solubility parameters of polymer and solvent (δp and δs) should be as close as possible (Jankovic et al., 2019) such that difference, δp - δs should be close to 0 or χ ≈ 0. From this, an inference can be drawn that if a solvent has a solubility parameter close to the given polymer, more likely it will be absorbed by the polymer.

Table 2.2

Solubility Parameter of some Common Solvents and Polymers (Novo & Curvelo, 2019)

Solvent	Solubility Parameter ($MPa^{1/2}$)	Polymer	Solubility Parameter ($MPa^{1/2}$)
DI water	48.0	PMMA	19.0
Ethanol	26.2	PET	20.5
Methanol	29.7	PVA	18.05
Isopropanol	23.8	PCS	20.3
Glycerol	36.2	PVC	19.6

2.6 Swelling of Polymer and Change in Refractive Index

It is already explained that polymer chains have empty spaces which get filled by the solvent molecules due to mutual diffusion. When solvent acquires the available space inside the polymer matrix, the new state of this solvent absorbed layer becomes different from the rest of the dry polymer. This new state of polymer is called swelled

polymer and the depth up to which solvent molecules penetrate polymer is called the swelling layer. It is found that due to the absorption of the solvent, polymers also reflect a change in their physical state that included an increase in the volume and mass (Tokmachev et al., 2017) of the polymer. Due to the presence of solvent inside the swelling layer the physical characteristic of the polymer-like appearance, transparency and color also change (Koziara et al., 2016). This can be utilized to visibly inspect and judge whether the polymer is swelled or not.

The Homogeneity of this swelling layer depends on the miscibility between the given polymer and the solvent (Marcombe et al., 2010). If a solvent has a strong affinity towards a given polymer, it would be able to diffuse inside the polymer matrix in a homogenous fashion (Kozanecki et al., 2016) which will result in a more continuous swelling layer but if the solvent has a poor affinity towards the polymer the swelling response will be weaker at times without absorbing any solvent at all. This swelling process is reversible in nature (Cimadoro & Goyanes, 2020) and it was found that solvent molecules leave the polymer due to the application of an external process like drying or heating (T. Sakai et al., 2012). Hence after the removal of solvent molecules, if the polymer can show its previous properties like in the dry state, the polymer can be said de-swelled (T. Sakai, 2020). This reversibility of the polymeric swelling process gives us more flexibility with application-based sensing applications and the polymer sensor can be retained after usage.

The effective refractive index of the solvent-polymer swelling layer can be calculated using the effective medium theory (EMT) (Kappert et al., 2019). Since the polymer absorbs the solvent, it acts as a host matrix and the solvent acts as inclusion and the net refractive index of the polymer-solvent swelling layer can be calculated as shown in Eq. (2.3). Where n_{sol}, n_{sw}, and n_p are the refractive indices of the solvent, swelled polymer matrix, and original polymer, Vf_{sol} is the volume fraction of the solvent in the swelled polymer matrix. An example of the refractive index of the swelled methacrylate-based polymer with common solvents like methanol, ethanol, and isopropanol is shown in Figure 2.6 and refractive indices of some common solvents are presented in Table 2.3.

$$n_{sw} = Vf_{sol}n_{sol} + (1 - Vf_{sol})n_p \qquad (2.3)$$

Figure 2.6

Variation in Effective Refractive Index of the Swelled PMMA Matrix Corresponding to Change in the Volume Fraction of the Solvent for Methanol, Ethanol, and Isopropanol
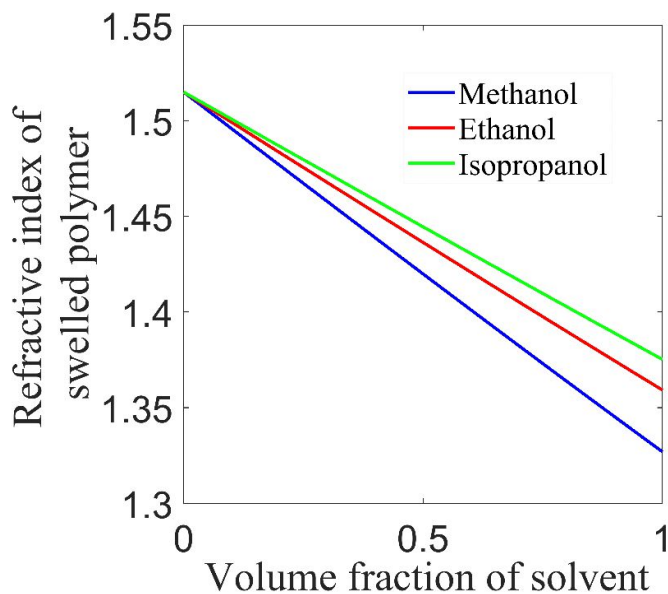
Table 2.3

Refractive Indices of Some Common Solvents at 632nm (Sudarsan, 2012)

Sr. No	Solvent	Refractive Index
1.	DI water	1.33
2.	Methanol	1.3264
3.	Ethanol	1.3604
4.	Isopropanol	1.3752
5.	Glycerol	1.4707

From this, it can be observed that the refractive index of swelled polymer matrix due to solvent absorption depends on the refractive index of the polymer, solvent, and

volume fraction of the solvent. For the same polymer and keeping the volume fraction of the solvent constant, it is found that the refractive index of the swelled polymer matrix decreases when the refractive index of the solvent is lowered (Ogieglo et al., 2015). For example, since the refractive index of methanol is lower than ethanol, then at the same volume fraction, the refractive index of a swelled polymer layer with absorbed methanol is lower than ethanol absorbed swelled polymer layer. Also, with an increase in the volume fraction of the solvent, the refractive index of the swelled polymer further decreases.

2.7 Effect of Swelling on Light Transmission in Polymer Waveguide

Due to the change in the refractive index of the polymer because of the swelling, it is natural to consider that there will be some change in the light transmission through the polymer waveguide (Kazakov, 2012). Since swelling occurs mostly on the surface of the polymer structure as solvent molecules diffused more in the surface in comparison to the deep core (Marcon & van der Vegt, 2014) it is safe to assume that in this condition the core and surface of the waveguide might be having relatively different refractive indices. Hence, there is a strong possibility that the newly formed swelling layer may be able to act as cladding and the propagated light inside the waveguide, interacts with this swelling layer rather than the rough surface of the polymer waveguide as shown in Figure 2.7. This idea can be related to a humidity sensor that uses a plastic optical fiber (POF) with PVA and PMMA as cladding material (Harith et al., 2019).

The working approach of this sensor relies on the refractive index of the cladding material and the change in scattering happens due to the absorption of environmental humidity. In another research, it was found that the main principle of humidity sensor utilizes the change of surface scattering in the cladding deposited on a POF which changes with increasing moisture absorption which further affects transmitted optical power through the sensor (Hu et al., 2020). In another humidity sensing application, a cladding material which is a hydrogel coating based on poly-dimethyl-acrylamide (PDMAA) is used to detect a change in the optical signals due to moisture absorption by the cladding material (Kelb et al., 2017). In a polymer optical fiber Bragg grating (POFBG) (Lu et al., 2009), it was found that because of fiber swelling induced by the atmospheric humidity there was a change in the wavelength spectrum. Hence it is

justified to expect that the optical transmission through a polymeric waveguide, 3D printed from a hydrophilic polymer can be affected by the polymeric swelling which has the potential to lower surface scattering.

Figure 2.7

A Possible Depiction of Swelling Layer Acting as Cladding Leads to Reduction in Surface Scattering Losses
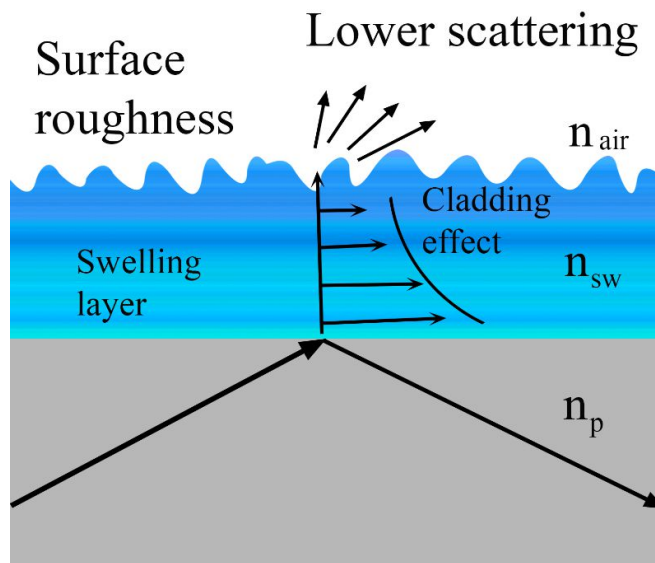
Note. n_p is the refractive index of the polymer material which is used for 3D printing of waveguide, n_{sw} is the refractive index of the swelling layer due to absorption of solvent molecules by dry polymer, and n_{air} is the refractive index of the environment in which the waveguide is placed, most commonly air.

2.8 Effect of Temperature on the Physical Properties of Polymers

Polymers are long-chain molecules that are crosslinked with each other, hence with the application of temperature, it is natural for these bonds to undergo certain transformations which would result in the change of chemical and physical properties. The effect of temperature on the shear and tensile strength of polymeric materials has been fairly reported over the years (Reis, 2012). Research has been conducted to report the thermal degradation of polymeric composites (Witkowski et al., 2016) in thermoset polymers. Any continuous fluctuation of temperature within a range of 20

°C to 80 °C can lead to heat distortions (Liang, 2013) which can further reduce the lifetime of the material. The behavior of a polymeric material under different temperatures is an important factor to be considered while using a polymer for any application as it can affect the overall performance of the respective system. Recommended working temperature of common polymers has a limit of 60 °C to 250 °C while for glasses it can vary from 400 °C to 700 °C.

Polymeric materials are viscoelastic in nature and due to their sensitivity towards high-temperature problems like creep and thermal fatigue occur in the structure (Alothman et al., 2014). Common Polymers like PMMA and PC exhibits glass-transition temperature (T_g) where individual polymer chains of the cross-linked polymer become reasonably mobile at the molecular level (Xie et al., 2020) and start to behave more independently than the entire rigid structure. This event can also be observed as softening of the polymer, and for fabrication purposes, polymer material loses many of its natural physical properties (Kawaguchi et al., 2014). Studies have been conducted on epoxies and unsaturated polyester (Plushchik & Aniskevich, 2000) under different temperatures to evaluate their mechanical performance. It was found that after the limit of 60 °C, the flexural and compressive strength of the polymer decreases sharply as temperature increases, and at higher temperatures, a loss of more than 50 % was observed.

2.8.1 Thermo-Optical Property of Polymers

Since temperature affects the structural properties of the polymers, it is natural that it would also affect the optical properties of the polymers. While applying temperature, it was found that the coefficient of thermal expansion for polyacrylic has an average value of 7×10^{-5} K^{-1} (Wang et al., 2012) while for the N-BK7 glass it is 0.71×10^{-5} K^{-1}, which shows polymers expands much faster due to the application of temperature. It is found that the basic optical property of polymers i.e., the refractive index also changes with temperature (Konopelnik et al., 2005) and it is called the thermo-optic coefficient of polymers. This corresponds to the variation in refractive index with temperature and donated by dn/dt. The thermo-optic coefficient of polymers depends on two factors: (1) the change in density caused by the coefficient of thermal expansion and (2) the increase in polarizability with temperature change (Trenti et al., 2018).

The values of dn/dt of polymer materials are generally larger in comparison to optical glasses (M. F. Hossain et al., 2010) which means polymers are more optically sensitive to temperature in comparison to glasses. Since polymers have a larger thermo-optic coefficient, any variation in temperature would be affecting light transmission through an optical component (Zhang et al., 2006) and the overall performance of the optical system. Since the measurement of thermo-optical coefficient requires precise equipment and sophisticated technology, and complex sample preparation it makes the process difficult (Wietzke et al., 2011).

In a noteworthy research, a polymer-based fiber Bragg grating (FBG) based sensor is fabricated to detect the change in the temperature of the surrounding (Sidhu et al., 2019). This sensor utilizes the thermo-optic properties of the given polymeric material, where a change in the refractive index of the polymer grating due to a change in the temperature results in the change of the peak wavelength. In another research, a polymer-based fiber interferometer is fabricated (Lian et al., 2020) that utilizes large thermo-optical and thermal expansion coefficients of the polymer material to show high sensitivity towards change in the surrounding temperature. Optical simulations (Suar et al., 2020) have also shown a decrement in normalized optical power through a PMMA waveguide when the temperature of the surroundings increases. These researches are significant and show that the optical properties of the polymers are significantly affected by the variation in their ambient temperature

2.9 Chapter Summary

This chapter focuses on the research works that have been previously done but more importantly, it helps to identify the research gaps that will be answered in this doctoral study. Swelling of polymers has been reported previously but its effect on light transmission through a polymer waveguide has not been categorically reported. Swelling of polymers is affected by mutual diffusion between polymer and solvent, but the optical transmission through a waveguide generally depends on the refractive index, hence it is very crucial to identify that in the case of a polymer waveguide, what will be the dominating factor that would affect the light transmission through a polymer-based waveguide. To use photopolymers for practical applications in integrated optics like developing an optical sensor, it is required to understand how

the given photopolymer would respond when interacting with different analytes or solvents.

Also, there is a need to develop a theoretical model that can illustrate the swelled polymer layer as a natural cladding for a polymer-based waveguide and how it affects light transmission through the waveguide. Available models either depict swelling in a polymeric system or surface scattering losses in the regular waveguide but do not demonstrate their combined effect. Similarly, the effect of temperature on the optical properties of the polymeric materials has been reported but how exactly a polymer waveguide would perform with the change in its surrounding temperature has not been reported. How modification of polymer material by addition of nanoparticles would affect the performance of a polymer waveguide has not been studied. These gaps in previous research served as motivation to undertake this doctoral research work.

CHAPTER 3
METHODOLOGY

In this chapter steps and methods that have been employed to conduct this research work are presented. This includes the development of a theoretical model for the solvent-methacrylate-based photopolymer waveguide interaction, characterization methods to analyze properties of the methacrylate-based photopolymer, 3D printing of methacrylate-based photopolymer waveguides, followed by physical experiments to verify the theoretical model. Physical testing includes testing of methacrylate-based photopolymer waveguide with different solvents, testing at different temperatures, synthesis of gold nanoparticles, and embedding them in the methacrylate-based photopolymer waveguide. Further gold nanoparticles embedded methacrylate-based photopolymer waveguide was subjected to repeated temperature testing to study its optical stability and was compared with methacrylate-based photopolymers waveguide without gold nanoparticles.

3.1 Theoretical Model for Solvent and Methacrylate-based Photopolymer Waveguide Interaction

A first-order theoretical model was derived to study the solvent and methacrylate-based photopolymer waveguide interactions. The model considers the formation of a swelling layer due to the absorption of solvent molecules in the polymer matrix and its potential use as a natural cladding layer in reducing surface scattering losses. The first-order model also assumes adsorption or diffusion of the solvent in the polymer matrix in one direction only increasing the thickness of the waveguide by swelling effect and does not consider the diffusion in other directions.

First, the thickness of the swelling layer (d_t) was estimated using Eq. (3.1), which depends primarily on the mutual diffusion coefficient (D_m) between a polymer and a solvent at any time (t).

$$d_t = \sqrt{D_m t} \tag{3.1}$$

Then, considering short-time Fickian diffusion in only one direction (along with the thickness) of the waveguide, the mass of the solvent absorbed by the polymer matrix at any time (t) is defined using Eq. (3.2).

28

$$(M_t/M_s) = (d_t/T_t) \tag{3.2}$$

Where M_t is the absorbed mass of the solvent at any time (t), M_s is the maximum possible mass of solvent that the waveguide can absorb, and T_t is the total thickness of the methacrylate-based photopolymer waveguide. T_t, therefore, also represents the maximum thickness up to which solvent molecules can diffuse inside the methacrylate-based photopolymer waveguide. Assuming that the density of the solvent remains constant during the swelling process, dividing mass with the density of the solvent in Eq. (3.2) and substituting d_t from Eq. (3.1), Eq. (3.2) can be rewritten as:

$$(M_t/M_s) = (V_t/V_s) = \sqrt{D_m t}/T_t \qquad \text{or}$$

$$V_t = V_s(\sqrt{D_m t}/T_t) \tag{3.3}$$

where V_t is the absorbed volume of solvent at any time (t) and V_s is the maximum possible volume of solvent that the waveguide can absorb. It is assumed here that the maximum possible volume of the solvent absorbed by the methacrylate-based photopolymer waveguide cannot be more than the total volume of the waveguide. Hence in the theoretical calculation, V_s is taken as the total volume of the given waveguide.

The Value of D_m was calculated using Eq. (3.4), where the diffusion coefficient at a given temperature (T) between a given polymer-solvent pair is expressed, where A is a pre-exponential factor and B is the rate constant.

$$D_m = Ae^{-B/T} \tag{3.4}$$

The diffusion of solvent molecules in the polymer matrix results in swelling of the polymer leading to guided mode transmission in the methacrylate-based photopolymer waveguide producing a cladding effect. To explore this, a lower order guided mode was considered having a propagation constant β which varies close to $k_0 n_{poly}$ (where $k_0 = 2\pi/\lambda$ is the wavenumber in space or air in this case) and n_{poly} is the refractive index of the polymer. The attenuation coefficient (κ) of the guided light can be therefore approximated as,

$$\kappa \approx k_o \sqrt{n_{poly}^2 - n_{sw}^2} = (2\pi/\lambda)\sqrt{n_{poly}^2 - n_{sw}^2} \tag{3.5}$$

where, n_{sw} is the refractive index of the newly formed swelled layer, which can be calculated using effective medium theory, as shown in Eq. (3.6).

$$n_{sw} = Vf_{sol}n_{sol} + (1 - Vf_{sol})n_{poly} \tag{3.6}$$

where, n_{sol} is the refractive index of the solvent and Vf_{sol} is the volume fraction of the solvent in the solvent-polymer matrix. Considering V_{poly} as the volume of the polymer matrix, Vf_{sol} can be obtained as,

$$Vf_{sol} = V_t/(V_t + V_{poly}) \tag{3.7}$$

Therefore, Eq. (3.5) can be rewritten as,

$$\kappa = (2\pi/\lambda)\sqrt{n_{poly}^2 - (Vf_{sol}n_{sol} + (1 - Vf_{sol})n_{poly})^2} \tag{3.8}$$

The strength of the evanescent wave at the surface of the waveguide in terms of the electric field component (E_0) of the propagating light, which is a function of the thickness of the swelled layer that varies with time, is then expressed as

$$E(d) = E_0 \, e^{-\kappa d(t)} \tag{3.9}$$

The scattering coefficient mostly depends on the difference in permittivity between the swelled layer and the superstrate ($\Delta\varepsilon$, region above waveguide) and the mode propagation constant β and can be written as $\Psi_{scat}(\beta, \Delta\varepsilon)$. Here, we assumed that the leakage is happening only due to the forward scattering from the rough waveguide surface, where E_{scat} is the scattered (or lost) field which can be estimated as

$$E_{scat} = E_o \, e^{-\kappa d(t)} e^{-\psi_{scat}(\beta, \Delta\varepsilon)} \tag{3.10}$$

Converting the electric field components to power terms, Eq. (3.10) was then used to estimate the guided optical power (P_{guid}) transmitted through the waveguide which is simply given by the difference between the total power (P_0) and the scattered power (obtained from Eq. (3.10)), is shown in Eq. (3.11).

$$P_{guid} = P_o[1 - e^{-2\kappa d(t)} e^{-2\psi_{scat}(\beta,\Delta\varepsilon)}] \qquad\qquad (3.11)$$

3.2 Characterization of the Methacrylate-based Photopolymer

For the experimental design, we used a commercially available photopolymer Px8880 (hex-polymer brand) which is a transparent methacrylate-based photopolymer and used the SLA-based 3D printing technique to print waveguides. The basic properties of the Px8880 photopolymer are listed in Table 3.1. Recommended curing wavelength range for this methacrylate-based photopolymer is 365 nm-420 nm and the minimum thickness for the SLA-based 3D printing machine is 25 μm, which depends on the resolution of the 3D printer and complexity of the intended design. Two characterization methods (1) UV-Vis spectroscopy and (2) liquid contact angle measurements are performed on the photopolymer to investigate their optical and surface wetting properties.

Table 3.1

Basic Properties of Px8880 Photopolymer

Sr. No	Photopolymer Property	Value
1.	Polymer type	Acrylate base
2.	Curing Wavelength	365-420 nm
3.	Shore hardness	85 D
4.	Viscosity	500 cps
5.	Color	Clear or Transparent

3.2.1 UV-Vis Absorbance Spectroscopy

A UV-Vis spectrophotometer (Make: Ocean Optics, Model: USB4000) was used to study the optical absorption of the Px8880 photopolymer. The light source that was used is a combination of a deuterium lamp (for UV region) and a halogen lamp (for visible). First, a blank cuvette was used to set the reference, and then a similar cuvette filled with the methacrylate-based photopolymer was used for recording absorbance by the spectrophotometer. This experiment was performed to get two important pieces

of information, first, the wavelength that photopolymer absorbs strongly to identify the correct light band where the methacrylate-based photopolymer will be cured during 3D printing, and second the wavelength range in which the methacrylate-based photopolymer does not absorb light to identify the wavelength band that can transmit through the methacrylate-based photopolymer waveguide without getting significant attenuation.

3.2.2 Contact Angle Measurement

To check the surface wetting behavior of the given methacrylate-based photopolymer contact angle (CA) measurements with three solvents DI water, isopropanol, and glycerol were performed on the methacrylate-based photopolymer using the sessile drop method as shown in Figure 3.1. First, a thin layer of photopolymer was coated on clean regular microscopic glass slides using the spin-coating method. These glass slides after spin-coating were cured under UV light (wavelength: 370 nm) to complete the crosslinking and form a uniform solid surface. A 5μL volume of solvent was dropped on the methacrylate-based photopolymer film and CA was measured using a goniometer (C60 drop shape analysis system) that utilizes a high-resolution camera to capture the profile of the solvent drop on the photopolymer surface.

Figure 3.1

Contact Angle Measurement Setup for Methacrylate-based Photopolymer Films
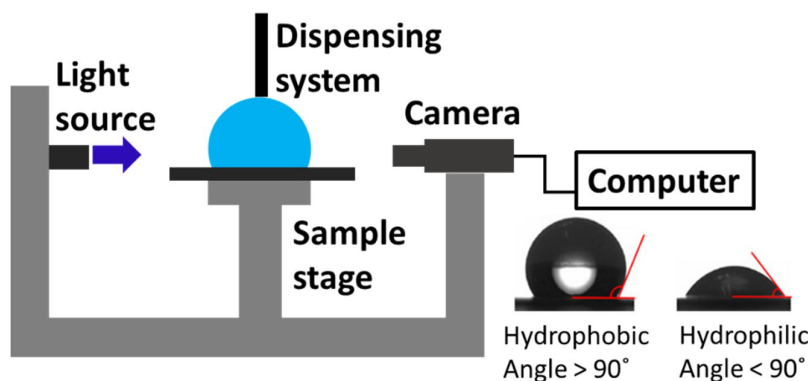
From the profile of the drop, the inbuilt software of the goniometer calculates the contact angle made by the solvent at the solid/liquid/gas interface by putting tangent

on the solvent drop with respect to the photopolymer surface. 10 CA readings were recorded from different locations of the methacrylate-based photopolymer film, and the averaged value of the CA was calculated from these individual readings. Finally, the average CA value is reported in the result section with measurement standard deviation.

3.3 Waveguide Design for 3D Printing

Waveguide structure was designed using 123 design software that converts designed CAD file into STL file, the format which is supported by SLA 3D printer. The basic dimensions of the waveguide are 700 μm high, 500 μm wide and 20,000 μm in length. The waveguide was placed on a support with a reduced width of 250 μm as shown in Figure 3.2. The thinner support ensures less leakage of light from the waveguide to the substrate by confining the light more into the waveguide.

Figure 3.2

Design of Waveguide (a) Side View (b) Top View
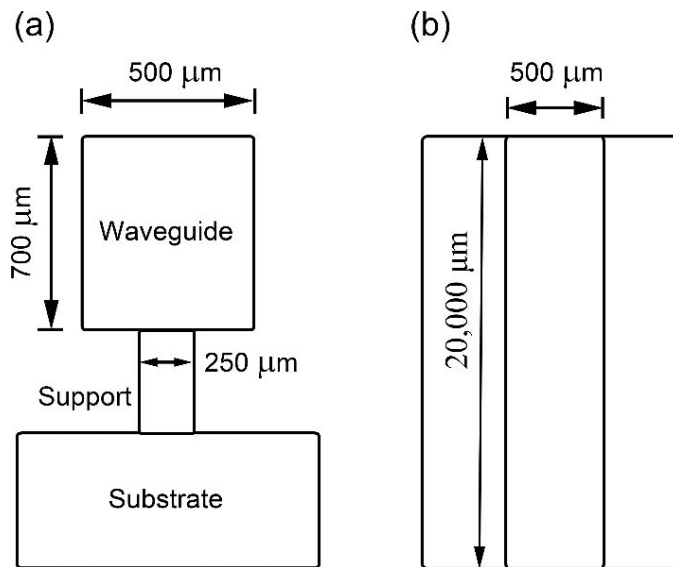
3.4 Methacrylate-based Photopolymer Waveguide Fabrication using SLA-based 3D Printing

The entire waveguide structure was fabricated using an SLA-based 3D printer (Duplicator 7, Wanhao Make). This 3D printer uses an upside-down 3D printing

configuration. The generated STL file was uploaded in the printer software which generates G-codes, and the inbuilt microcontroller of the 3D printer read these G-codes to carry out the 3D printing process. A 50 µm thickness of each layer for the slicing process for the 3D printing process was chosen. Details of the 3D printing process are presented in Table 3.2.

Table 3.2

Details of 3D Printing Process used in this Study

Sr. No	Characteristics	Description
1.	Printer type	SLA
2.	Make	Duplicator 7 by Wanhao
3.	Thickness of slicing layer	50 µm
4.	Printing time	4 hours 15 minutes
5.	Printing style	Upside-down
6.	Post curing time	30 minutes under UV light
7.	Format of CAD file	STL

After 3D printing, post-curing of the structure was performed using the conditions recommended by the resin manufacturer. First, the waveguide was cleaned in isopropanol and rinsed in DI water to remove any unwanted impurities at the surface, and dried using an air blower. After cleaning, the printed waveguide was further cured for 30 minutes under a UV lamp (wavelength 370 nm) to complete the crosslinking of the methacrylate-based photopolymer which imparts strength and helps in achieving full mechanical properties of the photopolymer.

3.5 Testing of Solvent and Methacrylate-based Photopolymer Waveguide Interactions

After 3D printing of the waveguide, they were tested with solvents to physically observe the effect of solvent and methacrylate-based photopolymer interaction on the optical transmission of the waveguide. The main purpose of this experiment was to

account for two important things: (1) verification of the theoretical model that was presented in the previous section 3.1, and (2) to understand optically, what is the dominating factor in the methacrylate-based photopolymer waveguide and solvent interactions, is it the mutual diffusion coefficient between the solvent and methacrylate-based photopolymer or the refractive indices of the solvent and the methacrylate-based photopolymer.

3.5.1 Interaction with Solvent Vapor

First solvents with different refractive indices were physically tested with a 3D printed waveguide for possible optical gain. The solvents chosen for this study are methanol and ethanol having distinct refractive indices at 650 nm of wavelength. A testing chamber of inner dimensions 40 mm in length, 25 mm in width, and 20 mm in height and thickness 5 mm was fabricated using a filament-based (PLA) 3D printer having openings to collect optical signals. Optical fibers were used to shine and collect light at the ends of the waveguide and the change in the transmitted optical power was recorded in an optical power meter (Make: Thor Labs, Model: PM100USB) at 650 nm wavelength. The inner volume of this chamber was designed in such a way that 1 µL of the solvent inside is equivalent to 50 ppm with respect to the chamber's volume. An opening as shown in Figure 3.3, was made in the chamber for solvent vapors to get released inside the chamber.

Figure 3.3

Schematic of Testing Methacrylate-based Photopolymer Waveguide Interaction with Solvent's Vapor to Observe Gain in the Optical Power
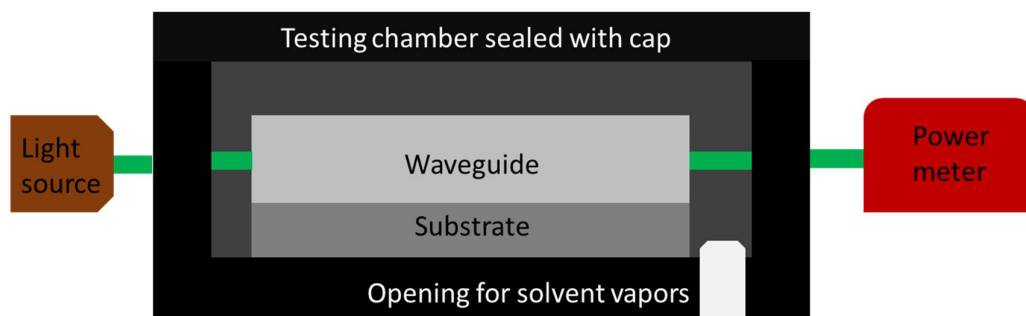
Solvents were used in vapor form to let the solvent interact with the entire waveguide inside the chamber, mimicking a natural atmosphere that any optically sensitive system should work with. Since both ethanol and methanol are highly volatile solvents that can present in the natural environment, using them in vapor form would also help us to understand the functioning of the waveguide if it might come in contact with volatile organic compounds (VOCs) present in the environment. The waveguide was placed smoothly at the center of the chamber and aligned with the path of the light source and the detector. Both solvents in 250 ppm quantity were used. The top of the testing chamber was sealed using a tight cap such that no solvent vapor could escape in the ambient environment. Once the saturation level of gain in the optical power was reached, the cap was removed, and the system was allowed to revert to its original conditions by releasing the solvent vapors.

3.5.2 Interaction with Liquid Solvent with Similar Refractive Indices

Next, the methacrylate-based photopolymer waveguide was tested with solvents keeping their refractive indices in a similar range. For this, two solvents isopropanol and glycerol were chosen, and they were diluted in DI water at different concertation in such a way that the refractive indices of the two sets remain in a similar range. For isopropanol samples, the concentration of isopropanol in DI water (v/v) was chosen as 20 %, 40 %, and 60 %, and corresponding refractive indices were observed as 1.346, 1.358, and 1.367 respectively. For glycerol samples, concertation of glycerol in DI water (v/v) was chosen as 10 %, 15 %, and 20 % and corresponding refractive indices were 1.349, 1.355, and 1.365 respectively. The reason for choosing isopropanol and glycerol for this study is the difference between their solubility parameters while keeping their respective indices in a similar range.

The data mentioned in the literature review section 2.5, Table 2.2 shows that the solubility parameter of isopropanol (23.8 MPa$^{1/2}$) is closer to PMMA (19.0 MPa$^{1/2}$) which is similar to the methacrylate-based photopolymer used in this research, while glycerol (36.2 MPa$^{1/2}$) and DI water (48.0 MPa$^{1/2}$) have a much higher value. Since the refractive indices were kept similar, any differences in the optical output of both sets of solvents would mainly be dominated by the solvent and methacrylate-based photopolymer mutual diffusion rather than their optical properties. A 25 μl quantity of the respective solvent was dropped on the waveguide as illustrated in Figure 3.4 and

transmitted optical power in the waveguide was recorded in an optical power meter (Make: Thor Labs, Model: PM100USB) at 650 nm wavelength. After the optical power was reached to saturation, the methacrylate-based photopolymer waveguide was cleaned and dried gently with an air blower. This process was repeated several times to check the repeatability of the optical output.

Figure 3.4

Schematic of Testing Methacrylate-based Photopolymer Waveguide with Liquid Solvents Having Similar Refractive Indices
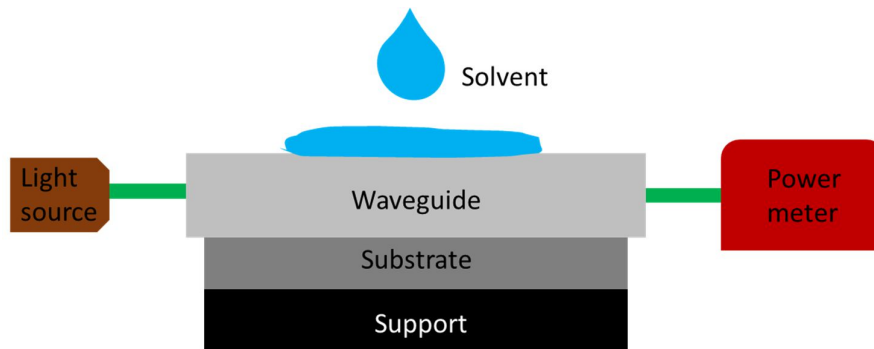
3.6 Testing of Methacrylate-based Photopolymer Waveguide- at Different Ambient Temperatures

After studying the effect of solvent absorption on the optical transmission of the photopolymer waveguide, the effects of temperature variation on the optical transmission were studied. It is already described in the literature review section (Chapter 2) that the refractive indices of common polymers vary with the change in temperature. Hence, an experiment was performed to check variation in the optical transmittance through the photopolymer waveguide due to the change in the surrounding temperature as shown in Figure 3.5. A 3D printed photopolymer waveguide was placed inside the testing chamber and connected with optical fiber cables for light input and output.

The change in the transmittance with respect to the change in the temperature chamber atmosphere controlled by a Peltier device (TEC1-12730) was recorded using a spectrophotometer (USB4000, Ocean Optics). A thermometer was placed inside the

testing chamber to measure the temperature variations in the chamber atmosphere. The top of the testing chamber was covered with an aluminum foil on which the Peltier plate was placed. The aluminum foil seals the testing chamber and provides uniform heating such that the heat generated by the Peltier plate uniformly dispatches to the entire testing chamber. A variable DC power was connected to the heating plate to change the temperature by varying voltage and current to the device.

Figure 3.5

Schematic of Testing Methacrylate-based Photopolymer Waveguide at Different Ambient Temperatures
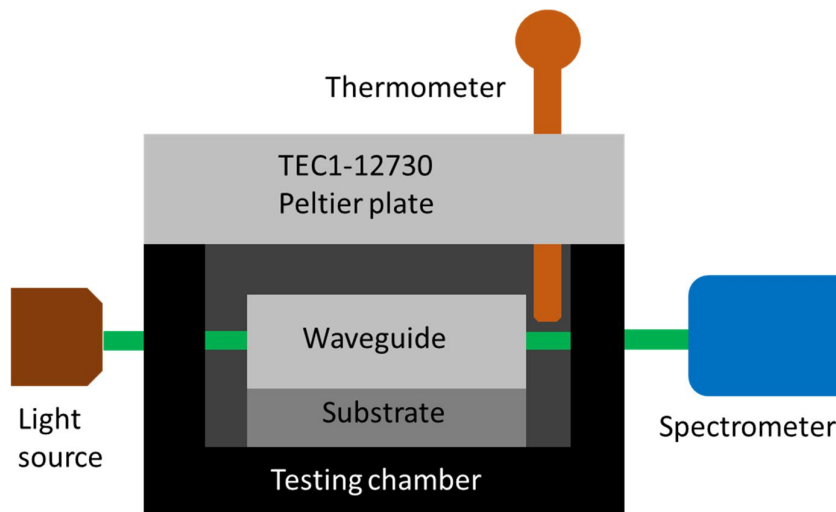
3.7 Fabrication of Gold Nanoparticles (Au-NP) Embedded Methacrylate-based Photopolymer Waveguide

Au-NP embedded waveguide was fabricated using the soft molding process as shown in Figure 3.6 and a detailed procedure is given below. Gold (Au) nanoparticles (NPs) were synthesized using the UV-light reduction method on zinc oxide (ZnO) nanorods as support and mixed uniformly with methacrylate-based photopolymer resin. This new photopolymer was used as a filler material for soft mold and by applying UV curing (wavelength: 370 nm) on Au-NP embedded methacrylate-based photopolymer, the waveguides were solidified. Fabricated waveguides were gently removed from the soft mold, rinsed with DI water, and stored in a cool dry place. Before pouring into

the mold, the resin was vacuum pumped in a dark chamber at room temperature for 30 minutes to remove air bubbles that got trapped in the resin during the mixing of the Au NPs. This way, it was made sure the Au-NP resin was free from air bubbles and other gaseous impurities. In this case, the soft molding process rather than 3D printing for the fabrication of Au-NP embedded waveguide was selected as the 3D printing happens in the ambient which would cause the absorption of environmental humidity in the waveguide. To avoid any absorption of humidity in the photopolymer structure of the waveguide soft molding was performed and humidity was sucked using a vacuum chamber. After fabrication, characterization of the waveguides was performed, and absorbance spectroscopy was measured.

Figure 3.6

Soft Molding Process for the Fabrication of Au-NP Embedded Waveguides (a) Fabrication of Master Mold in 3D Printer (b) Preparation of PDMS for Soft Molding (c) Curing of PDMS by Heating (d) Top View of Fabricated Soft Molds
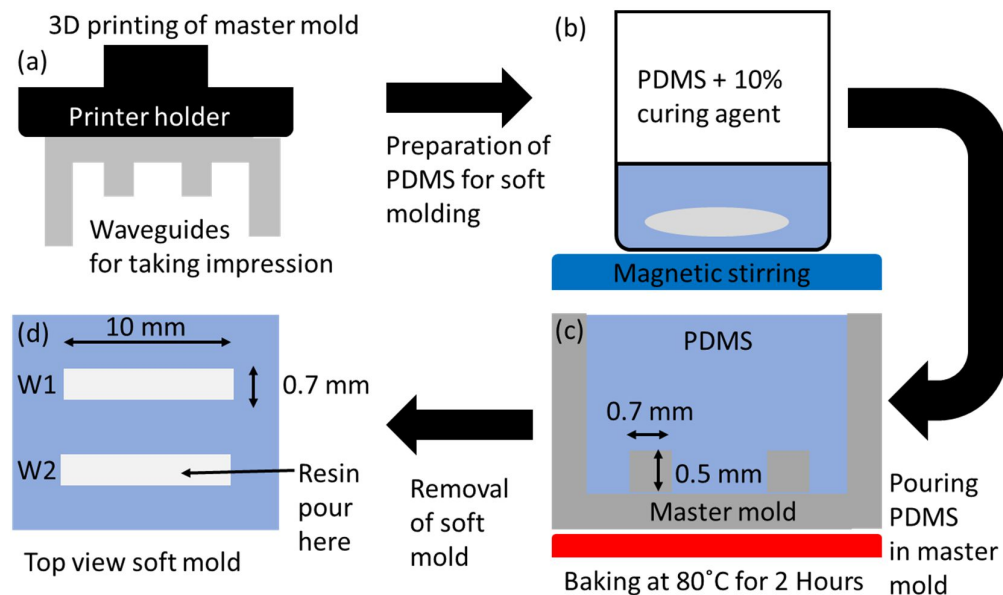
3.7.1 Fabrication of Soft Molds Using PDMS

A soft mold composed of polydimethylsiloxane (PDMS) was prepared to fabricate the Au-NP embedded photopolymer waveguide. To prepare the soft mold, a hard methacrylate photopolymer-based master mold was designed and fabricated using the

SLA-based 3D printing technique. The hard-master mold contains the exact replica of the waveguide with dimensions 10 mm x 0.7 mm x 0.5 mm (length x width x height). Here the crosssection of the waveguide (0.7 mm x 0.5 mm) was modified in comparison to the 3D printed waveguide (0.5 mm x 0.7 mm) for better filling of the Au-NP resin in the soft mold due to larger width and better curing due to smaller height. PDMS elastomer (Sylgard 184) was poured into the 3D printed master mold and baked for 2 Hours at 80 °C. Part A and part B of the PDMS elastomer were mixed with a ratio of 10:1 respectively. After 2 hours master mold was allowed to cool down to normal temperature and the soft PDMS mold was gently taken out and flushed with water to remove unused PDMS. The soft mold was then allowed to naturally dry for another 12 hours.

3.7.2 Synthesis of Au-NP and Au-NP Embedded Methacrylate-based Photopolymer

The Au-NP was prepared using UV reduction of chloroauric acid in the presence of ZnO nanorods as the catalyst. First regular microscopic glass slides were cleaned with acetone, followed by DI water, and thoroughly dried in an oven. 1 mM zinc acetate dihydrate solution in pure ethanol was prepared and sprayed gently on the glass side while keeping the temperature around 100 ˚C. After thoroughly coating glass sides it was annealed at 250 ˚C for 5 hours to obtain a uniform coating of tiny ZnO seeds on the glass substrate. Next, a 5 mM solution of hexamine and zinc nitrate hexahydrate was prepared in water. This solution acts as the growth solution for zinc oxide nanorods. Glass slides coated with ZnO seeds were placed in an upside-down position inside a petri-dish and submerged with 45 ml of the growth solution and sealed completely. The petri-dish was then placed in a microwave oven and run at light heating mode for 30 minutes (solution temperature ~90 °C).

After that the growth solution was drained, samples were cleaned thoroughly in DI water and the process was repeated for 4 more times. The samples finally were rinsed with an ample amount of DI water and annealed again at 350 °C for 1 hour. The resultant sample gave a uniform coating of ZnO nanorods on the glass substrate which was then used as catalyst and support for the Au NPs. Next gold nanoparticles were synthesized using reduction of chloroauric acid in UV-light having a wavelength of 370 nm. A 0.2 mM solution of chloroauric acid was prepared in 50 % ethanol and 50 % DI water. Glass substrates containing ZnO nanorods were submerged in 25 ml of

this solution under UV light (to promote the reduction of Au NPs) for 5 minutes and then annealed in an oven at 150 ˚C for 1 hour. This process was repeated 6 times and then samples were annealed at 350 ˚C for 1 hour in a furnace. The resultant sample produced Au-NPs decorated on the surface of the ZnO nanorods. A schematic of the synthesis of the Au-NP process is shown in Figure 3.7.

Figure 3.7

Synthesis of Gold Nanoparticles on Glass Slide (a) Spraying Seeding solution on Glass Slide (b) Hydro-thermal Growth of Zinc Oxide Nanorods (c) Synthesis of Gold Nanoparticles Using UV Light Reduction Method from Chloroauric Acid (d) Development of Gold Nanoparticles on Zinc Oxide Nanorods
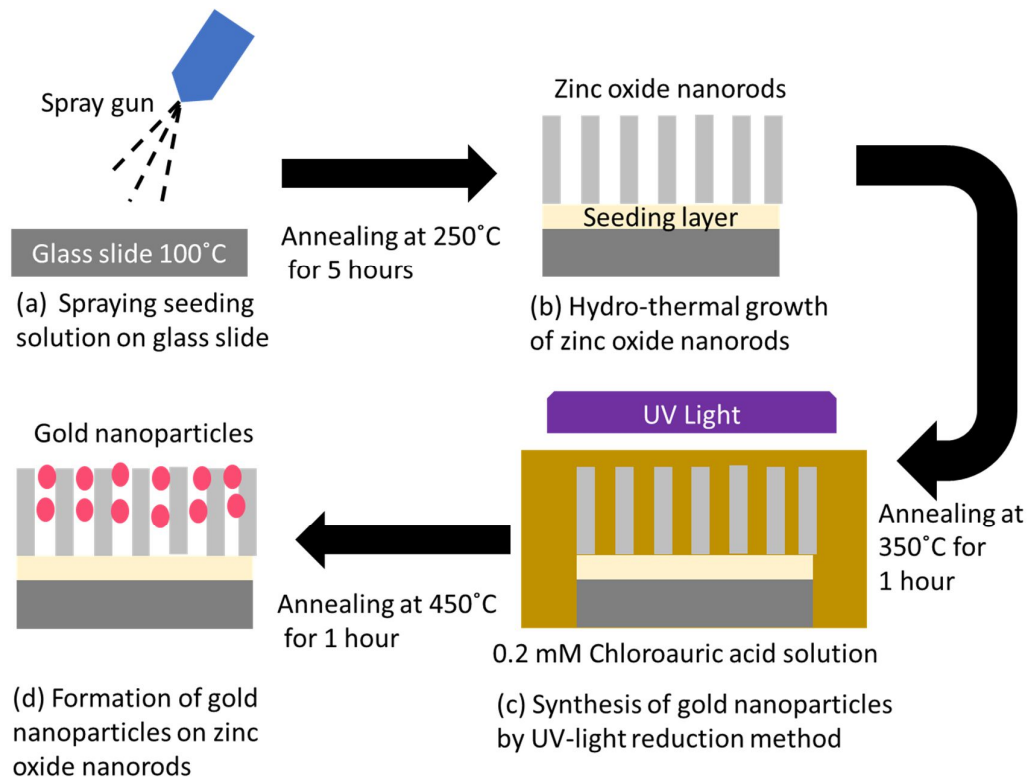
After synthesis, Au NPs decorated on ZnO were characterized using the following methods: 1. Energy Dispersive X-ray Spectroscopy (EDS) for elemental analysis (Oxford X-Max 20) 2. Field Emission Scanning Electron Microscope (FE-SEM) for ZnO and Au/ZnO surface morphology (JEOL JSM7800F) 3. UV/VIS Spectroscopy

for Absorbance Measurement of Au NPs (Ocean Optics USB4000). After characterization, gold nanoparticles were removed from the glass slides by gently scratching them and the powder obtained in this way was mixed uniformly with the methacrylate-based photopolymer to obtain the Au-NP embedded methacrylate-based photopolymer. The Au-NP embedded methacrylate-based photopolymer was then poured into the PDMS soft mold containing the negative replica of the waveguide and placed in a vacuum chamber to remove air bubbles from the mixture. Subsequently, the Au-NP embedded methacrylate-based photopolymer was cured under UV light (wavelength: 370 nm) for 2 hours to obtain the solid Au-NP embedded methacrylate-based photopolymer waveguide.

3.8 Effect of Temperature on the Optical Transmission through the Au-NP Embedded Waveguide

The effect of temperature on the optical transmission through the Au-NP embedded methacrylate-based photopolymer waveguide was studied using the same setup as described in section 3.6, Figure 3.5. First, the plain methacrylate-based photopolymer waveguide of similar dimensions was used as a reference to set the reference spectrum. Then the Au-NP embedded photopolymer waveguide was placed, and the transmittance spectrum was recorded in a spectrometer (Ocean Optics USB4000). Change in the optical transmittance due to change in the surrounding temperature was recorded and then repeatability test was performed in continuous cycles. During the repeatability experiment, first heating was provided to raise the temperature of the chamber, and then the system was cooled using the cooling effect of the Peltier plate by reversing the polarity of the DC power source.

The cyclic process of heating-cooling was continuously repeated for 20 cycles (or till the waveguide reaches a steady-state and is no longer affected by surrounding temperature). The transmittance spectrum was recorded continuously with respect to change in the temperature. This experiment helped to understand how thermo-optically stable the waveguide is when it undergoes repeated thermo-cyclic loading. This experiment was performed on both plain methacrylate-based photopolymer, and Au-NP embedded waveguides and their performances were compared to understand which waveguide is more stable and shows higher repeatability in optical signals. After recording the transmittance spectrum, in the case of Au-NP embedded

methacrylate-based photopolymer waveguide, the data was further analyzed to calculate the change in the peak height of the spectrum at different temperatures. The highest point and the lowest point on the transmittance spectrum were located and the difference in transmittance values was calculated as peak height at the given temperature. Later, experimental values of peak heights were compared with theoretical values to compare the trends shown by the results.

CHAPTER 4

RESULTS AND DISCUSSION

4.1. Theoretical Model to Study Solvent-Photopolymer Waveguide Interaction

In this section, a solution to solvent and methacrylate-based photopolymer waveguide interaction and its effect on the dynamic optical gain in the methacrylate-based photopolymer waveguide is presented. First, the thickness of the swelling layer due to the absorption of solvent in the methacrylate-based photopolymer waveguide is estimated. Then dynamic gain in optical power which occurred due to the reduction in surface scattering losses because of the developed swelling layer in the methacrylate-based photopolymer waveguide is presented.

4.1.1 Estimation of Thickness of the Swelling Layer

Polymeric swelling is the process where solvent molecules diffuse into the polymer matrix through a molecular motion which results in the absorption of the solvent in the polymer. The extent of swelling inside a polymer depends on the coefficient of mutual diffusion (D_m) between the polymer and the solvent. D_m is the relative factor between a solvent and a polymer and is different for different polymer-solvent combinations. The estimated thickness of the swelled layer (d_t) is the measure of how far the solvent molecules have penetrated inside the polymer matrix which depends on D_m and time (t). Considering short-time Fickian diffusion in only one side of the waveguide, the mass of the solvent absorbed by the polymer matrix at any time is presented in the equations in Chapter 3, section 3.1.

Swelling is a volumetric concept, but since here we have considered a first-order model, we have assumed that swelling in the other 2 directions (width and length) is negligible and absorption of solvent only increases the thickness of the polymer film in one direction only as shown in Figure 4.1. Value of D_m is then calculated using Eq. (3.4), where the mutual diffusion coefficient at a given temperature (T) between a given polymer-solvent pair shows how poly-methyl methacrylate (closest polymer to our methacrylate-based photopolymer) would interact with our chosen solvents: methanol and ethanol. The value of D_m at T = 298K is calculated and found to be 35.60×10^{-12} cm^2/s for methanol and 13.63×10^{-12} cm^2/s for ethanol. Using these values

thickness of the swelling layer for the given methacrylate-based photopolymer waveguide was calculated and results are presented in Figure 4.2.

Figure 4.1

Schematic Showing the Formation of Swelling Layer in the Methacrylate-based Photopolymer Waveguide due to Solvent Diffusion in Polymer Matrix
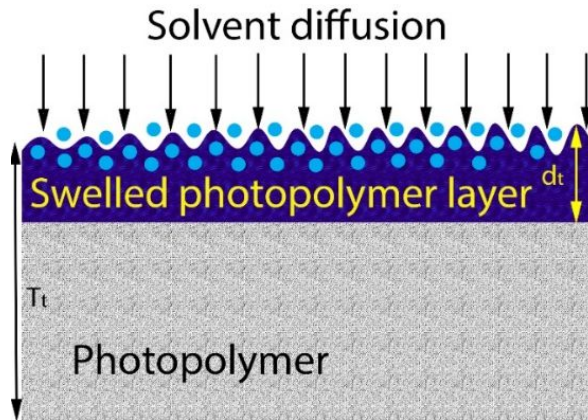
Figure 4.2

Theoretically Estimated Thickness of Swelling Layer for Poly-methyl Methacrylate (PMMA) with Methanol and Ethanol as Solvents
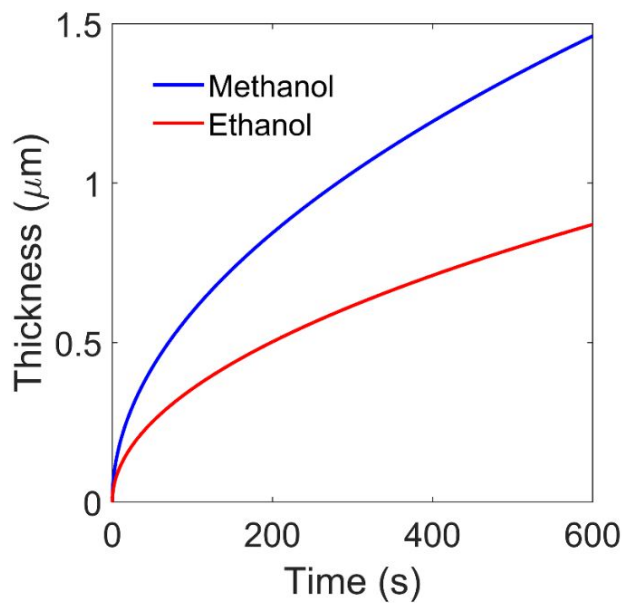
It can be observed that the thickness of the swelling layer increases with respect to time for both the solvents. The thickness of the swelling layer at a given time is higher in the case of methanol followed by ethanol which means methanol molecules can swell the polymer network more swiftly penetrating to a higher depth in comparison to ethanol. This is because methanol (35.60×10^{-12} cm^2/s) shows a higher coefficient of mutual diffusion for the methacrylate-based photopolymer in comparison to ethanol (13.63×10^{-12} cm^2/s). Due to a higher mutual diffusion, the polymer network accepts solvent molecules with less resistance. Therefore, the swelling effect produced by a solvent for the given methacrylate-based photopolymer depends on their coefficient of mutual diffusion, where a higher mutual diffusion will lead to a higher extent of swelling.

4.1.2 Gain in the Transmitted Power due to Swelling Layer

A first-order optical model that exploits the swelling layer as cladding and its effects in the reduction of surface scattering losses is used here to estimate the optical gain in the transmitted optical power through the waveguide before and after the swelling. A 3D printed methacrylate-based photopolymer waveguide typically has a considerable amount of surface roughness resulting in surface scattering of the transmitted light through the waveguide, as illustrated in Figure 4.3 (a). The formation of a swelling layer reduces the interaction of the light with the rough waveguide surface and rather light interacts more with the swelling layer which is more homogenous in comparison to the rough waveguide surface. This swelling layer has a new refractive index (n_{sw}) than the actual waveguide refractive index (n_{poly}) as shown in Figure 4.3 (b).

Formation of this swelled layer then results like a guided mode transmission in the methacrylate-based photopolymer waveguide and to explore this, a lower order guided mode is considered having a propagation constant β which would be very close to $k_o n_{poly}$ ($k_o = 2\pi/\lambda$ is the wavenumber in space or air in this case). The refractive index of the swelled layer (n_{sw}) is then calculated using effective medium theory as described in Chapter 3, section 3.1. Considering E_o as the electric field component of the propagating light, the strength of the evanescent wave (E_d) at the surface of the waveguide, which is a function of the thickness of the swelled layer (d_t) was determined. The scattering coefficient mostly depends on the difference in

permittivity ($\Delta\varepsilon$) between the swelled layer and the region above waveguide and the mode propagation constant β and can be written as $\psi_{scat}(\beta, \Delta\varepsilon)$ in the functional form.

Figure 4.3

Surface Scattering Losses in 3D Printed Waveguide (a) Before Swelling and (b) After Swelling due to the Solvent Diffusion into the Methacrylate-based Photopolymer
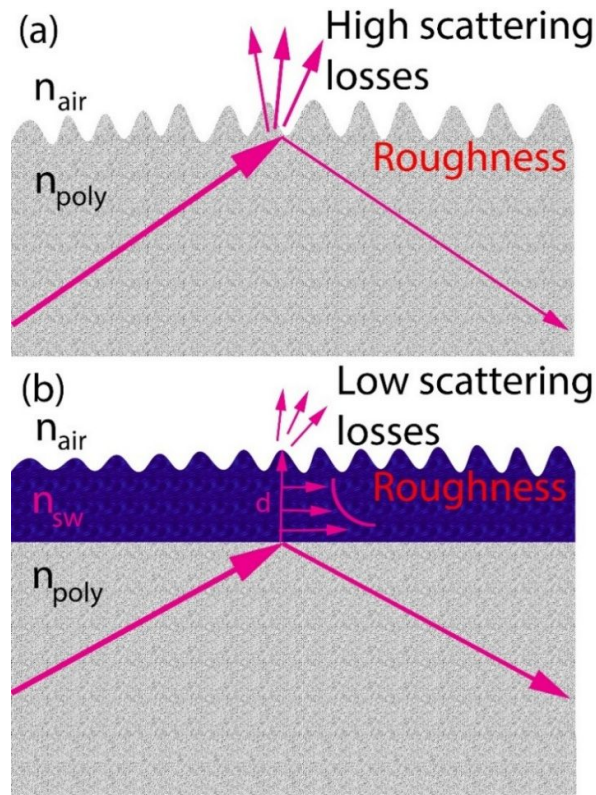
Here, we assumed that the leakage is happening only due to the forward scattering from the rough waveguide surface and no other kind of losses are being considered. The scattering loss that depends on the scattering loss component ($e^{-\psi_{scat}(\beta, \Delta\varepsilon)}$) and attenuation component ($e^{-2\kappa d(t)}$) was then used to estimate the transmitted optical power. The attenuation component is responsible for the dynamic optical gain the methacrylate-based photopolymer waveguide. This optical gain will majorly depend on the refractive index of the methacrylate-based photopolymer and solvent pair and the thickness of the swelling layer. The detailed model is described in Chapter 3,

section 3.1. The normalized dynamic gain in optical power with respect to time was plotted and results are shown in Figure 4.4 for both methanol and ethanol.

Figure 4.4

Comparison of Theoretical and Experimental Increase in the Normalized Optical Power due to Solvent and Methacrylate-based Photopolymer Interaction when Solvent used are (a) Methanol (b) Ethanol
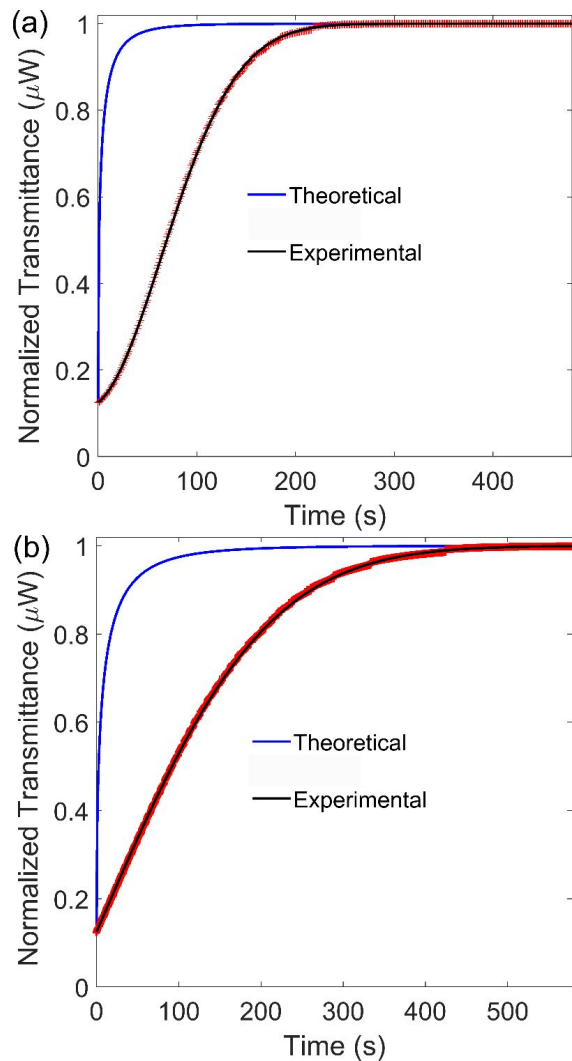
From this model, it was observed that when there is an increase in the thickness of the swelling layer, there is an exponential increase in the guided optical power through the waveguide. Model is solved for two solvent ethanol and methanol having

refractive indices of 1.3269 and 1.3592 respectively and the polymer is taken as PMMA with refractive index 1.49 at $\lambda = 650$ nm. Optical power increases with time and gets saturated in both cases. In the same Figure 4.4, the results of physical testing of the waveguide with methanol and ethanol are presented and compared with the theoretical results. Experimentally, it can be observed that whenever solvent vapor interacts with the methacrylate-based photopolymer waveguide there is an increase in the transmitted optical power till the optical power saturates. The absolute gain in optical power for methanol and ethanol is presented in Appendix A, Figure A1. The increase in the optical power is faster in the case of methanol than ethanol and the same trend was seen in both theoretical and experimental results.

The significant increase in the transmitted optical power is mainly due to the reduction of the surface scattering losses in the waveguide. Due to surface roughness guided light normally would scatter while transmitting through the waveguide resulting in a loss of light. But, due to the formation of the swelling layer, there is an optical gain in the waveguide which results in the increase of the transmitted optical power through the waveguide. This shows that the swelled methacrylate-based photopolymer layer is physically capable of showing the cladding effects in the waveguide. The faster increase in the optical power in the methanol and methacrylate-based photopolymer pair confirms the development of the more effective swelling layer in comparison to the ethanol and methacrylate-based photopolymer pair. The time to reach saturation point is compared for both the solvents. It is observed that for methanol theoretical value is around 110 s to reach full saturation and the experimental value is 215 s. For ethanol, it is 220 s and 420 s respectively.

Both theoretical and experimental results show that methanol results in a faster diffusion, and hence the formation of the swelling layer is faster than ethanol which is primarily because of the higher mutual diffusion between methanol and methacrylate-based photopolymer in comparison to ethanol. Although both theoretical and experimental values show a similar trend, the experimental time values are larger than the theoretical values. It is already mentioned previously that in our model swelling is considered only in one direction (along with the height of the waveguide) while in reality, the swelling would happen in all directions in the waveguide and the actual experiments are affected by other atmospheric factors, are the reasons why the

experimental and theoretical values might not match exactly, but we do observe a similar trend which was the main reason to develop a theoretical model as it helps us the envisage the experimental output. Also, it can be seen that the ratio of experimental time to theoretical time is 1.95 for methanol and 1.90 for ethanol which are quite close and within the limits of practical conditions. From this, we can say that the swelled methacrylate-based photopolymer layer due to the diffusion of solvent molecules inside the methacrylate-based photopolymer can show cladding effects and can significantly contribute to the dynamic optical gain in the waveguide which increases with time until saturation is reached.

4.2 Characterization of Methacrylate-based Photopolymer used for 3D Printing

4.2.1 UV-Visible Absorbance for Methacrylate-based Photopolymer

The UV-Visible absorption spectrum was performed on the methacrylate-based photopolymer (Px8880) and the absorbance of the methacrylate-based polymer is shown in Figure 4.5. It can be observed that the methacrylate-based photopolymer is absorbing wavelength from 300 nm to 410 nm which falls in the UV and violet light region of the electromagnetic (EM) spectrum while the methacrylate-based photopolymer does not absorb any light in the visible region where the wavelength is more than 410 nm.

Figure 4.5

UV-Vis Absorption Spectrum for Methacrylate-based Photopolymer (Px8880)
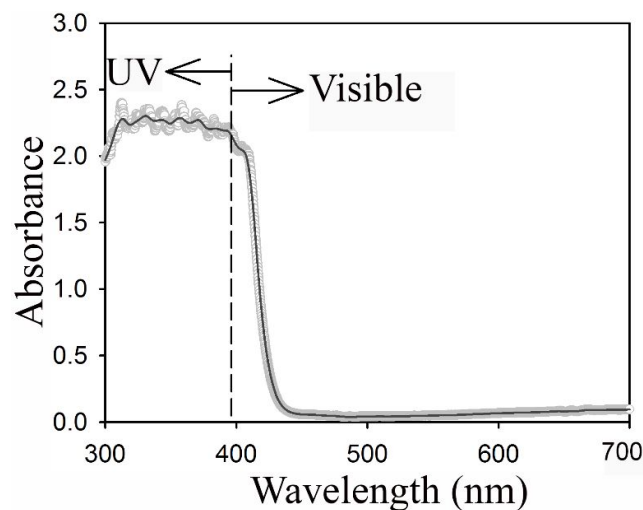
From this, it can be said that the given methacrylate-based photopolymer is sensitive to the UV and violet light region of the wavelength while it is not affected by the remaining visible region of the EM spectrum. Hence it can be suggested that the optical components being fabricated using methacrylate-based photopolymer would be suitable to work in the wavelength region higher than 410 nm of the EM spectrum as the methacrylate-based photopolymer does not absorb any wavelength in this region.

4.2.2 Solvophilic Nature of the Methacrylate-based Photopolymer Surface

To check the solvophilic nature of the methacrylate-based photopolymer surfaces, contact angles (CAs) for different solvents are measured at the methacrylate-based photopolymer surface. From the results, as shown in Figure 4.6, it can be observed that CAs for three solvents DI water, isopropanol, and glycerol are around 45.4º, 31.9º, and 47.9º respectively. Since CA for all solvents is less than 90º, the given methacrylate-based photopolymer is solvophilic in nature and has a tendency to absorb solvents and produce a considerable amount of swelling when solvents interact with the methacrylate-based photopolymer surface.

Figure 4.6

Contact Angle of DI Water, Isopropanol and Glycerol on the Methacrylate-based Photopolymer (Px8880) Surface
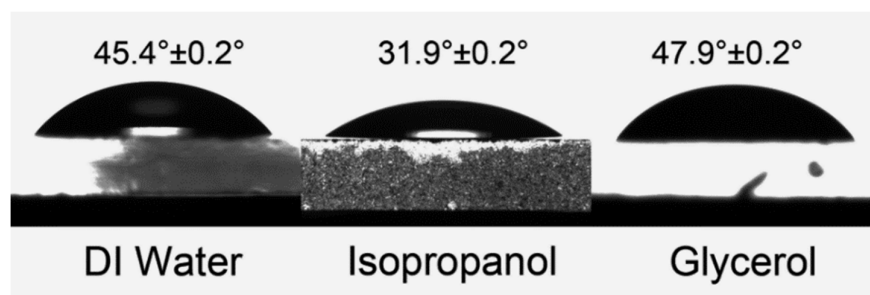
It can also be observed that isopropanol shows a much lower CA in comparison to DI water and glycerol, hence it can be said that isopropanol results in more surface wetting leading to higher interaction between the methacrylate-based photopolymer and solvent which would correspond to higher swelling of the methacrylate-based

photopolymer. CA shown by DI water and glycerol are very close, it can be suggested that the extent of swelling produce by DI water and glycerol would be closer and lower than what would be produced by isopropanol.

4.2.3 Microscopic Images of 3D Printed Methacrylate-based Photopolymer Waveguide

Photopolymer waveguides were 3D printed for physical testing with solvents. After the fabrication of the waveguides, microscopic images of the waveguide were taken to check the physical conformity. From microscope images, it was found that waveguide printed using a 3D printer has considerable surface roughness as shown in Figure 4.7 (b). This roughness is originated due to the slicing process during the 3D printing which was explained earlier in the literature review section. Due to this surface roughness, the given 3D printed methacrylate-based photopolymer waveguide is likely to have significant surface scattering losses.

Figure 4.7

Microscopic Images of 3D Printed Waveguides (a) Side View (b) Top View (c) Magnified Image of Waveguide for Pixel Analysis to Calculate Slicing Thickness
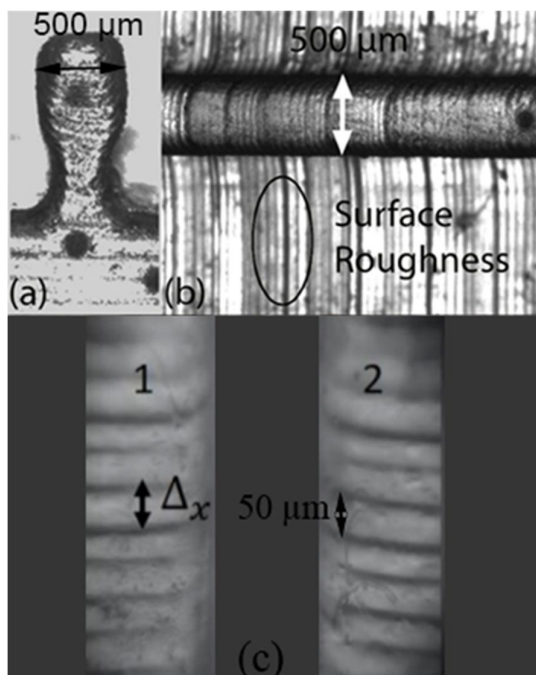
Figure 4.7(c) shows the top view of the waveguide structure taken from a monochrome camera (DCC1545M-CL) which is used to estimate the effective thickness (Δx) of the slicing layers. The 3D printer uses the slicing technique to print waveguides in a layer-by-layer format and due to the adjoining of every layer some roughness occurs which is clearly seen in Figure 4.7 (c). Using pixel analysis from the value of the acquired image, Δx was calculated to be 55.9 ± 5.8 μm, which is close to the chosen slicing thickness of 50 μm.

4.3 Optical Transmitted Power with Solvents of Similar Refractive Indices

The 3D printed methacrylate-based photopolymer waveguide was first tested with the three different solvents: DI water, isopropanol, and glycerol. These solvents were dropped on the waveguide and the change in the output power was recorded, as shown in Figure 4.8.

Figure 4.8

Transmitted Optical Power in the Methacrylate-based Photopolymer Waveguide in the Presence of Isopropanol, DI Water, and Glycerol
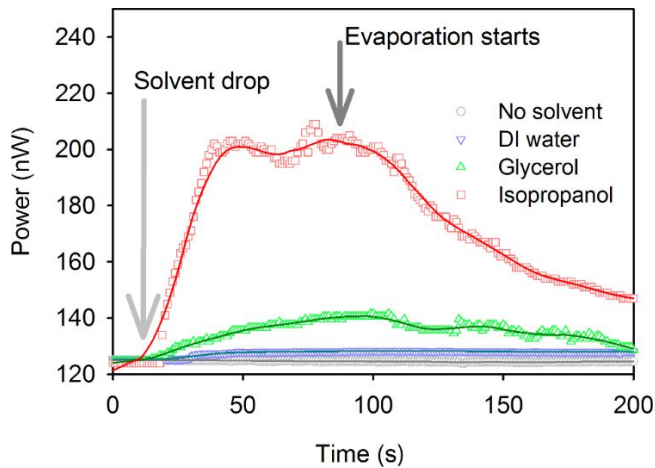
It can be observed that isopropanol shows the largest increase in the optical power when dropped on the waveguide (around 60 % increase in transmitted power) which is much larger in comparison to DI water and glycerol. This is due to the higher absorption affinity of isopropanol as a solvent towards the given methacrylate-based

photopolymer producing higher transmitted optical power in the waveguide. From these results, it can be said that the extent of increase in optical power depends on the type of solvent as the nature of a solvent affects the degree of swelling in the methacrylate-based photopolymer which further affects the surface scattering that occurs at the waveguide surface. To separate the effect of refractive index from the swelling behavior of the optical responses due to solvent-photopolymer interaction, two solvents samples having nearby refractive indices were tested with the methacrylate-based photopolymer waveguide and results are shown in Figure 4.9. Trend lines were added to show the continuity and repeatability in the results

Figure 4.9

Optical Power with (a) 20 % Isopropanol in DI Water (v/v) and (b) 10 % Glycerol in DI Water (v/v) Dropped on Methacrylate-based Photopolymer Waveguide
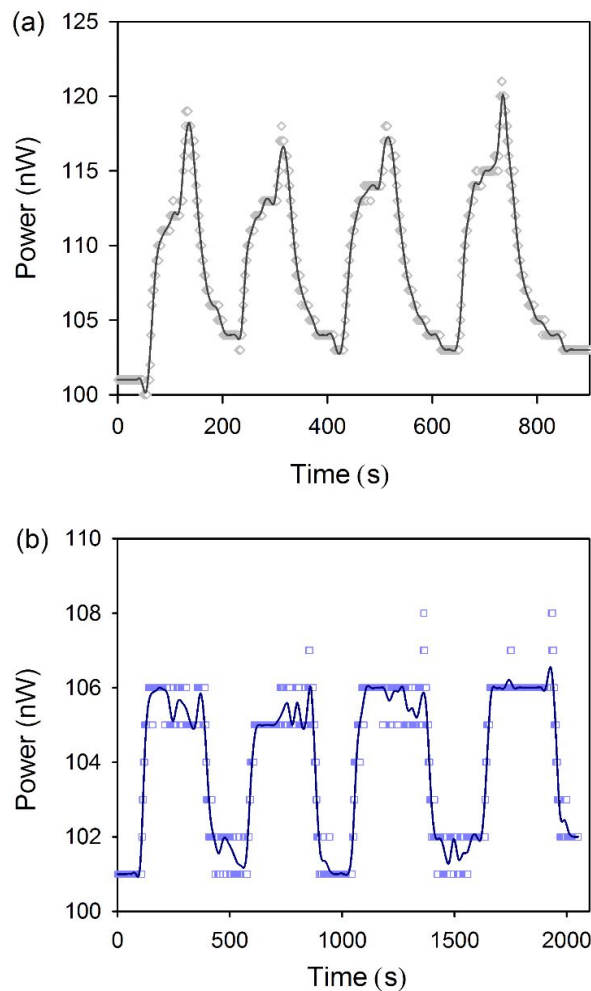
It was also observed that when samples were dropped repeatedly, while wiped and dried in between each repeated drop, optical power settles to the original level during drying and went back to a high value once solvents are reintroduced. This shows repeatability in the optical responses in the solvent-photopolymer interaction. Also in results, a sudden increase in the optical power is observed before settling to the initial power levels. This happened when the unabsorbed solvent was cleaned using a handy air blower (this is already mentioned in section 3.5.2) which made the remaining solvent further interact with the waveguide. For the calculation, we have not considered this part and the natural increase in the optical power due to solvent-photopolymer interaction was considered. We choose to present our results in the actual way we recorded because we think it gives us a better understanding of how the photopolymer waveguide would interact in the natural environment as these kinds of situations would happen in the natural environment and understanding them makes us develop better sensing system that can work in the ambient. From the results, it can be seen that the optical response was consistent and repetitive which shows the stability and precision of our experiment.

To further analyze the solvent-photopolymer interaction effect on the optical power of the methacrylate-based photopolymer waveguide, waveguide was further tested with more samples containing (i) isopropanol and (ii) glycerol in DI water in different concentrations (v/v). These samples were prepared in order to keep the refractive indices of corresponding samples approximately in the same range as presented in Table 4.1. Samples were dropped on the waveguide and the percentage increase in the optical power was recorded. It should be noted that when a solvent is dropped on the methacrylate-based photopolymer waveguide, the solvent gets absorbed by the methacrylate-based photopolymer matrix, which depends on the absorption affinity of the solvent, defined by the solvent's solubility index (or solubility parameter).

A higher solubility parameter indicates a lower absorption affinity. It is already reported that the solubility parameters of glycerol (36.2 $MPa^{1/2}$) and water (48.0 $MPa^{1/2}$) are higher than isopropanol (23.8 $MPa^{1/2}$). The solubility parameter of our methacrylate-based photopolymer is approximately 19.0 $MPa^{1/2}$ which is closer to isopropanol. Hence isopropanol will have a higher absorption affinity and diffusion in the methacrylate-based photopolymer in comparison to glycerol or water and

develops a homogenous and effective swelling layer. A higher affinity of isopropanol for the methacrylate-based photopolymer was also reflected during the measurement of CA, where isopropanol (31.9º) showed a lower CA in comparison to glycerol (47.9º) and DI water (45.4°). Based on these results obtained from solvent-photopolymer interaction experiments, the increase in the output optical power of the waveguide in the presence of different solvents can be explained by using the below-mentioned theory.

Table 4.1

Refractive Index of Samples of Isopropanol and Glycerol in DI Water (v/v) at Different Concentrations and the Corresponding Increase in the Optical Power

Isopropanol in DI water			
Concentration (v/v)	20 %	40 %	60 %
Refractive index	1.346	1.358	1.367
Increase in optical power (%)	9.74 ± 0.15	20.50 ± 0.48	36.55 ± 0.68
Glycerol in DI water			
Concentration (v/v)	10 %	15 %	20 %
Refractive index	1.349	1.355	1.365
Increase in optical power (%)	4.91 ± 0.03	4.91 ± 0.03	4.93 ± 0.03

When any solvent interacts with a methacrylate-based photopolymer, it gets absorbed and diffuse inside the methacrylate-based photopolymer resulting in the development of a swelling layer in the methacrylate-based photopolymer waveguide. This swelling layer has the capability to act as a cladding layer, having a lower refractive index than the core of the waveguide, and the majority of the transmitted light interacts with this swelling layer lowering the surface scattering losses and hence increase in the transmitted optical power improving the overall dynamic optical gain of the waveguide. Higher is the absorption affinity of a solvent for the methacrylate-based photopolymer, more effective and homogenous will be the swelling layer, and hence

higher will be the optical power gain through the methacrylate-based photopolymer waveguide. Thus, the absorption affinity of a solvent in the methacrylate-based photopolymer is the dominant factor affecting the dynamic optical gain in the waveguide, over the refractive index of the solvent.

4.4 Role of Temperature on the Optical Transmittance in the Methacrylate-based Photopolymer Waveguide

After the studies on the solvent-photopolymer interactions, we investigated the role of surrounding temperature on the optical transmission in the methacrylate-based photopolymer waveguide. The transmittance spectrum of the methacrylate-based photopolymer waveguide at different ambient temperatures is presented in Figure 4.10. The temperature was varied between 27 °C to 45 °C using a Peltier plate as described in Chapter 3, section 3.6, and optical transmittance in the methacrylate-based methacrylate-based photopolymer waveguide was recorded using a UV-Visible spectrophotometer. A low-temperature range was chosen for this study to avoid any permanent damage or deformation that may happen to the methacrylate-based photopolymer waveguide and the experiment was started from the ambient temperature (27 °C) to study the photopolymer waveguide in its naturally swelled state.

Figure 4.10

Transmittance Spectrum in a Methacrylate-based Photopolymer Waveguide at Different Ambient Temperatures
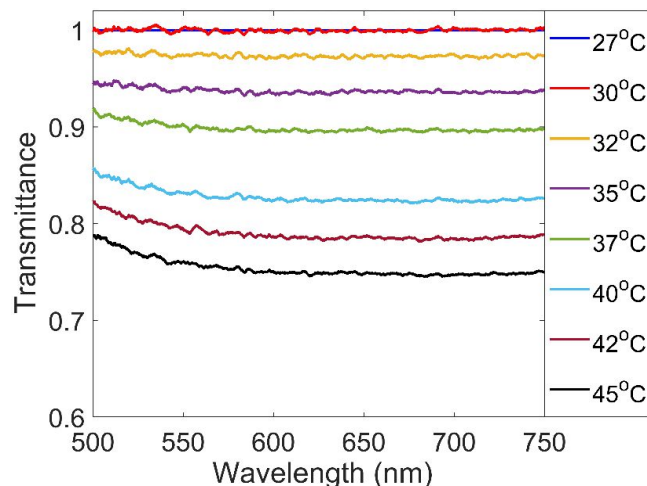
It was observed that optical transmittance through the methacrylate-based photopolymer waveguide decreases with an increase in the ambient temperature. Normalized transmittance at 27 °C showed an almost flat response over the wavelength range from 500 nm to 750 nm and up to 30 °C there was no significant change in the optical transmittance. Beyond 30 °C, optical transmittance in the waveguide was observed to drop gradually demonstrating almost a 25 % drop in the overall transmittance over the wavelengths 500 to 750 nm when the ambient temperature was increased from 30 °C to 45 °C. The overall change in the optical transmittance in the waveguide obtained by averaging and normalizing the transmittance over the wavelength range between 500 nm to 750 nm was then estimated for different ambient temperatures and is presented in Figure 4.11.

Figure 4.11

Change in Average Transmittance in the Waveguide as a Function of the Ambient Temperature
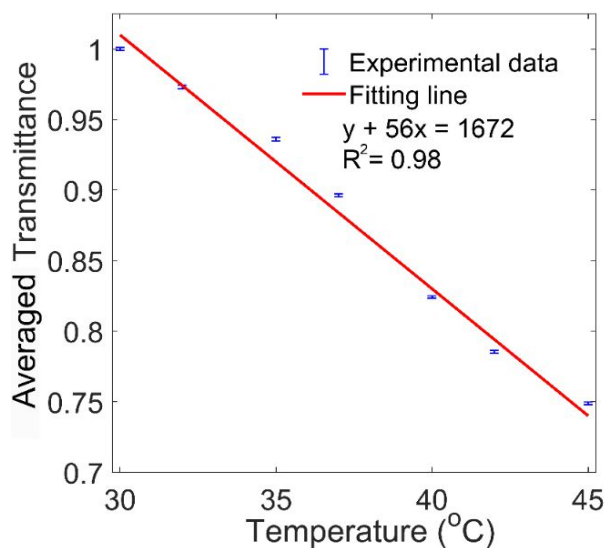
It can be observed that the average transmittance in the waveguide decreases with increasing ambient temperatures (from 30 °C to 45 °C) following a linear relation with slope –0.0178 /°C and the goodness to fit (R^2) is 0.98 shows a low error in the experimental results. The effect of temperature on the optical transmission through the methacrylate-based photopolymer waveguide can be explained in the following

way. Methacrylate-based Photopolymers have a natural tendency to swell by absorbing humidity that is present in the surrounding atmosphere which results in changes in the refractive index of the swelled polymer layer (n_{sw}) at the surface. As described earlier, this swelled polymer layer can act as a cladding layer guiding more light through the waveguide, as shown in Figure 4.12 (a).

Figure 4.12

Schematic Representation Showing the Effect of Ambient Temperature on the Methacrylate-based Photopolymer Waveguide. (a) Light Transmission Through a Naturally Swelled Photopolymer Waveguide and (b) Higher Scattering Losses due to Deswelling and Drying of the Photopolymer Waveguide with Increasing Temperature
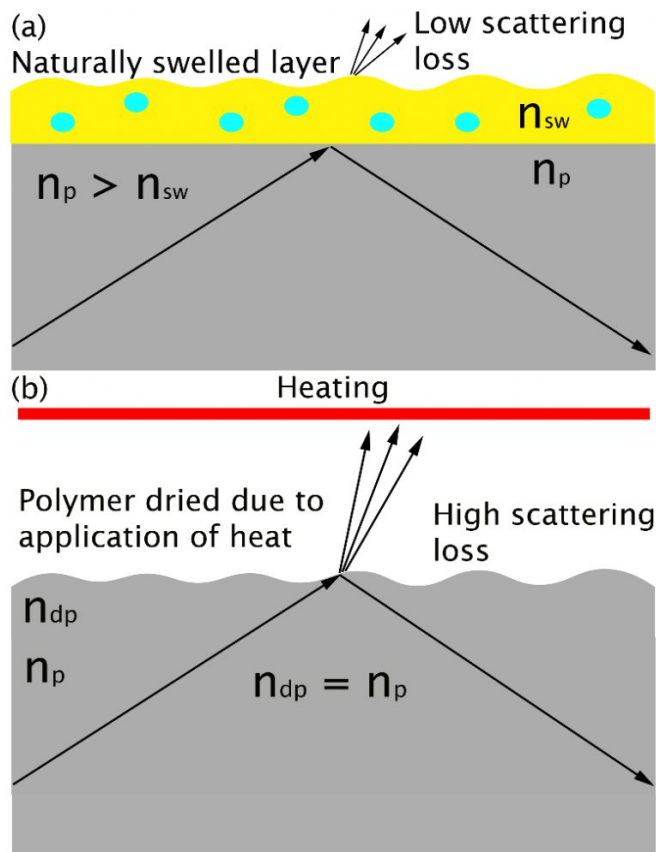
When the surrounding temperature rises, adsorbed humidity present near the surface of the photopolymer waveguide leaves the polymer matrix reducing the swelling and thus producing a dried polymer whose refractive index (n_{dp}) moves towards the

original photopolymer before swelling. As a result, scattering losses increase at the waveguide surface reducing the overall transmittance through the waveguide, as illustrated in Figure 4.12 (b). It should be noted here that the refractive index of methacrylate-based polymers typically decreases with increasing temperatures, e.g., PMMA refractive index drops from 1.492 to 1.488 as temperature increases from 30 °C to 45 °C (Kovačević & Djordjevich, 2009). A drop in the refractive index usually means more light transmission, which is not the case in our study. Therefore, we ruled out the effect of change in the refractive index of the photopolymer due to the increasing temperature on the observed decreasing optical transmittance and concluded that de-swelling of the polymer is the predominant factor resulting in lower optical transmission through the waveguide as ambient temperature rises.

4.5 Optical Transmission through the Methacrylate-based Photopolymer Waveguide with Repeated Heating and Cooling Cycles

In order to study the repeatability of the optical transmission behavior, we subjected the methacrylate-based photopolymer waveguide to repeated heating and cooling cycles. The testing chamber was repeatedly heated from room temperature 27 °C to 45 °C and cooled down to 27 °C using the Peltier plate and the optical transmittance through the waveguide was continuously recorded. From Figure 4.13 it can be observed that the optical transmittance dropped during the heating cycles and during the cooling cycles recovery of the optical transmittance was observed. However, the recovery of the optical transmission was not 100% and for the 1st heating-cooling cycle almost a 10 % drop in the recovered average transmittance value was recorded compared to the initial average transmittance. This drop was observed to gradually increase with subsequent heating-cooling cycles and after the 5th cycle, the waveguide did not produce any considerable change in the optical transmittance irrespective of the ambient temperature.

The drop in optical transmittance with increasing ambient temperature is already explained in the previous section. During cooling, the photopolymer waveguide reabsorbs the available humidity from the surrounding resulting in the formation of the swelling layer at the surface of the waveguide again trapping more light in the waveguide and thus increasing the optical transmission during cooling. As the heating and cooling cycles increases, this release and reabsorption of the humidity from the

surrounding also repeat resulting in reduction and restoration of the optical transmittance through the waveguide, respectively. However, the process of water molecules (humidity) released from the waveguide surface during heating and their reabsorption during the cooling cycles is not completely reversible. As the number of water molecules in the surrounding drops due to the repeated heating/cooling of the surrounding stopping the waveguide from further absorption of water molecules, the optical transmission output from the waveguide becomes steady and remained constant at around 80 % of the initial value as observed in the Figure 4.13.

Figure 4.13

Average Optical Transmittance Through the 3D Printed Methacrylate-based Photopolymer Waveguide with Repeated Heating and Cooling Cycles. The Red Graph Represents the Change in the Ambient Temperature Inside the Testing Chamber, while the Blue Graph Represents the Corresponding Average Optical Transmittance Through the Waveguide
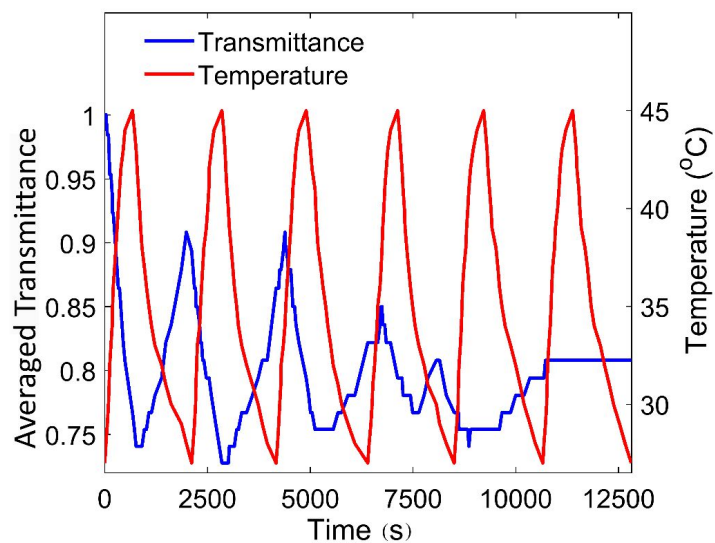
4.6 Fabrication of Au-NP Embedded Photopolymer Waveguide

In order to obtain a steady optical transmittance output from the waveguide with variable ambient temperatures, we then prepared a methacrylate-based photopolymer waveguide with gold nanoparticles (Au-NP) embedded in the polymer. The idea here was to utilize the localized surface plasmon resonance (LSPR) properties of the Au

NPs as an indicator of the variations of the ambient temperature rather than the optical transmittance. The LSPR property of Au NPs, which is highly sensitive to temperature and refractive index of the surrounding medium, is well-studied and used widely to fabricate sensors and other optical devices (Chang et al., 2018), (Mayer & Hafner, 2011). The preparation, characterization of the Au-NP, fabrication of the Au-NP embedded methacrylate-based photopolymer waveguide and its optical characteristics with respect to the ambient temperature are discussed below.

4.6.1 Synthesis and Characterization of Au NPs

The detailed synthesis process of Au NPs is described in Chapter 3. Briefly, we used a ZnO nanorod support to synthesize Au NPs in-situ on the ZnO surface using a photoreduction method. Figure 4.14 shows the SEM micrographs of ZnO nanorod support and Au NPs deposited on the surface of the ZnO nanorods. The ZnO nanorods showed their characteristic hexagonal shape with size of around 50 nm ± 15 nm. Au NPs deposited on the ZnO surface were found to be almost spherical in shape and with sizes smaller than 50 nm.

Figure 4.14

SEM Micrographs of (a) Zinc Oxide Nanorods and (b) Au NPs In-situ Deposited Zinc Oxide Nanorods
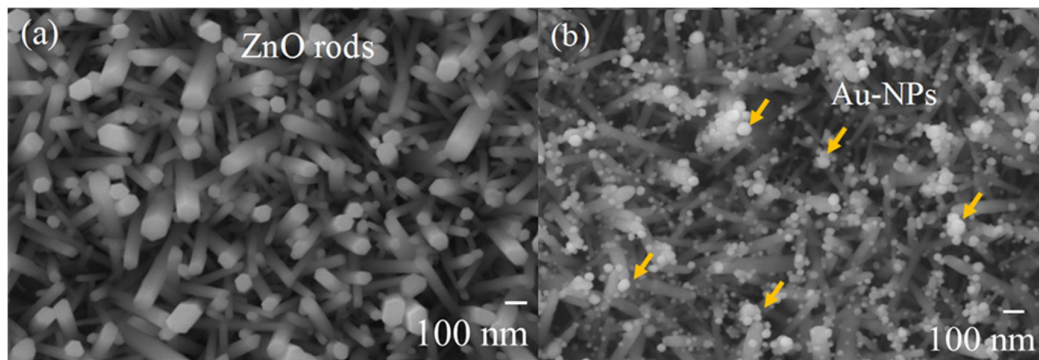
The size range of Au NPs was quite broad indicating poor control over the size of the in-situ deposited nanoparticles. But no agglomeration was observed, and Au NPs were found to cover the ZnO surface uniformly. The optical absorption of the Au NPs in-situ deposited on ZnO nanorods is shown in Figure 4.15. The Au NPs exhibited the

characteristic LSPR peak at 527 nm. However, due to their wide size distribution, the LSPR peak showed a slight broadening. An LSPR peak around 530 nm generally represents Au NPs of size around 30 nm, which corroborates with the size of the Au NPs observed in the SEM results. Another peak is absorbed at 360 nm in the UV region due to the presence of ZnO nanorods in the samples. However, no abnormal peak broadening was observed until 750 nm indicating the presence of individual Au NPs without any agglomeration.

Figure 4.15

Absorbance Spectrum of Gold Nanoparticles In-situ Deposited on ZnO Nanorod Surface a Glass Substrate
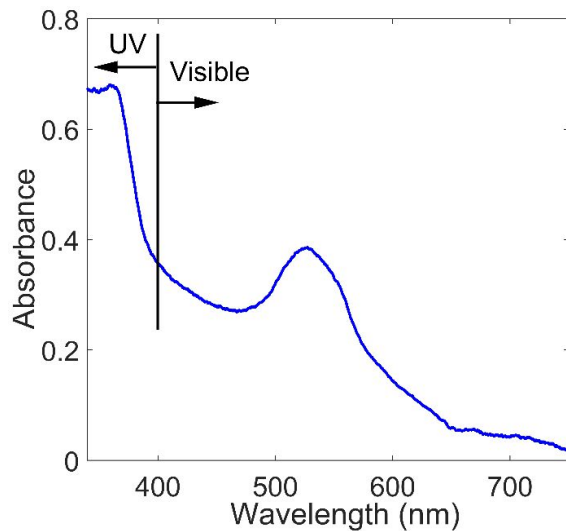
4.6.2 Fabrication of Au-NP Embedded Photopolymer Waveguide

Au-NP embedded photopolymer waveguides were then fabricated using a soft PDMS mold, as described in chapter 3. The volume fraction of Au NPs in the photopolymer was 0.000055 estimated from the atomic percentage of Au to Zn obtained from EDS of the Au NPs decorated ZnO nanorods. This value was selected based on the experimental precision as when a value of volume fraction 0.000062 was selected there was no output observed through the waveguide. This happened due to the agglomeration of Au NPs in the waveguide at a higher volume fraction, while if the lower volume fraction would have chosen the LSPR effect through the waveguide

was not prominent. The dimension of the Au-NP embedded methacrylate-based photopolymer waveguide was measured using a microscopic camera and found to be 0.651 mm × 0.456 mm against the original dimensions of 0.700 x 0.500 mm as shown in Figure 4.16 (a). These measured dimensions are acceptable and are within the limits of practicality. Also, the volume shrinkage of the waveguide was calculated by subtracting the designed volume of the waveguide (3.50 mm^3) and observed volume (2.97 mm^3) of the fabricated waveguide and found to be 0.53 mm^3.   After fabrication of Au-NP embedded methacrylate-based photopolymer waveguides absorbance spectroscopy was performed again on the samples to observe the LSPR peak of the Au NPs, as presented in Figure 4.16 (b).

Figure 4.16

(a) Microscopic Images of Au-NP Embedded Waveguide (b) Absorbance Spectrum Showing the LSPR Peak of the Au NPs Embedded in the Photopolymer Waveguide
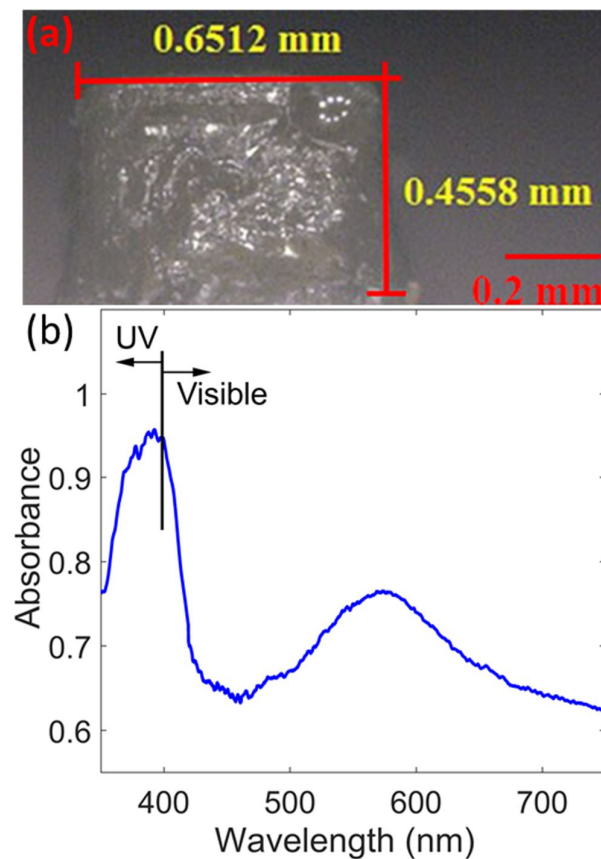
From the absorbance curve, it can be seen that the Au-NP waveguide has a peak absorbance first at a wavelength of 385 nm which is due to the presence of ZnO nanorods, and then at 580 nm due to the presence of Au NPs in the waveguide.. Generally, Au NPs LSPR peak shifts to higher values when the refractive index of the surrounding increases. The optical absorption shown in Figure 4.15 was measured in normal air conditions which has a refractive index of 1 at 589.2 nm. However, in the case of the methacrylate-based photopolymer waveguide, the refractive index of the polymer surrounding the Au NPs is much higher (1.492) than air and as a result the LSPR peak shifts to a higher wavelength value. The other absorbance characteristics of the embedded Au NPs were found to be more or less similar to the absorbance of the Au NPs prior to embedding in the polymer which shows an orderly distribution of the Au NPs and ZnO nanorods in the waveguide as initially observed before their embedding.

4.7 Effect of Temperature on the Optical Transmittance of the Au-NP Embedded Photopolymer Waveguide

Au-NP embedded waveguide was tested for its optical properties at different ambient temperatures. First, the temperature was increased from 28 ˚C to 45˚C and then cooled down back to the initial temperature using a similar setup described in sections 4.4 and 4.5. Change in visible light optical transmittance through the waveguide was recorded and presented in Figure 4.17, where Figure 4.17 (a) represents the variations in the optical transmittance during the heating cycle and 4.17 (b) represents the changes during the cooling cycle. Due to the strong LSPR absorption by the Au NPs, the lowest transmittance through the waveguide was observed at 580 nm, which gradually decreased with increasing ambient temperature varied from 28 °C to 45 °C.

Recovery of the optical transmittance to its initial value was observed during the cooling cycle when the ambient temperature was allowed to return to 28 °C. There is no disorder in the transmittance spectrum throughout the experiment which happens due to the uniform distribution of Au NPs in the waveguide and the absence of environmental humidity (or water molecules) in the core of the waveguide which was achieved by vacuum suction during the soft molding process. The Au-NP methacrylate-based photopolymer waveguide was then subjected to repeated heating and cooling cycles to investigate its stability. Figure 4.18 shows the normalized

optical transmittance response of the Au-NP methacrylate-based photopolymer waveguide at 580 nm for 20 heating and cooling cycles.

Figure 4.17

Transmittance Spectra of Au-NP Embedded Waveguide at Different Ambient Temperatures During (a) Heating and (b) Cooling Cycle
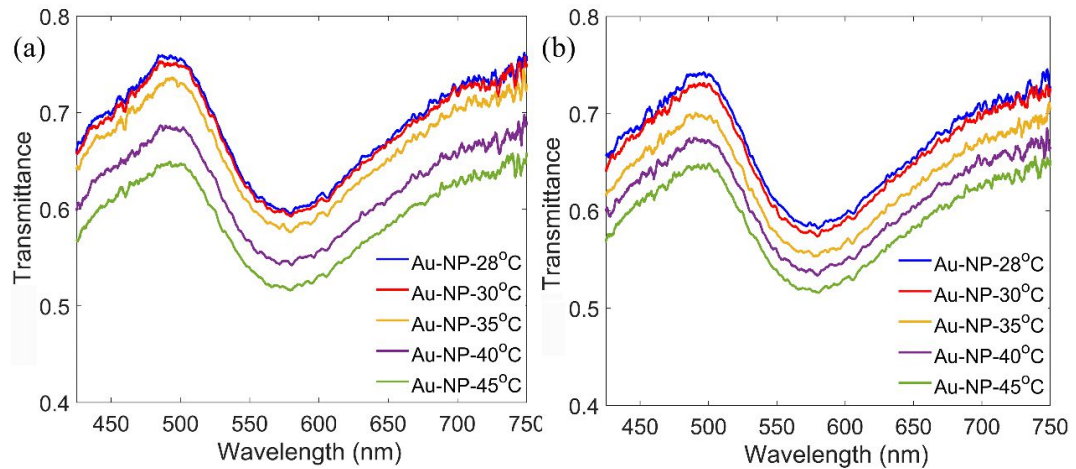
Figure 4.18

Repeatability of the Optical Response of Au-NP Embedded Waveguide for 20 Cycles of Heating and Cooling. The Reported Normalized Optical Transmittance was Measured at 580 nm
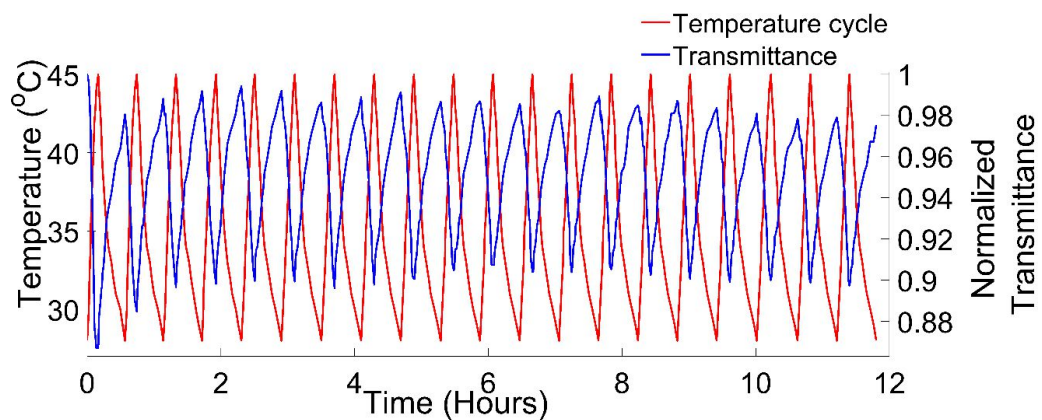
As described, the optical transmittance of the waveguide at 580 nm (LSPR peak) was found to decrease with increasing temperature (from 28 °C to 45 °C) and retired to its initial value when the temperature was allowed to cool down to near room temperature. Unlike the plain photopolymer waveguides without the embedded Au NPs, the optical transmittance behavior of the Au-NP embedded methacrylate-based photopolymer waveguide was found consistent throughout the 20 repeated heating and cooling cycles, showing only a small variation (within ±2.5%). The optical transmittance behavior of the Au-NP embedded photopolymer waveguide at 580 nm for the individual heating and cooling cycles is shown in Appendix B. The experiment was repeated several times which took about 12 hours to complete 20 heating and cooling cycles and during this continuous long 12 hours, we did not observe any physical damage to the waveguide. Figure 4.19 shows the overall variation of the optical transmittance of the Au-NP embedded methacrylate-based photopolymer waveguide averaged at 580 nm from the 20 repeated heating cycles.

Figure 4.19

Overall Change in the Optical Transmittance of Au-NP Embedded Waveguide at 580 nm (LSPR wavelength) with Increasing Ambient Temperature
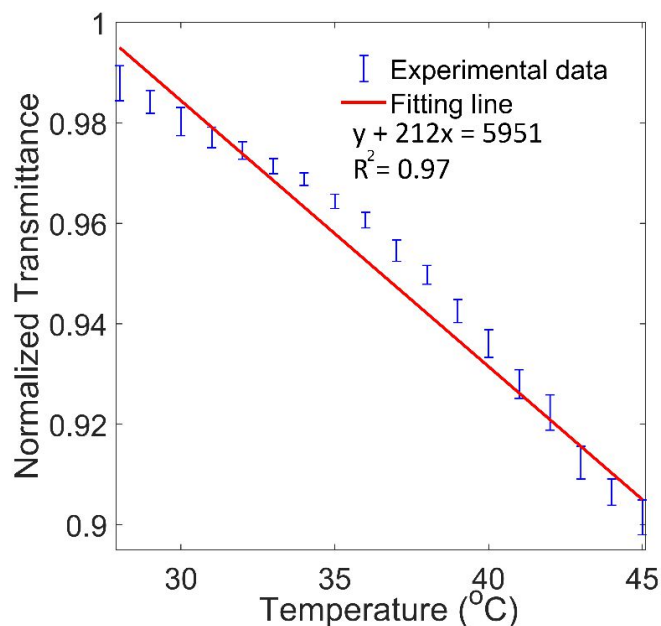
The change in the optical transmittance at the LSPR wavelength (580 nm) of the Au NPs with increasing ambient temperature was found to have nearly linear behavior, with slope around –0.0047 /°C and the goodness to fit (R^2) is 0.97 shows a low error in the experimental results. Compared to the plain photopolymer waveguide in the absence of the Au NPs which showed a slope of –0.0178 /°C, the Au-NP embedded waveguide exhibited an optical responsivity of lesser order. However, the stability of the Au-NP embedded methacrylate-based photopolymer waveguide was found to be far better than the plain methacrylate-based photopolymer waveguides.

4.8 Theoretical Model of the Au-NP Embedded Photopolymer Waveguide

To further analyze the LSPR effect shown by Au-NP embedded methacrylate-based photopolymer waveguide and its dependence on temperature, a theoretical model was developed. The LSPR effect shown by the Au NPs depends on the refractive index of Au NPs and the refractive index of its surrounding which happens to be a methacrylate-based photopolymer in this case. The Refractive index (n) of a material depends on its dielectric constant (ε) as

$$n = \varepsilon^{1/2} \tag{4.1}$$

Dielectric constant also has both real and complex parts, hence it can be written that

$$\varepsilon_p = \varepsilon_p^1 + i\varepsilon_p^2 \tag{4.2}$$

$$\varepsilon_g = \varepsilon_g^1 + i\varepsilon_g^2 \tag{4.3}$$

Where ε_p is the dielectric constant for methacrylate-based photopolymer, which is the host matrix, ε_g is the dielectric constant for Au NPs which are embedded in the host matrix. The complex part of the dielectric constant is mainly responsible for the absorption of light by a material. Since the methacrylate-based photopolymer has no complex value in its dielectric constant so its dielectric constant, Eq. (4.2) can be modified as

$$\varepsilon_p = \varepsilon_p^1 \tag{4.4}$$

Considering the approximation of the Riccati–Bessel functions (Bohren & Huffman, 1998), the scattering cross-section (σ_{sca}) can be calculated. σ_{sca} depends on the dielectric constant of Au NPs (ε_g^1 & ε_g^2), the dielectric constant of the host matrix

which is methacrylate-based photopolymer (ε^1_p), the wavelength of light (λ) and volume of Au NPs (V) as shown in Eq. (4.5).

$$\sigma_{sca} = \frac{32\pi^4(\varepsilon^1_p)^2 V^2}{\lambda^4} \frac{\left(\left(\varepsilon^1_g - \varepsilon^1_p\right)^2 + \varepsilon^2_g\right)}{\left(\left(\varepsilon^1_g + 2\varepsilon^1_p\right)^2 + \varepsilon^2_g\right)} \tag{4.5}$$

For small particles, the scattering cross-section signifies the given cross-section of the particles where light interacts. This cross-section is the area on the particles which scatters light and hence this area can also absorb light for those particles which has light absorption properties, like our Au NPs, so Eq. (4.5) can be modified where σ_{sca} is replaced with σ_{abs} which is absorption cross-section.

$$\sigma_{abs} = \frac{32\pi^4(\varepsilon^1_p)^2 V^2}{\lambda^4} \frac{\left(\left(\varepsilon^1_g - \varepsilon^1_p\right)^2 + \varepsilon^2_g\right)}{\left(\left(\varepsilon^1_g + 2\varepsilon^1_p\right)^2 + \varepsilon^2_g\right)} \tag{4.6}$$

Eq. (4.6) is solved by using the size of Au NPs as 50 nm, dielectric constant value for Au (Johnson & Christy, 1972), and the dielectric constant for methacrylate-based photopolymer at different temperatures (Xiang et al., 2006), and results are shown in Figure 4.20. It can be seen that the maximum absorption cross-section is found at 545 nm of wavelength and it is the wavelength where the Au-NP embedded methacrylate-based photopolymer waveguide would show maximum theoretical absorption. Experimentally, the resonance wavelength occurred at 580 nm, here we have to consider that the theoretical model assumes an ideal situation where the experiment can be affected by practical factors which result in this difference.

From Figure 4.20, it can be observed that with an increase in the temperature there is no significant shift in LSPR wavelength. This is because the thermo-optic coefficient of our methacrylate-based photopolymer is around -0.127e-3 /°C, hence the change in the refractive index of the methacrylate-based photopolymer is small to observe any shift in the resonance wavelength, but it can also be observed that the height of the absorption peak is decreased when the temperature is decreased. This is because due to the increase in the temperature there is a small decrease in the refractive index of the methacrylate-based photopolymer which is the local atmosphere in which Au NPs are embedded. Due to this, the intensity of light that is absorbed by the Au NPs decreases which is the basic principle of LSPR. The change in the absorbed intensity

of light is small hence it would not able to generate any shift in the resonance wavelength, but it results in the decrease in the height of the absorbance peak which is observed in the graphs.

Figure 4.20

Theoretical Value of Absorption Cross-section for Au-NP Embedded Methacrylate-based Photopolymer Waveguide at Different Ambient Temperatures
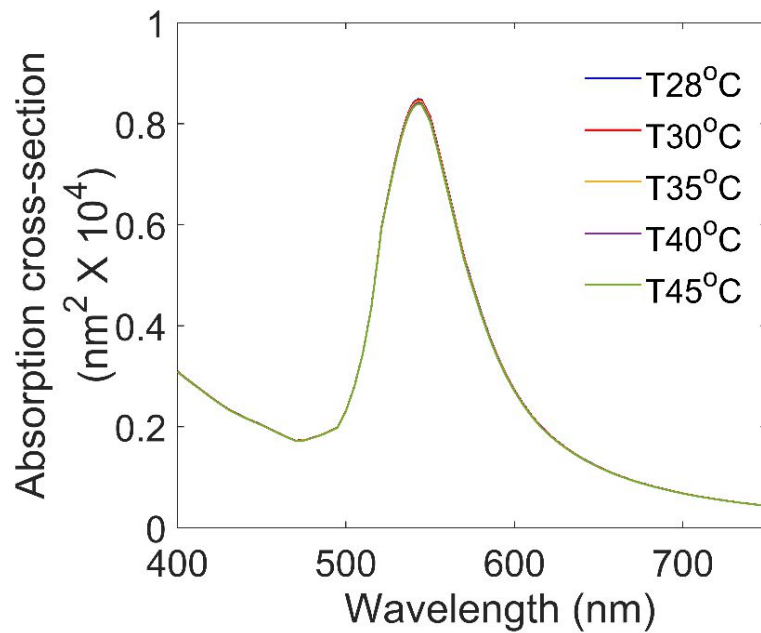
Next, using Lambert's Law of Absorption, the normalized transmittance (T_c) through the waveguide was then calculated as shown in Eq. (4.7) where α is the absorption coefficient of Au-NP embedded waveguide material and L is the length of the waveguide.

$$T_c = e^{-\alpha L} \tag{4.7}$$

α can be calculated from σ_{abs} as shown in Eq. (4.8) where η is the atomic number density which signifies the number of atoms of a given material per unit volume.

$$\sigma_{abs} = {\alpha}/{\eta} \quad \text{or} \quad \alpha = \sigma_{abs}\eta \tag{4.8}$$

η is calculated using Eq. (4.9) as shown below where N_A is the Avogadro's number, ρ is the density and M is the molecular weight.

$$\eta = \frac{\rho N_A}{M} \qquad\qquad (4.9)$$

Since in the Au-NP embedded methacrylate-based photopolymer waveguide, Au NPs are distributed over the entire volume of the waveguide, the effective molecular mass of the waveguide is calculated considering the combined effect of methacrylate-based photopolymer, ZnO and Au NPs. Mass of Au NPs and ZnO are calculated from the atomic percentage of Au to Zn which is obtained from EDS of the Au NPs decorated ZnO nanorods. The mass of the methacrylate-based photopolymer is calculated by multiplying its volume used in synthesis with its density and then individual mass % of all three components are calculated and used in Eq. (4.10).

$$M = \%m_{Au}\, M_{Au} + \%m_{ZnO}\, M_{ZnO} + \%m_{Poly}\, M_{Poly} \qquad\qquad (4.10)$$

In Eq. (4.10), $\%m_{Au}$, $\%m_{ZnO}$ & $\%m_{Poly}$ and M_{Au}, M_{ZnO} & M_{Poly} are mass percentage and molecular masses for Au, ZnO and methacrylate-based photopolymer respectively (for calculation the molecular mass of methacrylate-based photopolymer was taken same as of PMMA which the closest polymer to our methacrylate-based photopolymer), Avogadro's number was taken as 6.023×10^{23} /mol^{-1} and density of Au was taken as 19.3 gm/cm^3. Using these values in Eq. (4.9) and Eq. (4.8), α is calculated and then the value of α with a length of the waveguide (L) is substituted in Eq. (4.7) to calculate T_c through Au-NP embedded methacrylate-based photopolymer waveguide at different temperatures and results are shown in Figure 4.21.

From Figure 4.21 it can be observed that the LSPR peak is at 545 nm where the minimum transmittance is observed, it is the same wavelength where the peak in the absorption was observed in Figure 4.20 which shows the continuity of the model. From the inset in Figure 4.21, it can be observed that the resonance wavelength does not change with the increase in the temperature but the height of the peak changes due to a small change in the refractive index of methacrylate-based photopolymer which is already explained earlier.

Figure 4.21

Solution of Theoretical Model Showing Normalized Transmittance Through Au-NP
Embedded Methacrylate-based Photopolymer Waveguide at Different Temperatures
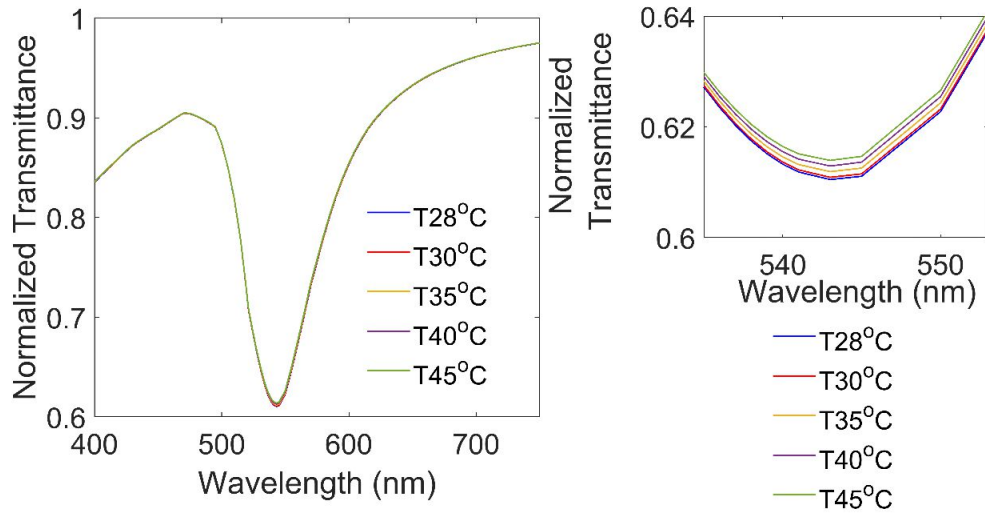
The change in the peak height due to an increase in the temperature is depicted in Figure 4.22 (a) where it can be seen that due to change in the temperature, the peak of the curve shifts upward, and this shift is denoted by Δh. Peak height is calculated for both theoretical model and experimental results at a different temperature, normalized and then peak height is plotted against temperature for both theoretical and experimental values as shown in Figure 4.22 (b). Figure 4.22 (b) shows the variations of the LSPR peak height with respect to the ambient temperature obtained from the theoretical model and experimental data. Both theoretical and experimental results indicate a gradual decrease in the peak height with an increase in temperature. This decrease in the peak height is due to the decrease in the refractive index of methacrylate-based photopolymer with the increase in the temperature which decreases the absorption intensity in the Au-NP embedded methacrylate-based photopolymer waveguide. The trend shown by the decrease in peak height for both theoretical and experimental values is linear, with the theoretical model having a higher slope than the experimental values. This difference between the experimental values and theoretical model is possible as the theoretical model considers a uniform decrease in the refractive index I the entire waveguide due to an increase in the

temperature while experimentally heating mostly affects the upper part of the waveguide and the lower part does not affect as much which results in the lower decrease in the experimental values in the peak height. Also, the experimental results could be affected by external factors while in the theoretical model, we consider ideal conditions.

Figure 4.22

(a) Depiction of Change in Peak Height (Δh) with Increase in Temperature for Theoretical Model (b) Comparing Change in the Peak Height for Theoretical and Experimental Results with Respect to Temperature
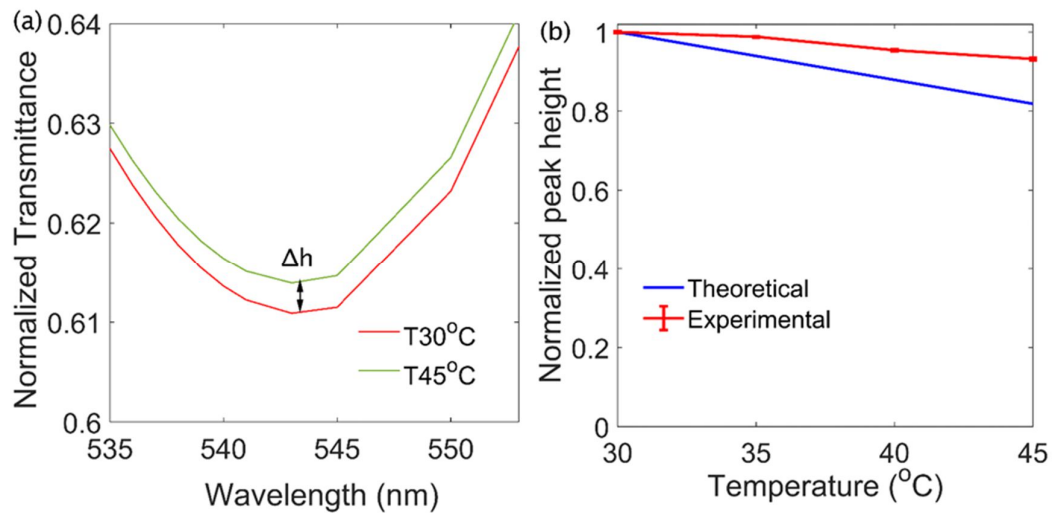
In these experiments, the effect of ambient temperature on the optical properties of the given methacrylate-based photopolymer is studied. It has been observed when the ambient temperature of plain methacrylate-based photopolymer waveguide is increased there is a decrease in the transmittance through it. Methacrylate-based photopolymer has a natural tendency to swell by absorbing humidity from the atmosphere. When heat is applied humidity is removed from the polymer matrix and it gets dried, due to which the refractive index of the surface of the methacrylate-based photopolymer waveguide increases which results in higher surface scattering losses and a decrease in the transmittance. In the case of plain methacrylate-based

photopolymer waveguide, humidity can penetrate deep in the polymer matrix as shown in Figure 23 (a) and can reach up to the core of the polymer matrix.

Figure 4.23

Schematic Showing Absorption and Desorption of Water Molecules when Repeated Heating and Cooling is Performed on (a) Plain Methacrylate-based Photopolymer Waveguide (b) Au-NP Embedded Methacrylate-based Photopolymer Waveguide
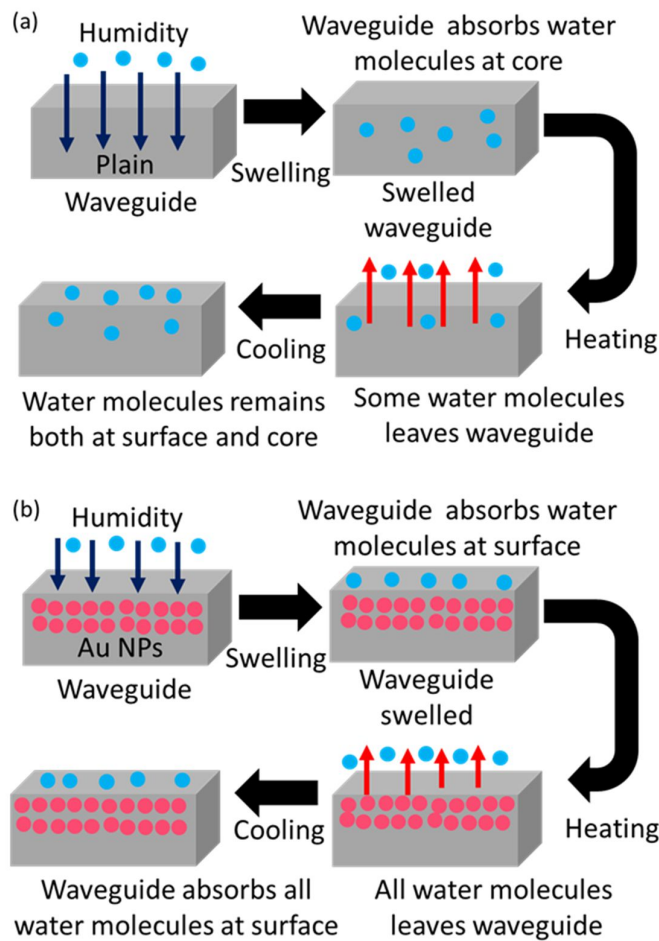
When the heat is applied water molecules would leave the core of the waveguide but there is a possibility that some would remain there. When the ambient is cooled, these water molecules can be reabsorbed within the waveguide, but it is not possible for them to go deep inside the waveguide core exactly like in the initial state and hence the transmittance level did not reach the initial level as shown in the Figure 4.13.

When the process of heating and cooling is continuously repeated, the water molecules which were not able to absorb by the waveguide leave the surroundings and there would be a drop in the number of the water molecules. As the number of water molecules in the surrounding drops, it stops the waveguide from further absorption of water molecules because of that the plain methacrylate-based photopolymer waveguide reaches the steady-state and the optical transmission output from the waveguide remained constant at around 80% of the initial value.

When Au NPs in-situ deposited on ZnO nanorods were added to the methacrylate-based photopolymer, they occupied the voids present in the photopolymer matrix and acts as a barrier for water molecules to go deep inside the waveguide as shown in Figure 4.23 (b). In this case, the humidity present in the ambient interacts with the surface of the waveguide and swelling happens only at the surface of the waveguide. When the temperature is applied these water molecules leave the surface and the waveguide's surface gets dried due to which the transmittance decreases. When the ambient is cooled, the water molecules get absorbed on the surface of the waveguide and transmittance reaches the initial level. Since in this case, the swelling is happening only at the surface of the waveguide, the absorption and desorption of the water molecular are regular and stable that is why the process shows a repeatable trend till the 20th cycle with a loss of 2.5 % of its initial transmittance value.

The presence of Au NPs in-situ deposited on ZnO inside the Au-NP embedded waveguide is detected through the transmittance spectrum. A strong peak at 580 nm of wavelength confirms the presence of Au NPs inside the methacrylate-based photopolymer matrix because the plain photopolymer does not absorb light in the visible region and ZnO nanorods absorbs light at 385 nm which is the UV region. From the theoretical model, it is also observed when the Au NPs are embedded in the methacrylate-based photopolymer a peak in the transmittance is observed due to the LSPR effect. From this, it can be said that the waveguide which is fabricated by embedding Au NPs in the methacrylate-based photopolymer shows the LSPR effect and the Au NPs present in the waveguide control the swelling behavior of the photopolymer waveguide. By adding Au NPs in the waveguide , the waveguide shows a repeatable and stable optical response.

CHAPTER 5

CONCLUSION AND RECOMMENDATIONS

5.1 Conclusion

Methacrylate-based photopolymer has been explored as a suitable waveguide material that has potential for integrated optical device applications. A photopolymer waveguide was fabricated using a stereolithography-based single-step 3D printing technique. It was observed that due to the slicing mechanism adopted in the 3D printing process, surface roughness was induced in the waveguide structure leading to surface scattering loss of the propagating light in the waveguide. Surface scattering in general results in forward scattering losses and waste of transmitted light through the waveguide, but in this research this surface scattering is shown as a useful tool to investigate the effect of polymeric swelling on the light transmission through the 3D printed photopolymer waveguide.

Surface wetting behavior of the photopolymer waveguide was measured using three different solvents, namely DI water, isopropanol, and glycerol, and for all cases a solvophilic nature was found with contact angles varying between 31° to 48°, indicating that the selected solvents have strong interaction with the solid photopolymer waveguide surface. The extent of the solvent interaction and its diffusion into the polymer matrix was then studied using a first-order theoretical model and verified with experimental results. The theoretical model showed the development of a swelling layer at the surface of the photopolymer waveguide due to the diffusion of the solvent molecules into the polymer matrix. The thickness of the swelling layer was found to depend highly on the coefficient of mutual diffusion between the solvent and the photopolymer.

Among the selected solvents, isopropanol shows the highest coefficient of mutual diffusion with the methacrylate-based photopolymer and exhibited the formation of a thicker swelling layer at the waveguide surface. In the same model, the swelling layer was further investigated for its capability of showing a cladding effect. Due to the development of an effective swelling layer, most of the transmitted light inside the core of the photopolymer waveguide interacted with the newly developed swelling layer rather than the rough surface of the photopolymer waveguide. This way newly

developed swelling layer acted as cladding which resulted in the reduction of surface scattering losses and consequently a dynamic gain was observed in the photopolymer waveguide. The solution to the theoretical model for optical power gain showed that due to polymeric swelling, the optical power through the photopolymer waveguide increases exponentially with time and saturates when solvent diffusion stops.

The results of the theoretical model were validated using experimental data. The 3D printed waveguide was exposed to the three selected solvent environments and the effects of their diffusion into the polymer matrix as well as their corresponding refractive index on the response of the transmitted light through the waveguide was investigated. Compared to the DI water and glycerol, isopropanol demonstrated a higher dynamic gain in the transmitted light through the waveguide attributed to its higher coefficient of mutual diffusion and produced an almost 60 % increase in the transmitted optical power due to the formation of a thicker swelling layer acting as cladding.

When solvents were diluted to adjust their refractive indices to similar values, isopropanol with a higher mutual diffusion coefficient continuously produced higher optical gains compared to the other solvents indicating that the solvent refractive index is not the primary deciding factor of the optical transmission through the photopolymer waveguide, but the solubility parameter of the polymer and solvent given as the coefficient of mutual diffusion is the dominant factor in this case.

Next, the effect of temperature on the optical transmission through the photopolymer waveguide was studied. It was observed that when the temperature of the ambient increases, transmittance through the photopolymer waveguide decreases. Photopolymers can naturally show swelling effect by absorbing humidity from the surrounding atmosphere. When heated, the trapped water molecules near the surface of the waveguide escape to the surrounding reducing the swelling. This leads to the homogenization of the refractive index of the polymer at the surface and as a result surface scattering losses increases reducing the transmitted optical power through the waveguide. Once the surrounding cools down, water molecules can be reabsorbed by the photopolymer waveguide reforming the swelling layer at the surface and thus optical transmittance returns to the original values. However, the recovery of the optical transmittance was not 100% and after a few heating and cooling cycles, the

photopolymer waveguide continuously exhibited a steady optical transmission output. This is possible when the trapped water molecules in the polymer matrix permanently stay within the polymer making the waveguide immune to the changes in the surrounding temperature.

To further investigate this, we embedded gold nanoparticles (Au NPs) into the photopolymer waveguide, where the voids in the polymer matrix are captured by the gold nanoparticles. With the Au NPs the photopolymer waveguide showed a sharp drop in the optical transmittance near 580 nm waveguide, which was attributed to the LSPR absorption of Au NPs which is sensitive to the ambient temperature and the surrounding refractive index. When tested the Au-NP embedded photopolymer waveguide with repeated heating and cooling cycles demonstrated a stable change in the optical transmittance response of the waveguide. During heating, the optical transmission was observed to drop gradually due to the drying of the polymer leading to higher surface scattering losses. The optical transmission was recovered when the ambient temperature was cooled down to normal room temperature. This behavior was consistently observed until 20 repeated heating/cooling cycles with only about a 2.5% drop in the recovery of the optical transmittance, indicating that in the presence of Au NPs the waveguide provides more stable changes.

The role of Au NPs can be explained as a barrier for the diffusion of the water molecules from the surrounding atmosphere into the photopolymer matrix. Most of the void spaces in the photopolymer matrix are occupied by these Au NPs and limit the water molecule diffusion into the polymer at its surface only. Since the absorbed water molecules in the photopolymer are mostly limited at the surface, they can easily escape and be reabsorbed during the heating and cooling cycles respectively, making the system more stable in terms of its optical response. Due to the presence of the gold nanoparticles capturing most of the void spaces in the photopolymer matrix, water molecules from the surrounding, therefore, cannot diffuse deep and permanently stay in the polymer matrix and thus produce a stable optical response in the Au-NP embedded photopolymer waveguide.

In summary, it can be concluded that methacrylate-based photopolymers, which are emerging potential materials in the field of integrated optics, are sensitive to the surrounding environment. The optical properties of the photopolymers are being

affected by different surrounding conditions, like the presence of solvent molecules or change in the ambient temperature which qualifies them to act as an optical material for integrated optics applications. How the optical transmission through photopolymers would be affected depends strongly on the mutual affinity of a solvent-photopolymer pair, rather than their refractive indices. The addition of nanoparticles in the photopolymer brings stability to the performance of the photopolymer waveguide for long-run applications.

5.2 Recommendations

Based on this study, the following recommendations are made that can be useful for further investigation.

1. Surface roughness that occurred due to slicing thickness during 3D printing contributes to scattering losses. By varying the surface roughness using different slicing thicknesses during 3D printing, it can be studied how the dynamic optical gain in the photopolymer is related to the surface roughness of the photopolymer waveguide.

2. A 3D printer with a higher resolution can be used to further reduce the dimension of the waveguide. In the present study, the dimension of waveguides is in 100s of microns which can be reduced to 10s of micron with a higher resolution 3D printer. This would result in better light confinement inside the waveguide and lower volumetric losses.

3. The absorption of solvent inside a polymer also depends on physical factors like the temperature and pressure of the given solvent. In the future solvent at different temperatures and pressures can be tested for their swelling effect which can be helpful in developing a flow sensor for industrial application, where a change in temperature or pressure in the flowing solvent can be detected.

4. In this research, only one size of gold nanoparticles (~50nm) was embedded in the photopolymer waveguide. In the future different sizes of gold nanoparticles as well as different types of nanoparticles and their shapes can be considered to investigate how they affect the performance of the waveguide.

5. The fundamental concept of this doctoral research work is to study changes in the optical properties of photopolymer due to the changes in some of the physical factors present in the ambient environment. Generally, optical properties of materials, like glass and silica do not show any swelling capacity and are not affected by factors like pressure, density, viscosity, current, or voltage. Hence in the future one can consider investigating other factors that can affect the swelling properties of photopolymer which could lead to the development of an integrated optical sensor to detect the change in these physical factors. In addition, photopolymers other than the methacrylate-based systems can also be a subject of future studies.

6. In the theoretical model, swelling is considered only in one direction. In the future, this model can be enhanced by considering swelling in all the relevant directions.

7. For the 3D printing fabrication of the waveguide, it is possible to set up the 3D printer in a humidifier that can control the humidity of the environment while printing. This way a greater control on the humidity can be achieved while 3D printing of the waveguide to have a better optical performance.

REFERENCES

Abdul Hamid, A. R., Osman, A. F., Mustafa, Z., Mandal, S., & Ananthakrishnan, R. (2020). Tensile, fatigue and thermomechanical properties of poly(ethylene-co-vinyl acetate) nanocomposites incorporating low and high loadings of pre-swelled organically modified montmorillonite. *Polymer Testing*. https://doi.org/10.1016/j.polymertesting.2020.106426

Abiad, M. G., Carvajal, M. T., & Campanella, O. H. (2009). A Review on Methods and Theories to Describe the Glass Transition Phenomenon: Applications in Food and Pharmaceutical Products. *Food Engineering Reviews*, *1*(2), 105–132. https://doi.org/10.1007/s12393-009-9009-1

Addanki, S., Amiri, I. S., & Yupapin, P. (2018). Review of optical fibers-introduction and applications in fiber lasers. *Results in Physics*, *10*, 743–750. https://doi.org/https://doi.org/10.1016/j.rinp.2018.07.028

Ahamed, M., El-Wahab, A., & Barakat, A. (2016). SPEEDING UP ALGORITHM FOR BUILDING THE STL MODEL USING 3D PRINTING. *17th International Conference on Applied Mechanics and Mechanical Engineering.*, *17*. https://doi.org/10.21608/amme.2016.35356

Ali, U., Abd Karim, K. J., & Buang, N. (2015). A Review of the Properties and Applications of Poly (Methyl Methacrylate) (PMMA). *Polymer Reviews*, *55*, 1–28. https://doi.org/10.1080/15583724.2015.1031377

Alothman, O. Y., Fouad, H., Al-Zahrani, S. M., Eshra, A., Al Rez, M. F., & Ansari, S. G. (2014). Thermal, creep-recovery and viscoelastic behavior of high density polyethylene/hydroxyapatite nano particles for bone substitutes: effects of gamma radiation. *BioMedical Engineering OnLine*, *13*(1), 125. https://doi.org/10.1186/1475-925X-13-125

Araujo, G. R., Pollmann, T., & Ulrich, A. (2019). Photoluminescence response of acrylic (PMMA) and polytetrafluoroethylene (PTFE) to ultraviolet light. *The European Physical Journal C*, *79*(8), 653. https://doi.org/10.1140/epjc/s10052-019-7152-2

Ballenger, V., Kaltenecker-Commerçon, J., Verdu, J., & Tordjeman, P. (2002). Interactions of solvents with poly(methyl methacrylate). *Polymer*. https://doi.org/10.1016/s0032-3861(96)01004-x

Barwicz, T., & Haus, H. A. (2005). Three-dimensional analysis of scattering losses due to sidewall roughness in microphotonic waveguides. *Journal of Lightwave Technology*. https://doi.org/10.1109/JLT.2005.850816

Beckers, M., Schlüter, T., Gries, T., Seide, G., & Bunge, C.-A. (2017). *6 - Fabrication techniques for polymer optical fibres* (C.-A. Bunge, T. Gries, & M. B. T.-P. O. F. Beckers (eds.); pp. 187–199). Woodhead Publishing. https://doi.org/10.1016/B978-0-08-100039-7.00006-3

Berglund, G. D., & Tkaczyk, T. S. (2019). Fabrication of optical components using a consumer-grade lithographic printer. *Opt. Express*, *27*(21), 30405–30420. https://doi.org/10.1364/OE.27.030405

Bernardo, V., Martin-de Leon, J., Pinto, J., Catelani, T., Athanassiou, A., & Rodriguez-Perez, M. A. (2019). Low-density PMMA/MAM nanocellular polymers using low MAM contents: Production and characterization. *Polymer*, *163*, 115–124. https://doi.org/10.1016/j.polymer.2018.12.057

Bhowmik, K., & Peng, G.-D. (2019). *Polymer Optical Fibers* (pp. 1–51). https://doi.org/10.1007/978-981-10-1477-2_38-1

Bisht, H. S., & Chatterjee, A. K. (2001). LIVING FREE-RADICAL POLYMERIZATION—A REVIEW. *Journal of Macromolecular Science, Part C*, *41*(3), 139–173. https://doi.org/10.1081/MC-100107774

Bohren, C. F., & Huffman, D. R. (1998). Absorption and Scattering of Light by Small Particles. In *Absorption and Scattering of Light by Small Particles*. https://doi.org/10.1002/9783527618156

Brinke, G. (2012). *1.11 - Phase Segregation/Polymer Blends/Microphase Separation* (K. Matyjaszewski & M. B. T.-P. S. A. C. R. Möller (eds.); pp. 287–313). Elsevier. https://doi.org/10.1016/B978-0-444-53349-4.00013-3

Brooks, H., Rennie, A., Abram, T., McGovern, J., & Caron, F. (2011). *Variable Fused Deposition Modelling - analysis of benefits, concept design and tool path generation* (pp. 511–517). https://doi.org/10.1201/b11341-83

Bussamra, B. C., Sietaram, D., Verheijen, P., Mussatto, S. I., da Costa, A. C., van der Wielen, L., & Ottens, M. (2021). A critical assessment of the Flory-Huggins (FH) theory to predict aqueous two-phase behaviour. *Separation and Purification Technology*, *255*, 117636. https://doi.org/10.1016/j.seppur.2020.117636

C. Y. Yu, H., Argyros, A., Barton, G., Eijkelenborg, M. A. van, Barbe, C., Finnie, K., Kong, L., Ladouceur, F., & McNiven, S. (2007). Quantum dot and silica nanoparticle doped polymer optical fibers. *Optics Express*, *15*(16), 9989–9994. https://doi.org/10.1364/OE.15.009989

Cennamo, N., Pesavento, M., & Zeni, L. (2021). A review on simple and highly sensitive plastic optical fiber probes for bio-chemical sensing. *Sensors and Actuators B: Chemical*, *331*, 129393. https://doi.org/10.1016/j.snb.2020.129393

Chang, C.-Y., Lin, H.-T., Lai, M.-S., Shieh, T.-Y., Peng, C.-C., Shih, M.-H., & Tung, Y.-C. (2018). Flexible Localized Surface Plasmon Resonance Sensor with Metal–Insulator–Metal Nanodisks on PDMS Substrate. *Scientific Reports*, *8*(1), 11812. https://doi.org/10.1038/s41598-018-30180-8

Chen, S. J., Fumeaux, C., Talemi, P., Chivers, B., & Shepherd, R. (2016). Progress in conductive polymer antennas based on free-standing polypyrrole and PEDOT: PSS. *2016 17th International Symposium on Antenna Technology and Applied Electromagnetics (ANTEM)*, 1–4. https://doi.org/10.1109/ANTEM.2016.7550191

Cimadoro, J., & Goyanes, S. (2020). Reversible swelling as a strategy in the development of smart membranes from electrospun polyvinyl alcohol nanofiber mats. *Journal of Polymer Science*, *58*(5), 737–746. https://doi.org/https://doi.org/10.1002/pol.20190156

Dall'Argine, C., Hochwallner, A., Klikovits, N., Liska, R., Stampf, J., & Sangermano, M. (2020). Hot-Lithography SLA-3D Printing of Epoxy Resin. *Macromolecular Materials and Engineering*. https://doi.org/10.1002/mame.202000325

Darvell, B. W. (2018). Chapter 5 - Acrylic. In B. W. Darvell (Ed.), *Materials Science for Dentistry (Tenth Edition)* (Tenth Edit, pp. 121–142). Woodhead Publishing. https://doi.org/10.1016/B978-0-08-101035-8.50005-5

Elson, J. M. (2003). Scattering losses from planar waveguides with material inhomogeneity. *Waves in Random Media*, *13*(2), 95–105. https://doi.org/10.1088/0959-7174/13/2/303

Esmizadeh, E., Khalili, S., Vahidifar, A., Naderi, G., & Dubois, C. (2018). *Waste Polymethyl Methacrylate (PMMA): Recycling and High-Yield Monomer Recovery BT - Handbook of Ecomaterials* (L. M. T. Martínez, O. V. Kharissova, & B. I. Kharisov (eds.); pp. 1–33). Springer International Publishing. https://doi.org/10.1007/978-3-319-48281-1_164-1

Evchuk, I., Makitra, R., & Pristanskii, R. (2005). Solubility of Polymethyl Methacrylate in Organic Solvents. *Russian Journal of Applied Chemistry - RUSS J APPL CHEM-ENG TR*, *78*, 1576–1580. https://doi.org/10.1007/s11167-005-0564-9

Falahati, M., Zhou, W., Yi, A., & Li, L. (2019). Fabrication of polymeric lenses using magnetic liquid molds. *Applied Physics Letters*. https://doi.org/10.1063/1.5090511

Fang, Q., Song, J. F., Tao, S. H., Yu, M. B., Lo, G. Q., & Kwong, D. L. (2008). Low Loss (~6.45dB/cm) Sub-Micron Polycrystalline Silicon Waveguide Integrated with Efficient SiON Waveguide Coupler. *Opt. Express*, *16*(9), 6425–6432. https://doi.org/10.1364/OE.16.006425

Frick, C., Dietz, A. C., Merritt, K., Umbreit, T. H., & Tomazic-Jezic, V. J. (2006). Effects of prosthetic materials on the host immune response: evaluation of polymethyl-methacrylate (PMMA), polyethylene (PE), and polystyrene (PS) particles. *Journal of Long-Term Effects of Medical Implants*, *16*(6), 423–433.

https://doi.org/10.1615/jlongtermeffmedimplants.v16.i6.20

Fuchs, Y., Soppera, O., & Haupt, K. (2012). Photopolymerization and
    photostructuring of molecularly imprinted polymers for sensor applications—A
    review. *Analytica Chimica Acta*, *717*, 7–20.
    https://doi.org/10.1016/j.aca.2011.12.026

Fujikake, H., Shibata, Y., & Ishinabe, T. (2016). Innovative polymer technologies for
    flexible liquid crystal displays. *SPIE Newsroom*.
    https://doi.org/10.1117/2.1201701.006774

Gervasio, M., Lu, K., & Davis, R. (2015). Experimental and Modeling Study of
    Solvent Diffusion in PDMS for Nanoparticle-Polymer Cosuspension Imprint
    Lithography. *Langmuir*. https://doi.org/10.1021/acs.langmuir.5b02617

Grillot, F., Vivien, L., Cassan, E., & Laval, S. (2008). Influence of waveguide
    geometry on scattering loss effects in submicron strip silicon-on-insulator
    waveguides. *Optoelectronics, IET*, *2*, 1–5. https://doi.org/10.1049/iet-
    opt:20070001

Guo, H., Guo, A., Gao, Y., & Liu, T. (2020). Influence of external swelling stress on
    the frequency characteristics of a volatile organic compound (VOC) sensor based
    on a polymer-coated film bulk acoustic resonator (FBAR). *Instrumentation
    Science and Technology*. https://doi.org/10.1080/10739149.2020.1737540

Guo, J., Gleeson, M. R., & Sheridan, J. T. (2012). A Review of the Optimisation of
    Photopolymer Materials for Holographic Data Storage. *Physics Research
    International*. https://doi.org/10.1155/2012/803439

Hällgren, S., Pejryd, L., & Ekengren, J. (2016). 3D Data Export for Additive
    Manufacturing - Improving Geometric Accuracy. *Procedia CIRP*, *50*, 518–523.
    https://doi.org/10.1016/j.procir.2016.05.046

Hamdi, D. A. (2020). Investigating the mechanical and microstructure properties of
    ceramic-PMMA polymer composite. *AIP Conference Proceedings*, *2213*(1),
    20043. https://doi.org/10.1063/5.0000429

Han, Q., Li, C., Guan, Y., Zhu, X. X., & Zhang, Y. (2014). Swelling-induced surface instability of a hydrogen-bonded LBL film and its self-healing. *Polymer*. https://doi.org/10.1016/j.polymer.2014.03.015

Han, X.-Y., Wu, Z.-L., Yang, S.-C., Shen, F.-F., Liang, Y.-X., Wang, L.-H., Wang, J.-Y., Ren, J., Jia, L.-Y., Zhang, H., Bo, S.-H., Morthier, G., & Zhao, M.-S. (2018). Recent Progress of Imprinted Polymer Photonic Waveguide Devices and Applications. *Polymers*, *10*(6), 603. https://doi.org/10.3390/polym10060603

Harith, Z., Zain, H., Batumalay, I. D. M., & Harun, S. W. (2019). A study on relative humidity sensors using PVA and PMMA coating. *Journal of Physics: Conference Series*, *1371*, 12027. https://doi.org/10.1088/1742-6596/1371/1/012027

Hartcher-O'Brien, J., Evers, J., & Tempelman, E. (2019). Surface roughness of 3D printed materials: Comparing physical measurements and human perception. *Materials Today Communications*, *19*, 300–305. https://doi.org/10.1016/j.mtcomm.2019.01.008

Henry, A., Tutt, T., Galloway, M., Davidson, Y., McWhorter, S., Soper, S., & McCarley, R. (2000). Surface Modification of Poly(methyl methacrylate) Used in the Fabrication of Microanalytical Devices. *Analytical Chemistry*, *72*, 5331–5337. https://doi.org/10.1021/ac000685l

Horák, D. (2003). Uniform polymer beads of micrometer size. *Acta Polymerica*, *47*, 20–28. https://doi.org/10.1002/actp.1996.010470103

Horvath, J. (2014). *A Brief History of 3D Printing* (pp. 3–10). https://doi.org/10.1007/978-1-4842-0025-4_1

Hossain, M. (2020). Modelling the curing process in particle-filled electro-active polymers with a dispersion anisotropy. *Continuum Mechanics and Thermodynamics*, *32*(2), 351–367. https://doi.org/10.1007/s00161-019-00747-5

Hossain, M. F., Chan, H. P., & Uddin, M. A. (2010). Simultaneous measurement of thermo-optic and stress-optic coefficients of polymer thin films using prism coupler technique. *Appl. Opt.*, *49*(3), 403–408.

https://doi.org/10.1364/AO.49.000403

Hu, Y., Ghaffar, A., Hou, Y., Liu, W., Li, F., & Wang, J. (2020). A Micro Structure POF Relative Humidity Sensor Modified With Agarose Based on Surface Plasmon Resonance and Evanescent Wave Loss. *Photonic Sensors*. https://doi.org/10.1007/s13320-020-0603-4

Huang, J., Qin, Q., & Wang, J. (2020). A Review of Stereolithography: Processes and Systems. *Processes*, *8*(9). https://doi.org/10.3390/pr8091138

Imoto, N., Shimizu, N., Mori, H., & Ikeda, M. (1983). Sputtered Silica Waveguides with an Embedded Three-Dimensional Structure. *Journal of Lightwave Technology*. https://doi.org/10.1109/JLT.1983.1072082

Jankovic, S., Tsakiridou, G., Ditzinger, F., Koehl, N. J., Price, D. J., Ilie, A.-R., Kalantzi, L., Kimpe, K., Holm, R., Nair, A., Griffin, B., Saal, C., & Kuentz, M. (2019). Application of the solubility parameter concept to assist with oral delivery of poorly water-soluble drugs – a PEARRL review. *Journal of Pharmacy and Pharmacology*, *71*(4), 441–463. https://doi.org/https://doi.org/10.1111/jphp.12948

Johnson, P. B., & Christy, R. W. (1972). Optical Constants of the Noble Metals. *Phys. Rev. B*, *6*(12), 4370–4379. https://doi.org/10.1103/PhysRevB.6.4370

Kappert, E. J., Raaijmakers, M. J. T., Tempelman, K., Cuperus, F. P., Ogieglo, W., & Benes, N. E. (2019). Swelling of 9 polymers commonly employed for solvent-resistant nanofiltration membranes: A comprehensive dataset. *Journal of Membrane Science*. https://doi.org/10.1016/j.memsci.2018.09.059

Kawaguchi, T., Lassila, L. V. J., Sasaki, H., Takahashi, Y., & Vallittu, P. K. (2014). Effect of heat treatment of polymethyl methacrylate powder on mechanical properties of denture base resin. *Journal of the Mechanical Behavior of Biomedical Materials*, *39*, 73–78. https://doi.org/10.1016/j.jmbbm.2014.07.012

Kazakov, S. (2012). *Hydrogel Films on Optical Fiber Core: Properties, Challenges, and Prospects for Future Applications* (pp. 25–70). https://doi.org/10.5772/48371

Kelb, C., Körner, M., Prucker, O., Rühe, J., Reithmeier, E., & Roth, B. (2017). PDMAA Hydrogel Coated U-Bend Humidity Sensor Suited for Mass-Production. *Sensors (Basel, Switzerland)*, *17*(3), 517. https://doi.org/10.3390/s17030517

Konopelnik, O., Aksimentyeva, O., & Martynyuk, G. (2005). Effect of Temperature on the Optical Properties of Conducting Polyaminoarenes and their Composites with Elastic Polymer Matrix. *Molecular Crystals and Liquid Crystals*, *427*(1), 37/[349]-47/[359]. https://doi.org/10.1080/15421400590891867

Kovačević, M. S., & Djordjevich, A. (2009). Variation of modal dispersion and bandwidth with temperature in PMMA based step-index polymer optical fibers. *Journal of Optoelectronics and Advanced Materials*, *11*(11), 1821–1825. https://www.scopus.com/inward/record.uri?eid=2-s2.0-75949092283&partnerID=40&md5=055076391d5995e3884fe2085494918d

Kozanecki, M., Halagan, K., Saramak, J., & Matyjaszewski, K. (2016). Diffusive properties of solvent molecules in the neighborhood of a polymer chain as seen by Monte-Carlo simulations. *Soft Matter*, *12*(25), 5519–5528. https://doi.org/10.1039/C6SM00569A

Koziara, B. T., Akkilic, N., Nijmeijer, K., & Benes, N. E. (2016). The effects of water on the morphology and the swelling behavior of sulfonated poly(ether ether ketone) films. *Journal of Materials Science*, *51*(2), 1074–1082. https://doi.org/10.1007/s10853-015-9437-7

Krasucka, P., Mergo, P., Wójcik, G., & Goworek, J. (2018). Mechanical experiments as a tool for study of swelling-deswelling and structural properties of porous polymers. *Chemical Engineering Science*. https://doi.org/10.1016/j.ces.2018.05.060

Kuila, B. K., Formanek, P., & Stamm, M. (2013). Multilayer polymer thin films for fabrication of ordered multifunctional polymer nanocomposites. *Nanoscale*, *5*(22), 10849–10852. https://doi.org/10.1039/C3NR03607C

Le, H. H., Carlson, E. M., Chua, J. P., & Belcher, S. M. (2008). Bisphenol A is

released from polycarbonate drinking bottles and mimics the neurotoxic actions of estrogen in developing cerebellar neurons. *Toxicology Letters*, *176*(2), 149–156. https://doi.org/10.1016/j.toxlet.2007.11.001

Leggat, P., Smith, D., & Kedjarune, U. (2009). Surgical Applications of Methyl Methacrylate: A Review of Toxicity. *Archives of Environmental & Occupational Health*, *64*, 207–212. https://doi.org/10.1080/19338240903241291

Leigh, J. A. (1975). Use of PMMA in expansion dental implants. *Journal of Biomedical Materials Research*, *9*(4), 233–242. https://doi.org/10.1002/jbm.820090426

Lian, X., Wu, Q., Farrell, G., & Semenova, Y. (2020). High-sensitivity temperature sensor based on anti-resonance in high-index polymer-coated optical fiber interferometers. *Optics Letters*, *45*(19), 5385–5388. https://doi.org/10.1364/OL.403050

Liang, J.-Z. (2013). Heat distortion temperature of PPS/PC blend, PPS/PC nanocomposite and PPS/PC/GF hybrid nanocomposite: *Journal of Polymer Engineering*, *33*(6), 483–488. https://doi.org/doi:10.1515/polyeng-2013-0064

Liu, J. G., & Ueda, M. (2009). High refractive index polymers: Fundamental research and practical applications. *Journal of Materials Chemistry*. https://doi.org/10.1039/b909690f

Lu, P., Men, L., & Chen, Q. (2009). Polymer-Coated Fiber Bragg Grating Sensors for Simultaneous Monitoring of Soluble Analytes and Temperature. *Sensors Journal, IEEE*, *9*, 340–345. https://doi.org/10.1109/JSEN.2009.2013499

Madani, A., & Azarinia, H. R. (2017). Design and fabrication of all-polymeric photonic waveguides in optical integrated circuits. *Optik*. https://doi.org/10.1016/j.ijleo.2017.03.021

Mahoney, E. J., Xiong, B., & Fang, Q. (2020). Optical model of light propagation in total internal reflection fluorescence sensors. *Appl. Opt.*, *59*(34), 10651–10660. https://doi.org/10.1364/AO.404112

Maines, E. M., Porwal, M. K., Ellison, C. J., & Reineke, T. M. (2021). Sustainable advances in SLA/DLP 3D printing materials and processes. *Green Chem.*, *23*(18), 6863–6897. https://doi.org/10.1039/D1GC01489G

Malacarne-Zanon, J., Pashley, D. H., Agee, K. A., Foulger, S., Alves, M. C., Breschi, L., Cadenaro, M., Garcia, F. P., & Carrilho, M. R. (2009). Effects of ethanol addition on the water sorption/solubility and percent conversion of comonomers in model dental adhesives. *Dental Materials*, *25*(10), 1275–1284. https://doi.org/10.1016/J.DENTAL.2009.03.015

Maradudin A. A., & Mendez E. R. (2007). Light scattering from randomly rough surfaces. *Science Progress (1933-)*, *90*(4), 161–221. http://www.jstor.org/stable/43423209

Marcombe, R., Cai, S., Hong, W., Zhao, X., Lapusta, Y., & Suo, Z. (2010). A theory of constrained swelling of a pH-sensitive hydrogel. *Soft Matter*. https://doi.org/10.1039/b917211d

Marcon, V., & van der Vegt, N. F. A. (2014). How does low-molecular-weight polystyrene dissolve: osmotic swelling vs. surface dissolution. *Soft Matter*, *10*(45), 9059–9064. https://doi.org/10.1039/C4SM01636J

Maruyama, T., Hirata, H., Furukawa, T., & Maruo, S. (2020). Multi-material microstereolithography using a palette with multicolor photocurable resins. *Opt. Mater. Express*, *10*(10), 2522–2532. https://doi.org/10.1364/OME.401810

Mat-Shayuti, M. S., Abdullah, M. Z., & Megat-Yusoff, P. S. M. (2017). Tensile Behaviour and Morphology of Polypropylene/Polycar-bonate/Polypropylene-graft-maleic Anhydride Blends. *MATEC Web of Conferences*. https://doi.org/10.1051/matecconf/201710901005

Mayer, K. M., & Hafner, J. H. (2011). Localized Surface Plasmon Resonance Sensors. *Chemical Reviews*, *111*(6), 3828–3857. https://doi.org/10.1021/cr100313v

Mendes-Felipe, C., Oliveira, J., Etxebarria, I., Vilas-Vilela, J. L., & Lanceros-Mendez, S. (2019). State-of-the-Art and Future Challenges of UV Curable

Polymer-Based Smart Materials for Printing Technologies. *Advanced Materials Technologies*, *4*(3), 1800618. https://doi.org/https://doi.org/10.1002/admt.201800618

Miller-Chou, B. A., & Koenig, J. L. (2003). A review of polymer dissolution. In *Progress in Polymer Science (Oxford)*. https://doi.org/10.1016/S0079-6700(03)00045-5

Naka, K. (2021). *Monomers, Oligomers, Polymers, and Macromolecules (Overview) BT - Encyclopedia of Polymeric Nanomaterials* (S. Kobayashi & K. Müllen (eds.); pp. 1–6). Springer Berlin Heidelberg. https://doi.org/10.1007/978-3-642-36199-9_237-1

Ngo, T. D., Kashani, A., Imbalzano, G., Nguyen, K. T. Q., & Hui, D. (2018). Additive manufacturing (3D printing): A review of materials, methods, applications and challenges. *Composites Part B: Engineering*, *143*, 172–196. https://doi.org/10.1016/j.compositesb.2018.02.012

Novo, L. P., & Curvelo, A. A. S. (2019). Hansen Solubility Parameters: A Tool for Solvent Selection for Organosolv Delignification. *Industrial \& Engineering Chemistry Research*, *58*(31), 14520–14527. https://doi.org/10.1021/acs.iecr.9b00875

Obreja, P., Cristea, D., Budianu, E., Rebigan, R., Kuncser, V., Bulinski, M., & Filoti, G. (2006). Effect of dopant on the physical properties of polymer films for microphotonics. *Progress in Solid State Chemistry*, 103–109. https://doi.org/10.1016/j.progsolidstchem.2005.11.051

Ogieglo, W., Wormeester, H., Eichhorn, K.-J., Wessling, M., & Benes, N. E. (2015). In situ ellipsometry studies on swelling of thin polymer films: A review. *Progress in Polymer Science*, *42*, 42–78. https://doi.org/10.1016/j.progpolymsci.2014.09.004

Okudan, A., & Altay, A. (2019). Investigation of the effects of different hydrophilic and hydrophobic comonomers on the volume phase transition temperatures and thermal properties of n-isopropylacrylamide-based hydrogels. *International*

Journal of Polymer Science. https://doi.org/10.1155/2019/7324181

Paquet, C., & Kumacheva, E. (2008). Nanostructured polymers for photonics. *Materials Today*, *11*(4), 48–56. https://doi.org/10.1016/S1369-7021(08)70056-7

Peters, K. (2011). Polymer optical fiber sensors - A review. In *Smart Materials and Structures*. https://doi.org/10.1088/0964-1726/20/1/013002

Plushchik, O. A., & Aniskevich, A. N. (2000). Effects of temperature and moisture on the mechanical properties of polyester resin in tension. *Mechanics of Composite Materials*, *36*(3), 233–240. https://doi.org/10.1007/BF02681875

Quan, H., Zhang, T., Xu, H., Luo, S., Nie, J., & Zhu, X. (2020). Photo-curing 3D printing technique and its challenges. *Bioactive Materials*, *5*(1), 110–115. https://doi.org/10.1016/j.bioactmat.2019.12.003

Ramponi, R., Osellame, R., & Marangoni, M. (2002). Two straightforward methods for the measurement of optical losses in planar waveguides. *Review of Scientific Instruments*, *73*(3), 1117–1120. https://doi.org/10.1063/1.1448143

Ravi, P. (2020). Understanding the relationship between slicing and measured fill density in material extrusion 3D printing towards precision porosity constructs for biomedical and pharmaceutical applications. *3D Printing in Medicine*, *6*. https://doi.org/10.1186/s41205-020-00063-8

Ravi, P., & Shiakolas, P. S. (2021). Effects of slicing parameters on measured fill density for 3D printing of precision cylindrical constructs using Slic3r. *SN Applied Sciences*, *3*(3), 390. https://doi.org/10.1007/s42452-021-04398-7

Reddy, K. R., El-Zein, A., Airey, D. W., Alonso-Marroquin, F., Schubel, P., & Manalo, A. (2020). Self-healing polymers: Synthesis methods and applications. *Nano-Structures & Nano-Objects*, *23*, 100500. https://doi.org/10.1016/j.nanoso.2020.100500

Reis, J. (2012). Effect of Temperature on the Mechanical Properties of Polymer Mortars. *Materials Research*, *15*, 645–649. https://doi.org/10.1590/S1516-14392012005000091

Rodriguez, E., Shahbikian, S., Marcos, B., & Huneault, M. A. (2018). Hydrolytic stability of polylactide and poly(methyl methacrylate) blends. *Journal of Applied Polymer Science*, *135*(11), 45991. https://doi.org/10.1002/app.45991

Roughton, B. C., White, J., Camarda, K. V, & Gani, R. (2011). Simultaneous Design of Ionic Liquids and Azeotropic Separation Processes. In E. N. Pistikopoulos, M. C. Georgiadis, & A. C. B. T.-C. A. C. E. Kokossis (Eds.), *21 European Symposium on Computer Aided Process Engineering* (Vol. 29, pp. 1578–1582). https://doi.org/10.1016/B978-0-444-54298-4.50094-5

Sakai, N. (2009). Photo-curable resin for UV-nanoimprint technology. *Journal of Photopolymer Science and Technology*. https://doi.org/10.2494/photopolymer.22.133

Sakai, T. (2020). Swelling and Deswelling. In *Physics of Polymer Gels* (pp. 77–107). https://doi.org/10.1002/9783527346547.ch4

Sakai, T., Kurakazu, M., Akagi, Y., Shibayama, M., & Chung, U. (2012). Effect of swelling and deswelling on the elasticity of polymer networks in the dilute to semi-dilute region. *Soft Matter*, *8*(9), 2730–2736. https://doi.org/10.1039/C2SM07043J

Schmitz, C., Pösch, P., Thelakkat, M., Schmidt, H. W., Montali, A., Feldman, K., Smith, P., & Weder, C. (2001). Polymeric light-emitting diodes based on poly(p-phenylene ethynylene), poly(triphenyldiamine), and spiroquinoxaline. *Advanced Funtional Materials*. https://doi.org/10.1002/1616-3028(200102)11:1<41::AID-ADFM41>3.0.CO;2-S

Shi, Ying, Ma, L., Zhuang, Y., & He, Z. (2020). Investigation on roughness-induced scattering loss of small-core polymer waveguides for single-mode optical interconnect applications. *Optics Express*, *28*(26), 38733–38744. https://doi.org/10.1364/OE.410283

Shi, Yingli, Hu, M., Xing, Y., & Li, Y. (2020). Temperature-dependent thermal and mechanical properties of flexible functional PDMS/paraffin composites. *Materials & Design*, *185*, 108219. https://doi.org/10.1016/j.matdes.2019.108219

Shi, Yongqiang, Zhang, C., Zhang, H., Bechtel, J. H., Dalton, L. R., Robinson, B. H., & Steier, W. H. (2000). Low (sub-1-volt) halfwave voltage polymeric electro-optic modulators achieved by controlling chromophore shape. *Science*. https://doi.org/10.1126/science.288.5463.119

Shukla, V., Bajpai, M., Singh, D. K., Singh, M., & Shukla, R. (2004). Review of basic chemistry of UV-curing technology. *Pigment & Resin Technology*, *33*, 272–279. https://doi.org/10.1108/03699420410560461

Sidhu, N., Sohi, P., & Kahrizi, M. (2019). Polymer based optical humidity and temperature sensor. *Journal of Materials Science: Materials in Electronics*, *30*. https://doi.org/10.1007/s10854-018-00586-1

Sinchenko, E., Gibbs, W. E. K., Mazzolini, A. P., & Stoddart, P. R. (2013). The Effect of the Cladding Refractive Index on an Optical Fiber Evanescent-Wave Sensor. *J. Lightwave Technol.*, *31*(20), 3251–3257. http://jlt.osa.org/abstract.cfm?URI=jlt-31-20-3251

Sinha, A. K., Narang, H. K., & Bhattacharya, S. (2020). Mechanical properties of hybrid polymer composites: a review. In *Journal of the Brazilian Society of Mechanical Sciences and Engineering*. https://doi.org/10.1007/s40430-020-02517-w

Stajanca, P., Topolniak, I., Pötschke, S., & Krebber, K. (2018). Solution-mediated cladding doping of commercial polymer optical fibers. *Optical Fiber Technology*, *41*, 227–234. https://doi.org/10.1016/j.yofte.2018.02.008

Suar, M., Baran, M., Günther, A., & Roth, B. (2020). Combined thermomechanical and optical simulations of planar-optical polymer waveguides. *Journal of Optics*, *20*. https://doi.org/10.1088/2040-8986/abc087

Sudarsan, V. (2012). 8 - Optical Materials: Fundamentals and Applications. In S. Banerjee & A. K. Tyagi (Eds.), *Functional Materials* (pp. 285–322). Elsevier. https://doi.org/10.1016/B978-0-12-385142-0.00008-8

Sudhakar, Y. N., Selvakumar, M., & Bhat, D. K. (2018). *Chapter 1 - An introduction of Biopolymer Electrolytes* (Y. N. Sudhakar, M. Selvakumar, & D. K. B. T.-B. E.

Bhat (eds.); pp. 1–34). Elsevier. https://doi.org/10.1016/B978-0-12-813447-4.00001-7

Suzuki, Y., Nakamura, A., & Morisawa, M. (2018). Effect of Double Cladding with the use of Scattering Upper Layer on the Sensitivity of Plastic Optical Fiber Alkane Sensors. *26th International Conference on Optical Fiber Sensors*, TuE6. https://doi.org/10.1364/OFS.2018.TuE6

Tawade, B. V, Apata, I. E., Pradhan, N., Karim, A., & Raghavan, D. (2021). Recent Advances in the Synthesis of Polymer-Grafted Low-K and High-K Nanoparticles for Dielectric and Electronic Applications. *Molecules*, *26*(10). https://doi.org/10.3390/molecules26102942

Tian, Y., Qian, K., Jacobs, E., Amstad, E., Jones, D. S., Stella, L., & Andrews, G. P. (2019). The Investigation of Flory-Huggins Interaction Parameters for Amorphous Solid Dispersion Across the Entire Temperature and Composition Range. *Pharmaceutics*, *11*(8), 420. https://doi.org/10.3390/pharmaceutics11080420

Tokmachev, M. G., Ferapontov, N. B., & Gagarin, A. N. (2017). Analysis of the swelling or shrinking kinetics of crosslinked hydrophilic polymers by mathematical modeling. *Journal of Mathematical Chemistry*, *55*(1), 142–152. https://doi.org/10.1007/s10910-016-0676-x

Trenti, A., Borghi, M., Biasi, S., Ghulinyan, M., Ramiro-Manzano, F., Pucker, G., & Pavesi, L. (2018). Thermo-optic coefficient and nonlinear refractive index of silicon oxynitride waveguides. *AIP Advances*, *8*(2), 25311. https://doi.org/10.1063/1.5018016

Trost, M., Herffurth, T., Schmitz, D., Schröder, S., Duparré, A., & Tünnermann, A. (2013). Evaluation of subsurface damage by light scattering techniques. *Applied Optics*, *52*(26), 6579–6588. https://doi.org/10.1364/AO.52.006579

Uyor, U., Popoola, P., Popoola, O., & V.S, A. (2020). Polymeric cladding materials under high temperature from optical fibre perspective: a review. *Polymer Bulletin*, *77*, 1–23. https://doi.org/10.1007/s00289-019-02830-y

Venkatraman, V., & Alsberg, B. K. (2018). Designing high-refractive index polymers using materials informatics. *Polymers*. https://doi.org/10.3390/POLYM10010103

Verrina, V., Edward, S., Zhang, H., Antoncecchi, A., Witte, S., & Planken, P. (2020). Role of scattering by surface roughness in the photoacoustic detectionof hidden micro-structures. *Appl. Opt.*, *59*(30), 9499–9509. https://doi.org/10.1364/AO.397264

Vidakis, N., Petousis, M., Vaxevanidis, N., & Kechagias, J. (2020). *Surface Roughness Investigation of Poly-Jet 3D Printing*. *8*, 14. https://doi.org/10.3390/math8101758

Vrentas, J. S., & Duda, J. L. (1977). DIFFUSION IN POLYMER - SOLVENT SYSTEMS - 1. REEXAMINATION OF THE FREE-VOLUME THEORY. *J Polym Sci Polym Phys Ed*. https://doi.org/10.1002/pol.1977.180150302

Vrentas, J. S., & Vrentas, C. M. (1994). Solvent Self-Diffusion in Glassy Polymer-Solvent Systems. *Macromolecules*. https://doi.org/10.1021/ma00098a009

Wang, J., Lee, M., Park, S.-M., Hong, S., & Kim, N. (2012). A study on the mechanical properties and deformation behavior of injection molded PMMA-TSP laminated composite. *Korea-Australia Rheology Journal*, *24*. https://doi.org/10.1007/s13367-012-0003-4

Wietzke, S., Jansen, C., Reuter, M., Jung, T., Kraft, D., Chatterjee, S., Fischer, B. M., & Koch, M. (2011). Terahertz spectroscopy on polymers: A review of morphological studies. *Journal of Molecular Structure*, *1006*(1), 41–51. https://doi.org/10.1016/j.molstruc.2011.07.036

Witkowski, A., Stec, A. A., & Hull, T. R. (2016). *Thermal Decomposition of Polymeric Materials BT - SFPE Handbook of Fire Protection Engineering* (M. J. Hurley, D. Gottuk, J. R. Hall, K. Harada, E. Kuligowski, M. Puchovsky, J. Torero, J. M. Watts, & C. Wieczorek (eds.); pp. 167–254). Springer New York. https://doi.org/10.1007/978-1-4939-2565-0_7

Xavier, S. F. (2003). Properties and Performance of Polymer Blends. In L. A. Utracki

(Ed.), *Polymer Blends Handbook* (pp. 861–950). Springer Netherlands.
https://doi.org/10.1007/0-306-48244-4_12

Xiang, L., Zhuang-Qi, C., Qi-Shun, S., Qing-Hua, M., De-Ying, H., Kun-Peng, G.,
Ling, Q., & Yu-Quan, S. (2006). Anisotropy in Thermo-Optic Coefficient of
Different Polymer Systems by Attenuated Total Reflection Configuration.
Chinese Physics Letters, *23*(4), 998–1001. https://doi.org/10.1088/0256-
307x/23/4/065

Xie, R., Weisen, A. R., Lee, Y., Aplan, M. A., Fenton, A. M., Masucci, A. E., Kempe,
F., Sommer, M., Pester, C. W., Colby, R. H., & Gomez, E. D. (2020). Glass
transition temperature from the chemical structure of conjugated polymers.
Nature Communications, *11*(1), 893. https://doi.org/10.1038/s41467-020-14656-
8

Xue, G.-H., & Fu, J.-Z. (2014). Fabrication of low cost soft tissue prostheses with the
desktop 3D printer. *Scientific Reports*, *4*, 1–7. https://doi.org/10.1038/srep06973

Yang, X., Shao, Q., Yang, L., Zhu, X., Hua, X., Zheng, Q., Song, G., & Lai, G.
(2013). Preparation and performance of high refractive index silicone resin-type
materials for the packaging of light-emitting diodes. *Journal of Applied Polymer
Science*, *127*. https://doi.org/10.1002/app.37897

Yoshida, K., Yamamoto, T., Tajima, K., Isono, T., & Satoh, T. (2019). Installing a
functional group into the inactive ω-chain end of PMMA and PS-b-PMMA by
terminal-selective transesterification. *Polymer Chemistry*, *10*(24), 3390–3398.
https://doi.org/10.1039/C9PY00315K

Yoshimura, S., Ikuse, K., Tsukazaki, Y., Kiuchi, M., & Hamaguchi, S. (2009). Effect
of ultraviolet light irradiation on etching process of poly(methyl methacrylate) by
ion beam injections. *Journal of Physics: Conference Series*, *191*.
https://doi.org/10.1088/1742-6596/191/1/012030

Zhang, Z., Zhao, P., Lin, P., & Sun, F. (2006). Thermo-optic coefficients of polymers
for optical waveguide applications. *Polymer*, *47*, 4893–4896.
https://doi.org/10.1016/j.polymer.2006.05.035

APPENDIX

APPENDIX A

EXPERIMENTAL OPTICAL POWER GAIN WHEN SOLVENT VAPORS INTERACTS WITH THE PHOTOPOLYMER WAVEGUIDE

Figure A1 represents the experimental increase in the optical power when methanol and ethanol vapors come in contact with the methacrylate-based photopolymer waveguide. From the figure, it can be observed that both of them show an exponential increase in the optical power where methanol reaches the saturation level faster (215 s) in comparison to ethanol (420 s). This is due to a higher mutual diffusion coefficient of methanol for the photopolymer in comparison to ethanol.

Figure A1

Experimental Gain in the Optical Power when the Solvent Vapors Interact with the Methacrylate-based Photopolymer Waveguides (a) Methanol (b) Ethanol
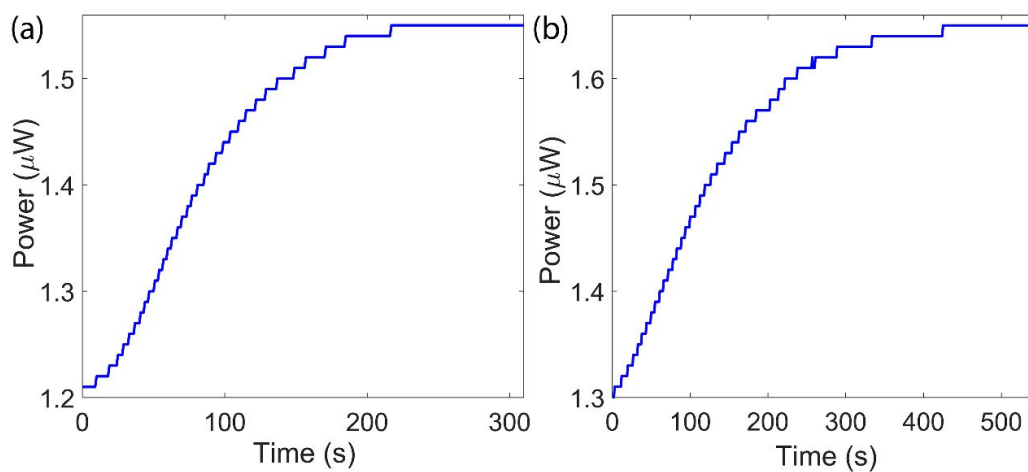
APPENDIX B

OPTICAL TRANSMITTANCE IN THE Au-NP EMBEDDED METHACRYLATE-BASES PHOTOPOLYMER WAVEGUIDE WITH HEATING AND COOLING CYCLES

In Figure B1, variation in the transmittance to temperature for Au-NP embedded methacrylate-based photopolymer waveguide is shown for heating and cooling cycles. The Au-NP embedded methacrylate-based photopolymer waveguide was heated from 28˚C to 45˚C, and then cool down to 28˚C which counts for one complete cycle. This experiment was repeated continuously for 20 complete cycles and normalized transmittance is presented below in graphs. To provide clarity in the presentation, 20 cycles are shown in four figures, a group of 5 cycles each. Here it can be observed that when the temperature of the testing chamber was increased, transmittance through the waveguide was decreased, when the testing chamber was cooled down, transmittance was increased and raised to the initial levels. This trend was repeatable for all 20 cycles and at the end of the 20th cycle, the net loss in the transmittance was only 2.75 %.

Figure B1

Transmittance vs Temperature Graphs for the Au-NP Embedded Waveguide for Individual Heating and Cooling Cycles (a) 1-5 Cycles (b) 6-10 Cycles (c)11-15 Cycles (b)16-20 Cycles
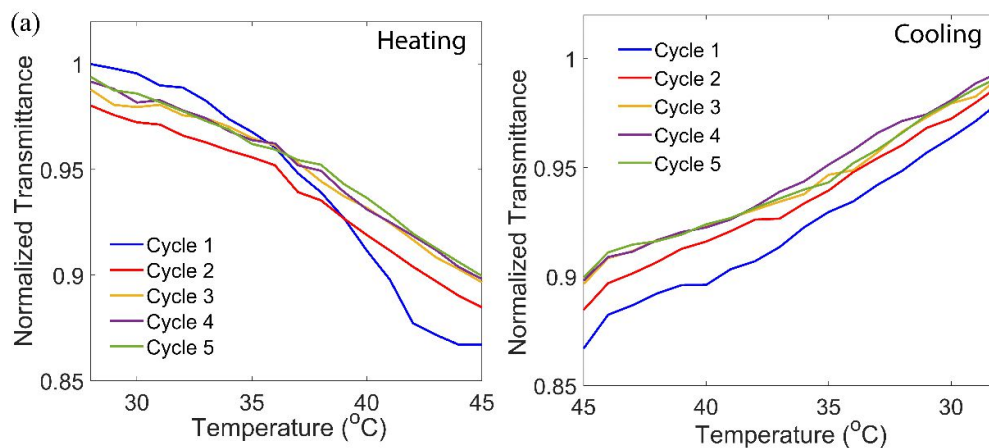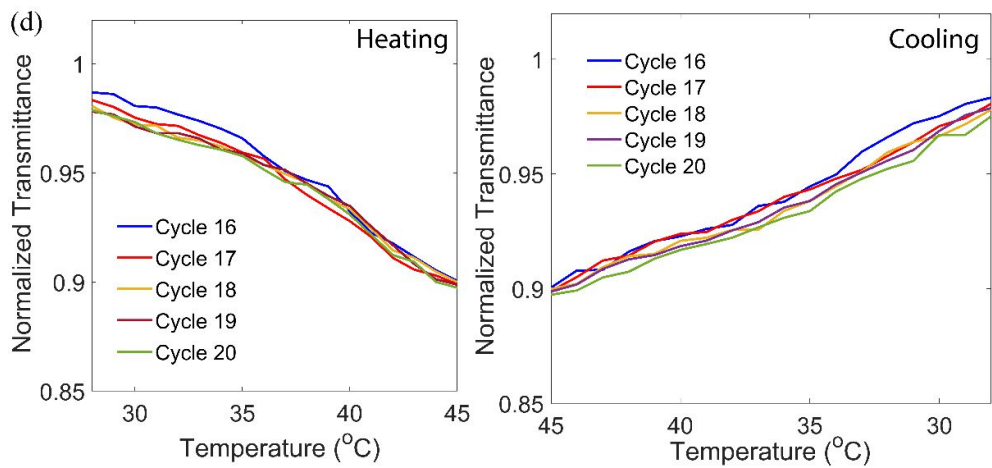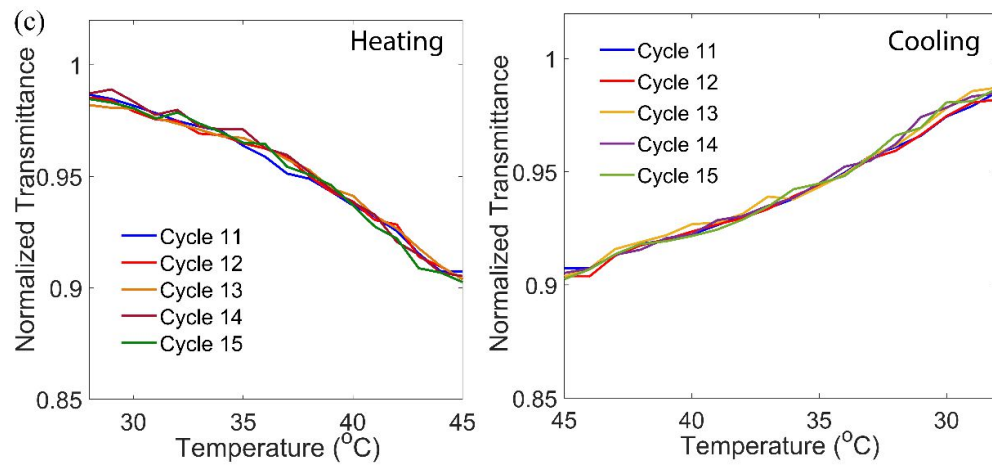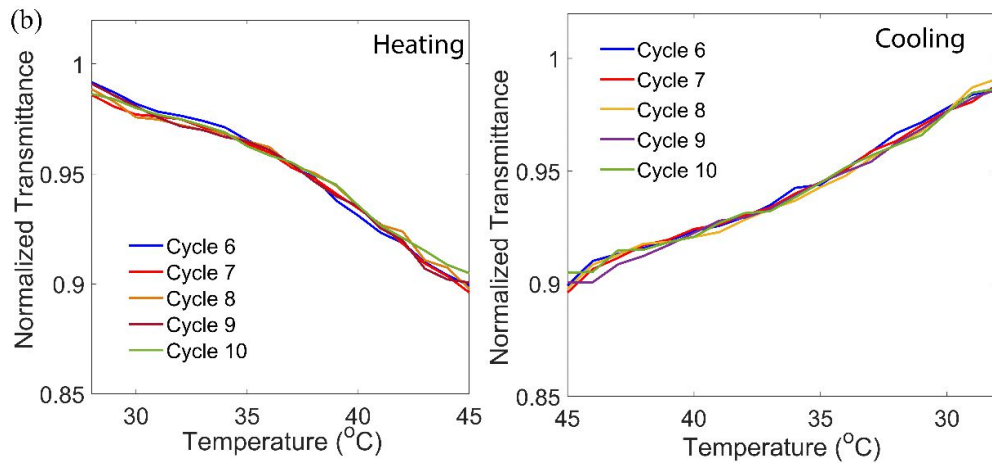
VITA

Born in 1986, Kunal Sharma earned his B.Tech. degree in Mechanical Engineering from Banaras Hindu University, Varanasi, India in 2008. During his bachelor's degree, he worked as an intern at Ashok Leyland, India. After graduating, he worked as Senior Engineer at Larsen & Toubro Ltd, India, and then to pursue higher education, he joined the Asian Institute of Technology master's degree program in Mechatronics. During his master's degree, he worked on control and dynamics of the system and human-machine interfaces using CAD / CAM modeling. After earning his master's degree, he joined the Doctor of Engineering in Nanotechnology program at the Asian Institute of Technology, Thailand where he received educational support through AIT-Fellowship and Ideal Fasteners. In his doctoral study, he primarily worked on the usage of photopolymers in the development of integrated optic sensors and 3D printing of waveguides. His research interest includes Nanoparticles-polymer-based optical composites, integrated optical sensors, multiphysics-simulation, and, theoretical modeling.